# Focusing on the Versatile Transcription-Coupled DNA Repair Pathway

Franziska Wienholz

# Focusing on the Versatile Transcription-Coupled DNA Repair Pathway

Een focus op het veelzijdige transcriptie-gekoppelde
DNA reparatieproces

Thesis

to obtain the degree of Doctor from the
Erasmus University Rotterdam
by command of the
rector magnificus

Prof.dr. R.C.M.E. Engels

and in accordance with the decision of the Doctorate Board.
The public defence shall be held on

Thursday, 14th of March 2019 at 15:30 hrs
by

Franziska Wienholz
born in Herdecke, Germany

**Doctoral Committee:**

| | |
|---|---|
| **Promotor:** | Prof. Dr. W. Vermeulen |
| **Other members:** | Dr. J.H.G. Lebbink |
| | Prof. Dr. J.H.J Hoeijmakers |
| | Prof. Dr. L.H.F. Mullenders |
| **Copromotor:** | Dr. J.A.F. Marteijn |

# Table of contents

# Chapter 1

## General Introduction

# Introduction

Genetic information, which is needed for building and maintaining organisms, is stored in the DNA. The ability to correctly storing and translating this genetic information is crucial for organisms to function properly.

## DNA Damage

The integrity of DNA is continuously challenged by the intrinsic chemical instability of DNA and its exposure to genotoxic agents. It has been proposed that approximately 10.000 - 100.000 DNA lesions per day and per cell are formed [1-3]. DNA damage can be classified based on its source of origin: 1) spontaneous reactions (for example hydrolytic deamination of cytosine and hydrolytic depurination of guanine), 2) cellular metabolism (for example reactive oxygen species) and 3) exogenous sources (for example chemicals, ultraviolet (UV)-light and ionizing radiation). The induced DNA damage consists of a wide spectrum of different types of DNA lesions including, for example, DNA breaks or chemically modified nucleotides (Table 1) [4].

**Table 1**
Overview of different agents inducing DNA damage that are repaired by NER, BER or MMR.

| DNA lesion | Damage source | Main Repair Pathway |
|---|---|---|
| CPD, 6-4PP | Sunlight | |
| Bulky adducts | Food, cigarette smoke | NER |
| Intrastrand crosslinks | Chemotherapy (e.g., Cisplatin) | |
| 8-oxoG | ROS, respiration | |
| ThymineIcol | ROS, respiration | |
| $N^7$-Alkyl-dG, $N^3$-Alkyl-dA | Food, pollutants | |
| Uracil, (Hypo)Xanthine | Spontaneous deamination | BER |
| Abasic site | Spontaneous hydrolysis | |
| Single-strand breaks | Ionizing radiation, ROS | |
| Mismatches | Replication errors | |
| Small insertion/deletion | Replication slippage | MMR |

Adapted from: Giglia-Mari et al., (2011)[4].

A well-known DNA damaging agent is UV-light, present in sunlight. DNA bases can directly absorb photons of UV-light [5], causing the formation of covalent bonds between two adjacent pyrimidines resulting in cyclobutane-pyrimidine dimers (CPD) or 6-4 pyrimidinepyrimidone photo products ((6-4)PPs) [6-8]. If left unrepaired, these DNA lesions might have effects on different processes in the cell, by interfering for example with transcription or replication, or by inducing mutations or other chromosomal aberrations [3, 9, 10]. A sophisticated and interwoven DNA-damage response (DDR) has evolved including DNA-damage repair mechanisms and DNA-damage signaling to maintain the integrity of the genetic information and to regulate the cell cycle and apoptosis or senescence [11].

### The repair of damaged DNA
In contrast to other macromolecules, such as proteins or RNA, DNA cannot be replaced and relies solely on DNA repair when damaged [9, 12]. Specific DNA-damage repair pathways are responsible for the removal of different types of DNA lesions (Table 1). The research presented in this thesis focusses on excision based DNA repair pathways, including DNA Mismatch Repair (MMR), Base Excision Repair (BER) and Nucleotide Excision Repair (NER), which are discussed below in more detail.

MMR, BER and NER all utilize a similar excision based strategy to remove DNA lesions present in only one of the two DNA strands. The DNA lesion is removed by incisions made in the DNA in proximity of the damage and is replaced with newly synthesised DNA, using the undamaged, complementary strand as template. Even though all excision-based DNA repair pathways utilize a similar damage removal mechanism, these repair pathways recognise different types of DNA damage (Table 1) and utilize principally different strategies to detect those DNA lesions.

### DNA Mismatch Repair
Base-base mismatches, or short nucleotide insertions or deletions that can occur spontaneously as a consequence of inaccurate replication or recombination are removed by the Mismatch Repair (MMR) pathway. MMR is mainly active during replication when mismatches are recognized by the heterodimeric MutSα (for base-base mismatches) or MutSβ (for larger nucleotide insertion/deletion loops) complexes [13]. MutSα and MutSβ are homologs of the prokaryotic homodimeric MutS protein. Amongst a number of eukaryotic heterodimeric MutS homologs, MutSα and MutSβ are the most prominent [14]. Upon mismatch recognition, the MutSα or MutSβ dimers undergo ATP-driven conformational

changes to recruit one of the dimeric MutL (α, β or ɣ) complexes activated by PCNA. This ternary complex creates single-stranded DNA nicks in the daughter strand and a stretch of nucleotides, including the mismatch, is subsequently excised by exonuclease 1 (EXO1). The resulting single-strand gap is eventually filled by PCNA and DNA Polymerase δ (Pol δ) and ligated by DNA ligase I [15]. The importance of functional MMR is illustrated by the severe cancer-prone phenotype of hereditary nonpolyposis colorectal cancer or Lynch syndrome patients, caused by mutations in the *MLH1* gene (coding for MutL) or the *MSH2* gene (coding for MutS) [16, 17].

## Base Excision Repair

Side products of cellular metabolism, such as oxygen radicals and alkylating agents can alter nucleotide bases without significant disturbance of Watson-Crick base-pairing [1, 18]. The Base Excision Repair (BER) mechanism can remove those altered nucleotide bases from the DNA and is therefore an important repair system for maintaining genome stability and preventing mutagenesis following the numerous endogenous DNA damages acquired during the lifespan of an organism [19].

The BER reaction can be sub-divided into distinct steps [20] (Figure 1). Firstly, oxidized, alkylated or deaminated nucleotide bases are recognized by specific DNA glycosylases, each recognizing a specific type of base damage. For example, the 8-Oxoguanine glycosylase (OGG1), specifically recognizes 8-oxo-7,8-dihydroguanine (8-oxoG), one of the major oxidation-induced base lesions [9]. The glycosylases excise and remove the damaged or inappropriate bases by cleaving the N-glycosidic bond between the base and the deoxyribose, leaving an apurinic/apyrimidinic (AP) site (Figure 1). This AP site is then further processed by AP-endonuclease 1 (APE1), which incises the deoxyribose at the AP site, resulting in a 3' OH and 5' deoxyribose phosphate termini [21, 22]. Subsequently, the Poly(ADP-ribose)-Polymerase 1 (PARP-1) binds to these ssDNA breaks and gets activated to catalyze the synthesis of ADP-ribose polymer chains to proteins, including PARP-1 itself [23, 24]. The ssDNA breaks and PARylated proteins recruit the X-ray repair cross-complementing protein 1 (XRCC1), which functions as a scaffold protein coordinating the further processing by either short-patch (replacement of a single nucleotide) or by long-patch (replacement of 2-10 nucleotides) BER. In short-patch BER, ssDNA is subsequently filled and ligated by the activity of DNA Polymerase β (Polβ) and DNA ligase IIIα (Lig III) (Figure 1). The long-patch is repaired by the action of Proliferating cell nuclear antigen (PCNA) and Pol δ, the resulting stretch of displaced nucleotides is cleaved by the Flap endonuclease 1
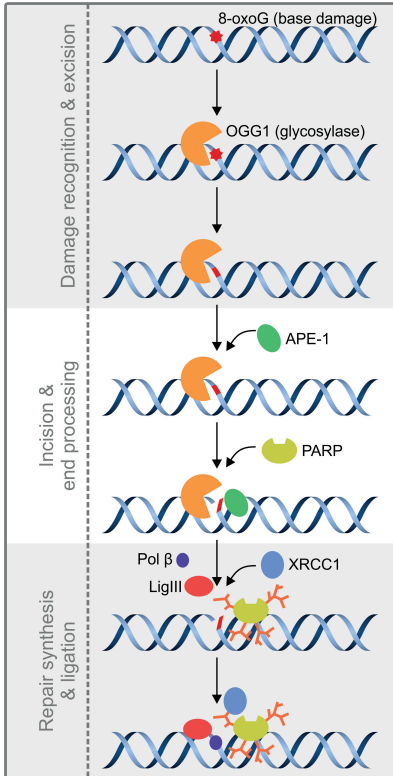
**Figure 1**

**Base excision repair of oxidative lesions.** BER can be subdivided into three steps. First, damaged bases are recognized and removed by glycosylases resulting in an AP site. For example, the prevalent 8-oxoG lesion is recognized by the glycosylase OGG1. Secondly, APE1 incises the DNA backbone adjacent to the AP site, thereby creating a single strand break. The last step includes the binding of PARP to the single strand break, followed by the recruitment of XRCC1. XRCC1 then functions as scaffold, binding DNA Polymerase β and Ligase III, which respectively fill and ligate the DNA.

(FEN1) and ligated by Ligase I.

Reduced BER activity, mostly due to polymorphic, less functional variants of BER proteins, seems to play a role in the development of cancer and neurodegeneration [25-27]. Polβ, responsible for gap-filling during short-patch BER is mutated in 30% of solid tumors [28] and mutations in its catalytic domain increase genomic instability and cellular transformation [29].

## Nucleotide Excision Repair

Nucleotide Excision Repair (NER) is a highly versatile and evolutionary conserved repair pathway capable of recognizing and removing helix distorting lesions, which are for example caused by UV-light [12, 30]. In contrast to most other DNA repair pathways, NER does not recognize the DNA lesion itself, but rather the DNA-damage induced distortion of the DNA helix. This indirect manner of damage recognition explains its capability to remove a wide variety of structurally unrelated DNA lesions [7, 12, 30].

## DNA damage recognition

NER consists of two sub-pathways, Global Genome NER (GG-NER) and Transcription coupled NER (TC-NER), distinct by how and where in the genome lesions are detected [6, 31]. GG-NER recognizes DNA damage throughout the entire genome, whereas TC-NER specifically repairs lesions in the transcribed strand of active genes [12].

## DNA damage recognition in GG-NER

Within GG-NER, DNA damage is recognized by the heterotrimeric XPC complex, consisting of XPC, RAD23B and centrin2 [32, 33]. XPC constantly probes the DNA [34] and recognizes severe helix distortions caused by the DNA damage in the opposite strand, such as induced by (6-4)PPs, and binds to the undamaged strand [35] (Figure 2). In addition to XPC, a second more lesion-specific sensor exists: the UV radiation – DNA Damage binding protein (UV-DDB) complex. The UV-DDB complex, consisting of the DDB1 and DDB2/XPE proteins, also recognizes the more modest helix-distorting CPDs [7, 36]. DDB2 has high affinity for DNA damage and its binding induces kinking of the DNA, which in turn enables the recruitment of XPC [37-39]. The UV-DDB complex is crucial for the recognition of CPDs, but also enhances the repair of (6-4)PPs [12] (Figure 2).

## DNA Damage recognition in TC-NER

TC-NER is initiated when RNA Polymerase II (RNAP II) stalls on a transcription-blocking DNA lesion (TBL), which is followed by a highly orchestrated maneuver of a complex process involving multiple proteins [7, 40, 41] (Figure 3). Upon RNAP II stalling on a lesion, Cockayne Syndrome protein B (CSB) binding to RNAP II is stabilized [42, 43]. CSB interacts transiently with RNAP II [18]. Recent cryo-EM studies of Rad26, the yeast homolog of CSB, show that it has a has a key-role in the lesion-recognition proces [44]. Mediated by its ATPase activity, Rad26 is capable of translocating RNAP II forward over naturally occurring pause sites or less bulky lesions.

However, Rad26 cannot translocate RNAP II over bulky, transcription-blocking DNA lesions [44]. This prolonged binding of CSB to lesion stalled Pol II is expected to be one of the first steps in the recruitment of other TC-NER proteins [45], such as Cockayne Syndrome A (CSA) (Figure 3) (see below). The binding of CSA is crucial for the recruitment of downstream TC-NER factors, such as xeroderma pigmentosum group A-binding protein (XAB) [45]. In addition, CSA directly interacts with DDB1 to form the E3-ubiquitin ligase complex together with Cullin4A, ROC1/Rbx1 and the COP signalosome [46, 47]. The precise function of

CSA remains unknown, but different findings suggest that the CSA complex might play a role in the ubiquitylation and subsequent degradation of CSB and RNAP II upon UV irradiation [47-49].

UVSSA is the most recently identified TC-NER factor [50-53]. UVSSA consists of 709 amino acids and contains a N-terminal Vps/Hrs/STAM (VHS) and a conserved C-terminal domain of unknown function (DUF) 2043 domain. Both domains have been shown to be required for TC-NER activity [51]. An important role of UVSSA is the recruitment of the de-ubiquitylating enzyme USP7 [50, 52]. Even though this UVSSA-USP7 interaction is reported to suppress the de-ubiquitylation activity of USP7, this interaction is still capable to protect UVSSA from proteasomal degradation [54]. More importantly, the UVSSA-mediated recruitment of USP7 to the TC-NER complex (Figure 3) counteracts the UV-induced ubiquitylation of CSB [55]. Additionally, a role for UVSSA in the ubiquitylation of RNAP II has been suggested, however its exact mechanism remains unknown [51]. Recently it was suggested that UVSSA also plays a crucial role in the recruitment of transcription factor II H (TFIIH), via a direct interaction with P62 [51, 56].
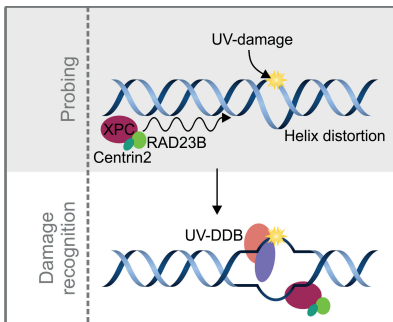


**Figure 2**

**DNA damage recognition during GG-NER.** The complex of XPC, RAD23B and Centrin2 continuously probes the DNA for helix-distorting lesions, such as (6-4)PPs. XPC serves as main initiator of GG-NER, but it has a poor ability to detect mild helix distorting lesions, such as CPDs. The recognition of those mildly destabilizing DNA lesions is accomplished by the UV–DDB complex, which consists of DDB1 and DDB2. Their binding to lesions subsequently stimulates the binding of XPC.

Since lesion-stalled RNAP II covers several nucleotides around the actual DNA lesion [57], the lesion needs to become accessible for repair factors, most likely by RNAP II displacement [55, 58]. To date, three possible mechanisms for RNAP II displacement have been proposed: backtracking, degradation and lesion bypass [59]. RNAP II backtracking is hypothesized to be the preferred pathway to induce TC-NER, such that the polymerase can directly resume transcription as soon as the blocking lesion is removed [41, 60], but thus far this mechanism has only been described in prokaryotes [61]. The lesion bypass and RNAP II degradation

**Figure 3**
**DNA damage recognition in TC-NER.** The DNA lesion is recognized by the stalling of elongating RNAP II. This results in an increased binding of the TC-NER factors CSB, CSA and UVSSA to lesion stalled RNAP II.

pathways, the latter dubbed as the last-resort mechanism [62], are considered to operate infrequently and only under specific conditions [31, 63-65]. Of note, while RNAP II degradation and bypass remove the lesion-stalled RNAP II, TC-NER is not init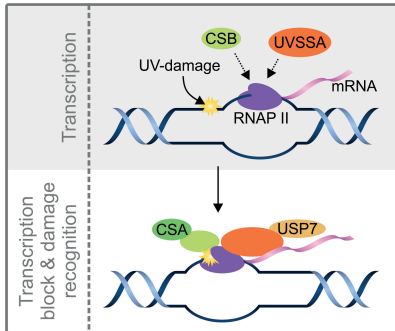iated and the TBL is not repaired. However, in this way unrepaired lesions become accessible for alternative repair pathways, thereby overcoming persistent lesion-stalled RNAP II, as it has been hypothesized that these are highly cytotoxic by triggering p53-dependent apoptosis [66, 67].

**Core NER mechanism**

After damage recognition by either GG-NER or TC-NER, both pathways use the same mechanism to repair the DNA damage by excision followed by gap-filling synthesis and ligation [30]. Firstly, the DNA helix is unwound by the general transcription factor II H (TFIIH) [68]. TFIIH contains 10 subunits, of which the two ATP-dependent helicase subunits Xeroderma Pigmentosum group B (XPB) and Xeroderma Pigmentosum group D (XPD) are responsible for the unwinding of the DNA [69] (Figure 4). Another important role for TFIIH in NER is its damage verification function [70, 71]. Translocation of TFIIH over the damaged strand is blocked by the presence of a lesion and results in the further assembly of the NER pre-incision complex [70, 71]. After unwinding, Xeroderma Pigmentosum group A (XPA), replication protein A (RPA) and Xeroderma Pigmentosum group G (XPG) are recruited [72, 73]. The binding of RPA to the non-damaged strand is assumed to help to position the two structure-specific endonucleases: XPG and the heterodimeric excision-repair cross complementing-1 (ERCC1) and Xeroderma Pigmentosum group F (XPF), on the damaged strand [73, 74]. The dual excision reaction is initiated by the ERCC1-XPF complex 5' of the lesion, followed by XPG, which makes an incision at the 3' site of the lesion [75] (Figure 4). The lesion containing ssDNA stretch is most likely released together with TFIIH and is finally degraded [76.] The last step of the NER reaction involves the recruitment of either DNA Polymerase

δ, ε or κ to the DNA polymerase auxiliary factor PCNA bound to the 3'-OH of the ssDNA gap, which enables the gap-filling DNA repair synthesis [77-79]. The nick in the DNA backbone is finally sealed by DNA ligase I or III [80, 81] (Figure 4).

**Transcription restart after TC-NER**
A crucial step following TC-NER mediated damage removal is the resumption of transcription [59]. It has been shown that especially factors involved in chromatin remodeling play a role in this process [82]. Eleven-nineteen lysine-rich leukemia (ELL) [83], histone regulator A (HIRA) [84]Genetic (Electronic, disruptor of telomeric silencing 1-like (DOT1L) [85] and FACT (facilitates chromatin transcription) [86] have all been identified to be important for transcription restart, for example, by serving as a docking site for proteins regulating transcription (ELL), or by generating transcription favorable chromatin environments (HIRA, DOT1L, FACT). However, a function of these proteins during the TC-NER mediated repair itself cannot be excluded [59, 82], mainly due to the lack of easy to use tools to assay specifically TC-NER activity.

**Clinical consequences of inherited NER-defect**
The biological relevance of NER is highlighted by the severe phenotypes of patients with autosomal recessive mutations in NER genes. These mutations cause different rare UV-hypersensitive NER syndromes, resulting in a wide variety of phenotypes, ranging from normal development with extreme cancer-predisposition to neurodevelopmental defects and premature aging, but without cancer predisposition [12].

## Xeroderma Pigmentosum
Xeroderma pigmentosum (XP) is characterized by severe photosensitivity, dry parchment-like skin, pigmentation abnormalities and a more than 1000-fold increased risk of cancer in sun-exposed areas of the skin [87]. The incidence rate of internal tumors is also increased in some XP cases [88]. XP arises from a deficiency to perform GG-NER [89, 90], leading to damage accumulation across the genome, thereby impinging replication fidelity leading to mutations and a concomitant increase in cancer incidence [9, 12].

## Cockayne Syndrome
Cockayne syndrome (CS) is classified as a progressive neurodevelopmental and premature aging disorder [55, 91]. To date, more than 180 cases of CS have been reported and patients show the following characteristics: microcephaly, mental retardation, progressive sensorineural deafness, cachexia and
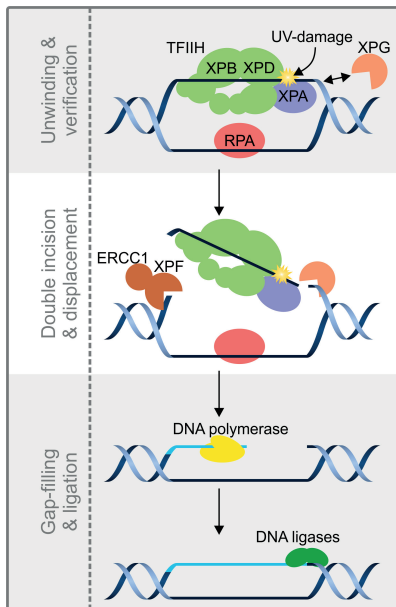
**Unwinding & verification**

TFIIH
UV-damage
XPG
XPB XPD
XPA
RPA

**Double incision & displacement**

ERCC1 XPF

**Gap-filling & ligation**

DNA polymerase

DNA ligases

**Figure 4**
**The core NER reaction.** After the recognition of DNA damage by GG-NER or TC-NER, the TFIIH complex is recruited to the lesion. XPG then binds to the pre-incision NER complex. The double helix is opened around the lesion by the helicase activity of TFIIH. After verification of the DNA damage by the TFIIH subunits XPD and XPB, the recruitment of XPA, binding to single-stranded, chemically altered nucleotides, and RPA, which binds to the undamaged strand, is induced. Subsequently, XPA recruits the XPF–ERCC1 heterodimer, which incises the DNA at the 5' of the lesion. XPG subsequently incises 3' of the DNA lesion, resulting in an about 30 nucleotide long excised DNA patch, containing the DNA lesion. DNA Polymerase δ, κ or ε are responsible for the gap-filling. DNA repair is completed after the DNA ligases seal the nick.

photosensitivity [91-93]. CS patients have a life expectancy of approximately 12 years. Mutations in CSA, CSB, or specific mutations in XPB, XPD or XPG were identified as causative for the development of CS [92, 94, 95]. The absence of TC-NER sensitizes to UV-light and oxidative damage inducing agents, such as hydrogen peroxide [96] or potassium bromate [97]. Persistent TBLs cause cellular dysfunction, senescence and apoptosis, eventually resulting in DNA damage-induced aging. Of note, in contrast to XP patients, TC-NER deficiency as in CS patients, does not lead to a high cancer incidence rate [98].

## UV-Sensitivity Syndrome

UV-sensitive syndrome (UV$^S$S) patients display cutaneous hypersensitivity to sunlight, demonstrated by acute sunburns and mild freckling [99, 100]. UV$^S$S patients are, just like CS patients, characterized by the inability to recover RNA synthesis after TBLs without affecting GG-NER [50, 99], which led to the conclusion that UV$^S$S is caused by a defect in TC-NER [40]. Although DNA lesions that stall RNAP II cannot be removed in cells originating from both UV$^S$S or CS patients, UV$^S$S patients strikingly lack the severe symptoms associated with CS [99, 100]. *UVSSA* was identified as the UV$^S$S causing gene in group A of UV$^S$S patients [50-53]. In addition to mutations in *UVSSA*, also specific mutations in *CSA* [101] or *CSB* [102] can cause UV$^S$S.

### The disparity of UV$^S$S and CS

Detailed insight into the precise molecular function of each of the TC-NER factors and their mechanism is required to unravel the striking phenotypic differences between CS and UV$^S$S [12, 99, 103, 104]. Thus far, several, not mutually exclusive, hypotheses have been proposed to explain those phenotypic differences. One such hypothesis is that the CSA and CSB proteins, in contrast to UVSSA, have additional functions beyond TC-NER. For example, CS proteins were implicated in specific transcriptional programs [105], transcription initiation [106], redox balance [107], repair of double strand breaks [108, 109] and maintenance of mitochondrial DNA stability [110, 111], while thus far no such roles for UVSSA were described. The difference between CS and UV$^S$S might also be based on the inability of CS cells to remodel or degrade lesion stalled RNAP II [12, 51, 112], which might still happen in UV$^S$S cells. In addition, it was suggested that the additional CS features may be derived from a defect in the repair of (endogenously produced) oxidative DNA damage interfering with transcription [9, 31], based on data that specifically CS cells but not UV$^S$S cells are sensitive to oxidative DNA damage [31]. Indeed, increasing evidence points to a role of CSB in the repair of oxidative damage and its involvement in BER. For example, repair intermediates of the glycosylase reaction during BER can stall elongating RNAP II and might activate TC-NER [113-115]. Furthermore, CSB has been shown to interact with proteins of the BER pathway (OGG1 [116, 117], PARP-1 [118] and APE1 [119]). More direct evidence for the involvement of CSB in BER has been shown recently, by demonstrating the recruitment of CSB to oxidative damage in a transcription dependent manner [120, 121] (Chapter 5). However, recent studies suggest that also UVSSA is involved in the repair of oxidative lesions, as shown by sensitive repair assays [122] and its recruitment on oxidative lesions (Chapter 4). Further research is needed to explain the striking differences between the CS and the UV$^S$S syndrome and to give additional mechanistic insights in the complex and highly regulated TC-NER reaction.

## Scope of this thesis

Many aspects of TC-NER have been described since the discovery of this versatile DNA damage repair pathway three decades ago [123]. However, many crucial questions regarding its exact molecular mechanism and the manner in which it deals with different types of lesions remain unanswered [31]. With the research presented in this thesis we aimed to further contribute to the understanding of TC-NER mechanisms.

To further unravel the TC-NER mechanism, sensitive techniques that can specifically measure TC-NER activity would be of great value. In **Chapter 2** the development of a new, single-cell assay that can quantify TC-NER activity is described. This immunofluorescence-based method allows the direct measurement of TC-NER activity in an user-friendly manner. Furthermore, this sensitive assay not only enables the measurements of TC-NER and GG-NER activity on low, physiological relevant, UV-C doses (2 J/m$^2$), but also allows detection and quantification of the activity of other excision repair pathways.

Thus far, the exact mechanism how UVSSA is recruited to the TC-NER complex remains elusive. Therefore, we studied the accumulation of UVSSA on UV-C induced DNA damage in **Chapter 3**. Using live cell microscopy, we showed that UVSSA is recruited to DNA damage in a CSA and CSB independent manner. We further showed, using specific UVSSA deletion mutants that the DUF2043 domain is important for its recruitment to UV-induced DNA damage. To identify factors involved in the recruitment of UVSSA to DNA damage, a quantitative mass spectrometry approach was used to reveal proteins that specifically interact with the DUF2043 domain. With this approach we identified the FACT subunit Spt16 as a novel UVSSA interactor and follow-up studies indicated that Spt16 is involved in the recruitment of UVSSA to sites of DNA damage.

As UVSSA is hypothesised to be involved in the response to both UV and oxidative induced DNA damage, in **Chapter 4** we used quantitative interaction proteomics to identify UVSSA interactions that were specifically induced following UV-C or $H_2O_2$ induced DNA damage. In this chapter we describe the damage-specific UVSSA interaction partners, discuss their potential roles and propose that UVSSA might have different functions following UV or oxidative DNA damage.

In **Chapter 5,** the function of the TC-NER factor CSB during the repair of oxidative damage was analysed. Live cell imaging studies indicated that the recruitment of XRCC1 to oxidative lesions is dependent on functional CSB and active transcription, whereas recruitment of the BER-initiating glycosylase OGG1 does not require transcription or CSB. Based on our data we propose a model in which CSB facilitates XRCC1 recruitment to RNA polymerase II complexes stalled at BER-intermediates. These results further establish the importance of CSB in BER.

In **Chapter 6** we discuss the main findings of the experimental work described in this thesis and provide future directions to study the role and molecular function of TC-NER factors in the repair of different types of DNA damage.

# References

1.  Lindahl, T., *Instability and decay of the primary structure of DNA.* Nature, 1993. **362**(6422): p. 709-15.
2.  Swenberg, J.A., et al., *Endogenous versus exogenous DNA adducts: their role in carcinogenesis, epidemiology, and risk assessment.* Toxicol Sci, 2011. **120 Suppl 1**: p. S130-45.
3.  Hoeijmakers, J.H., *Genome maintenance mechanisms for preventing cancer.* Nature, 2001. **411**(6835): p. 366-74.
4.  Giglia-Mari, G., A. Zotter, and W. Vermeulen, *DNA damage response.* Cold Spring Harb Perspect Biol, 2011. **3**(1): p. a000745.
5.  Ravanat, J.L., T. Douki, and J. Cadet, *Direct and indirect effects of UV radiation on DNA and its components.* J Photochem Photobiol B, 2001. **63**(1-3): p. 88-102.
6.  Gillet, L.C. and O.D. Scharer, *Molecular mechanisms of mammalian global genome nucleotide excision repair.* Chem Rev, 2006. **106**(2): p. 253-76.
7.  Nouspikel, T., *DNA repair in mammalian cells : Nucleotide excision repair: variations on versatility.* Cell Mol Life Sci, 2009. **66**(6): p. 994-1009.
8.  Cadet, J., E. Sage, and T. Douki, *Ultraviolet radiation-mediated damage to cellular DNA.* Mutat Res, 2005. **571**(1-2): p. 3-17.
9.  Hoeijmakers, J.H., *DNA damage, aging, and cancer.* N Engl J Med, 2009. **361**(15): p. 1475-85.
10. Gates, K.S., *An overview of chemical processes that damage cellular DNA: spontaneous hydrolysis, alkylation, and reactions with radicals.* Chem Res Toxicol, 2009. **22**(11): p. 1747-60.
11. Jackson, S.P. and J. Bartek, *The DNA-damage response in human biology and disease.* Nature, 2009. **461**(7267): p. 1071-8.
12. Marteijn, J.A., et al., *Understanding nucleotide excision repair and its roles in cancer and ageing.* Nat Rev Mol Cell Biol, 2014. **15**(7): p. 465-81.
13. Kunkel, T.A. and D.A. Erie, *DNA mismatch repair.* Annu Rev Biochem, 2005. **74**: p. 681-710.
14. Sharma, M., et al., *Differential mismatch recognition specificities of eukaryotic MutS homologs, MutSalpha and MutSbeta.* Biophys J, 2014. **106**(11): p. 2483-92.
15. Chatterjee, N. and G.C. Walker, *Mechanisms of DNA damage, repair, and mutagenesis.* Environ Mol Mutagen, 2017. **58**(5): p. 235-263.
16. Richman, S., *Deficient mismatch repair: Read all about it (Review).* Int J Oncol, 2015. **47**(4): p. 1189-202.
17. Tiwari, A.K., H.K. Roy, and H.T. Lynch, *Lynch syndrome in the 21st century: clinical perspectives.* QJM, 2016. **109**(3): p. 151-8.
18. Evans, M.D., M. Dizdaroglu, and M.S. Cooke, *Oxidative DNA damage and disease: induction, repair and significance.* Mutat Res, 2004. **567**(1): p. 1-61.
19. Parsons, J.L. and G.L. Dianov, *Co-ordination of base excision repair and genome stability.* DNA Repair (Amst), 2013. **12**(5): p. 326-33.
20. Krokan, H.E. and M. Bjoras, *Base excision repair.* Cold Spring Harb Perspect Biol, 2013. **5**(4): p. a012583.
21. Dianov, G.L. and U. Hubscher, *Mammalian base excision repair: the forgotten archangel.* Nucleic Acids Res, 2013. **41**(6): p. 3483-90.
22. Hegde, M.L., T.K. Hazra, and S. Mitra, *Early steps in the DNA base excision/single-strand interruption repair pathway in mammalian cells.* Cell Res, 2008. **18**(1): p. 27-47.
23. Khodyreva, S.N., et al., *Apurinic/apyrimidinic (AP) site recognition by the 5'-dRP/AP lyase in poly(ADP-ribose) polymerase-1 (PARP-1).* Proc Natl Acad Sci U S A, 2010. **107**(51): p. 22090-5.
24. Herceg, Z. and Z.Q. Wang, *Functions of poly(ADP-ribose) polymerase (PARP) in DNA repair, genomic integrity and cell death.* Mutat Res, 2001. **477**(1-2): p. 97-110.
25. Jeppesen, D.K., V.A. Bohr, and T. Stevnsner, *DNA repair deficiency in neurodegeneration.* Prog Neurobiol, 2011. **94**(2): p. 166-200.
26. Wallace, S.S., D.L. Murphy, and J.B. Sweasy, *Base excision repair and cancer.* Cancer Lett, 2012. **327**(1-2): p. 73-89.
27. Wallace, S.S., *Base excision repair: a critical player in many games.* DNA Repair (Amst), 2014. **19**: p.

14-26.

28.  Starcevic, D., S. Dalal, and J.B. Sweasy, *Is there a link between DNA polymerase beta and cancer?* Cell Cycle, 2004. **3**(8): p. 998-1001.

29.  Nemec, A.A., et al., *Colon cancer-associated DNA polymerase beta variant induces genomic instability and cellular transformation.* J Biol Chem, 2012. **287**(28): p. 23840-9.

30.  Scharer, O.D., *Nucleotide excision repair in eukaryotes.* Cold Spring Harb Perspect Biol, 2013. **5**(10): p. a012609.

31.  Hanawalt, P.C. and G. Spivak, *Transcription-coupled DNA repair: two decades of progress and surprises.* Nat Rev Mol Cell Biol, 2008. **9**(12): p. 958-70.

32.  Araki, M., et al., *Centrosome protein centrin 2/caltractin 1 is part of the xeroderma pigmentosum group C complex that initiates global genome nucleotide excision repair.* J Biol Chem, 2001. **276**(22): p. 18665-72.

33.  Sugasawa, K., et al., *Xeroderma pigmentosum group C protein complex is the initiator of global genome nucleotide excision repair.* Mol Cell, 1998. **2**(2): p. 223-32.

34.  Hoogstraten, D., et al., *Versatile DNA damage detection by the global genome nucleotide excision repair protein XPC.* J Cell Sci, 2008. **121**(Pt 17): p. 2850-9.

35.  Min, J.H. and N.P. Pavletich, *Recognition of DNA damage by the Rad4 nucleotide excision repair protein.* Nature, 2007. **449**(7162): p. 570-5.

36.  Kim, J.K., D. Patel, and B.S. Choi, *Contrasting structural impacts induced by cis-syn cyclobutane dimer and (6-4) adduct in DNA duplex decamers: implication in mutagenesis and repair activity.* Photochem Photobiol, 1995. **62**(1): p. 44-50.

37.  Payne, A. and G. Chu, *Xeroderma pigmentosum group E binding factor recognizes a broad spectrum of DNA damage.* Mutat Res, 1994. **310**(1): p. 89-102.

38.  Tang, J. and G. Chu, *Xeroderma pigmentosum complementation group E and UV-damaged DNA-binding protein.* DNA Repair (Amst), 2002. **1**(8): p. 601-16.

39.  Wakasugi, M., et al., *DDB accumulates at DNA damage sites immediately after UV irradiation and directly stimulates nucleotide excision repair.* J Biol Chem, 2002. **277**(3): p. 1637-40.

40.  Spivak, G., et al., *Ultraviolet-sensitive syndrome cells are defective in transcription-coupled repair of cyclobutane pyrimidine dimers.* DNA Repair (Amst), 2002. **1**(8): p. 629-43.

41.  Spivak, G., *Transcription-coupled repair: an update.* Arch Toxicol, 2016. **90**(11): p. 2583-2594.

42.  Selby, C.P. and A. Sancar, *Human transcription-repair coupling factor CSB/ERCC6 is a DNA-stimulated ATPase but is not a helicase and does not disrupt the ternary transcription complex of stalled RNA polymerase II.* J Biol Chem, 1997. **272**(3): p. 1885-90.

43.  van den Boom, V., et al., *DNA damage stabilizes interaction of CSB with the transcription elongation machinery.* J Cell Biol, 2004. **166**(1): p. 27-36.

44.  Xu, J., et al., *Structural basis for the initiation of eukaryotic transcription-coupled DNA repair.* Nature, 2017. **551**(7682): p. 653-657.

45.  Fousteri, M., et al., *Cockayne syndrome A and B proteins differentially regulate recruitment of chromatin remodeling and repair factors to stalled RNA polymerase II in vivo.* Mol Cell, 2006. **23**(4): p. 471-82.

46.  Groisman, R., et al., *The ubiquitin ligase activity in the DDB2 and CSA complexes is differentially regulated by the COP9 signalosome in response to DNA damage.* Cell, 2003. **113**(3): p. 357-67.

47.  Fischer, E.S., et al., *The molecular basis of CRL4DDB2/CSA ubiquitin ligase architecture, targeting, and activation.* Cell, 2011. **147**(5): p. 1024-39.

48.  Groisman, R., et al., *CSA-dependent degradation of CSB by the ubiquitin-proteasome pathway establishes a link between complementation factors of the Cockayne syndrome.* Genes Dev, 2006. **20**(11): p. 1429-34.

49.  Saijo, M., *The role of Cockayne syndrome group A (CSA) protein in transcription-coupled nucleotide excision repair.* Mech Ageing Dev, 2013. **134**(5-6): p. 196-201.

50.  Schwertman, P., et al., *UV-sensitive syndrome protein UVSSA recruits USP7 to regulate transcription-coupled repair.* Nat Genet, 2012. **44**(5): p. 598-602.

51.  Nakazawa, Y., et al., *Mutations in UVSSA cause UV-sensitive syndrome and impair RNA polymerase IIo processing in transcription-coupled nucleotide-excision repair.* Nat Genet, 2012. **44**(5): p. 586-92.

52.  Zhang, X., et al., *Mutations in UVSSA cause UV-sensitive syndrome and destabilize ERCC6 in*

*transcription-coupled DNA repair.* Nat Genet, 2012. **44**(5): p. 593-7.

53. Fei, J. and J. Chen, *KIAA1530 protein is recruited by Cockayne syndrome complementation group protein A (CSA) to participate in transcription-coupled repair (TCR).* J Biol Chem, 2012. **287**(42): p. 35118-26.

54. Higa, M., et al., *Stabilization of Ultraviolet (UV)-stimulated Scaffold Protein A by Interaction with Ubiquitin-specific Peptidase 7 Is Essential for Transcription-coupled Nucleotide Excision Repair.* J Biol Chem, 2016. **291**(26): p. 13771-9.

55. Vermeulen, W. and M. Fousteri, *Mammalian transcription-coupled excision repair.* Cold Spring Harb Perspect Biol, 2013. **5**(8): p. a012625.

56. Okuda, M., et al.

57. Brueckner, F., et al., *CPD damage recognition by transcribing RNA polymerase II.* Science, 2007. **315**(5813): p. 859-62.

58. Tornaletti, S., D. Reines, and P.C. Hanawalt, *Structural characterization of RNA polymerase II complexes arrested by a cyclobutane pyrimidine dimer in the transcribed strand of template DNA.* J Biol Chem, 1999. **274**(34): p. 24124-30.

59. Steurer, B. and J.A. Marteijn, *Traveling Rocky Roads: The Consequences of Transcription-Blocking DNA Lesions on RNA Polymerase II.* J Mol Biol, 2016.

60. Wang, W., et al., *Structural basis of transcriptional stalling and bypass of abasic DNA lesion by RNA polymerase II.* Proc Natl Acad Sci U S A, 2018. **115**(11): p. E2538-e2545.

61. Epshtein, V., et al., *UvrD facilitates DNA repair by pulling RNA polymerase backwards.* Nature, 2014. **505**(7483): p. 372-7.

62. Wilson, M.D., M. Harreman, and J.Q. Svejstrup, *Ubiquitylation and degradation of elongating RNA polymerase II: the last resort.* Biochim Biophys Acta, 2013. **1829**(1): p. 151-7.

63. Somesh, B.P., et al., *Multiple mechanisms confining RNA polymerase II ubiquitylation to polymerases undergoing transcriptional arrest.* Cell, 2005. **121**(6): p. 913-23.

64. Somesh, B.P., et al., *Communication between distant sites in RNA polymerase II through ubiquitylation factors and the polymerase CTD.* Cell, 2007. **129**(1): p. 57-68.

65. Walmacq, C., et al., *Mechanism of translesion transcription by RNA polymerase II and its role in cellular resistance to DNA damage.* Mol Cell, 2012. **46**(1): p. 18-29.

66. Ljungman, M. and F. Zhang, *Blockage of RNA polymerase as a possible trigger for u.v. light-induced apoptosis.* Oncogene, 1996. **13**(4): p. 823-31.

67. Yamaizumi, M. and T. Sugano, *U.v.-induced nuclear accumulation of p53 is evoked through DNA damage of actively transcribed genes independent of the cell cycle.* Oncogene, 1994. **9**(10): p. 2775-84.

68. Tapias, A., et al., *Ordered conformational changes in damaged DNA induced by nucleotide excision repair factors.* J Biol Chem, 2004. **279**(18): p. 19074-83.

69. Compe, E. and J.M. Egly, *TFIIH: when transcription met DNA repair.* Nat Rev Mol Cell Biol, 2012. **13**(6): p. 343-54.

70. Sugasawa, K., et al., *Two-step recognition of DNA damage for mammalian nucleotide excision repair: Directional binding of the XPC complex and DNA strand scanning.* Mol Cell, 2009. **36**(4): p. 642-53.

71. Li, C.L., et al., *Tripartite DNA Lesion Recognition and Verification by XPC, TFIIH, and XPA in Nucleotide Excision Repair.* Mol Cell, 2015. **59**(6): p. 1025-34.

72. Volker, M., et al., *Sequential assembly of the nucleotide excision repair factors in vivo.* Mol Cell, 2001. **8**(1): p. 213-24.

73. Rademakers, S., et al., *Xeroderma pigmentosum group A protein loads as a separate factor onto DNA lesions.* Mol Cell Biol, 2003. **23**(16): p. 5755-67.

74. de Laat, W.L., et al., *DNA-binding polarity of human replication protein A positions nucleases in nucleotide excision repair.* Genes Dev, 1998. **12**(16): p. 2598-609.

75. Staresincic, L., et al., *Coordination of dual incision and repair synthesis in human nucleotide excision repair.* EMBO J, 2009. **28**(8): p. 1111-20.

76. Kemp, M.G., et al., *Mechanism of release and fate of excised oligonucleotides during nucleotide excision repair.* J Biol Chem, 2012. **287**(27): p. 22889-99.

77. Shivji, M.K., et al., *Nucleotide excision repair DNA synthesis by DNA polymerase epsilon in the presence of PCNA, RFC, and RPA.* Biochemistry, 1995. **34**(15): p. 5011-7.

78. Araujo, S.J., et al., *Nucleotide excision repair of DNA with recombinant human proteins: definition of the minimal set of factors, active forms of TFIIH, and modulation by CAK.* Genes Dev, 2000. **14**(3): p. 349-59.

79. Lehmann, A.R., *DNA polymerases and repair synthesis in NER in human cells.* DNA Repair (Amst), 2011. **10**(7): p. 730-3.

80. Moser, J., et al., *Sealing of chromosomal DNA nicks during nucleotide excision repair requires XRCC1 and DNA ligase III alpha in a cell-cycle-specific manner.* Mol Cell, 2007. **27**(2): p. 311-23.

81. Nocentini, S., *Rejoining kinetics of DNA single- and double-strand breaks in normal and DNA ligase-deficient cells after exposure to ultraviolet C and gamma radiation: an evaluation of ligating activities involved in different DNA repair processes.* Radiat Res, 1999. **151**(4): p. 423-32.

82. Mandemaker, I.K., W. Vermeulen, and J.A. Marteijn, *Gearing up chromatin: A role for chromatin remodeling during the transcriptional restart upon DNA damage.* Nucleus, 2014. **5**(3): p. 203-10.

83. Mourgues, S., et al., *ELL, a novel TFIIH partner, is involved in transcription restart after DNA repair.* Proc Natl Acad Sci U S A, 2013. **110**(44): p. 17927-32.

84. Adam, S., S.E. Polo, and G. Almouzni, *Transcription recovery after DNA damage requires chromatin priming by the H3.3 histone chaperone HIRA.* Cell, 2013. **155**(1): p. 94-106.

85. Oksenych, V., et al., *Histone methyltransferase DOT1L drives recovery of gene expression after a genotoxic attack.* PLoS Genet, 2013. **9**(7): p. e1003611.

86. Dinant, C., et al., *Enhanced chromatin dynamics by FACT promotes transcriptional restart after UV-induced DNA damage.* Mol Cell, 2013. **51**(4): p. 469-79.

87. Black, J.O., *Xeroderma Pigmentosum.* Head Neck Pathol, 2016. **10**(2): p. 139-44.

88. Kraemer, K.H., et al., *Xeroderma pigmentosum, trichothiodystrophy and Cockayne syndrome: a complex genotype-phenotype relationship.* Neuroscience, 2007. **145**(4): p. 1388-96.

89. Cleaver, J.E., *Defective repair replication of DNA in xeroderma pigmentosum.* Nature, 1968. **218**(5142): p. 652-6.

90. Setlow, R.B., et al., *Evidence that xeroderma pigmentosum cells do not perform the first step in the repair of ultraviolet damage to their DNA.* Proc Natl Acad Sci U S A, 1969. **64**(3): p. 1035-41.

91. Karikkineth, A.C., et al., *Cockayne syndrome: Clinical features, model systems and pathways.* Ageing Res Rev, 2017. **33**: p. 3-17.

92. Laugel, V., *Cockayne syndrome: the expanding clinical and mutational spectrum.* Mech Ageing Dev, 2013. **134**(5-6): p. 161-70.

93. Wilson, B.T., et al., *The Cockayne Syndrome Natural History (CoSyNH) study: clinical findings in 102 individuals and recommendations for care.* Genet Med, 2016. **18**(5): p. 483-93.

94. Laugel, V., et al., *Mutation update for the CSB/ERCC6 and CSA/ERCC8 genes involved in Cockayne syndrome.* Hum Mutat, 2010. **31**(2): p. 113-26.

95. Cleaver, J.E., E.T. Lam, and I. Revet, *Disorders of nucleotide excision repair: the genetic and molecular basis of heterogeneity.* Nat Rev Genet, 2009. **10**(11): p. 756-68.

96. Spivak, G. and P.C. Hanawalt, *Host cell reactivation of plasmids containing oxidative DNA lesions is defective in Cockayne syndrome but normal in UV-sensitive syndrome fibroblasts.* DNA Repair (Amst), 2006. **5**(1): p. 13-22.

97. Ropolo, M., et al., *Complementation of the oxidatively damaged DNA repair defect in Cockayne syndrome A and B cells by Escherichia coli formamidopyrimidine DNA glycosylase.* Free Radic Biol Med, 2007. **42**(12): p. 1807-17.

98. Lehmann, A.R., *DNA repair-deficient diseases, xeroderma pigmentosum, Cockayne syndrome and trichothiodystrophy.* Biochimie, 2003. **85**(11): p. 1101-11.

99. Spivak, G., *UV-sensitive syndrome.* Mutat Res, 2005. **577**(1-2): p. 162-9.

100. Itoh, T., T. Ono, and M. Yamaizumi, *A new UV-sensitive syndrome not belonging to any complementation groups of xeroderma pigmentosum or Cockayne syndrome: siblings showing biochemical characteristics of Cockayne syndrome without typical clinical manifestations.* Mutation Research/DNA Repair, 1994. **314**(3): p. 233-248.

101. Nardo, T., et al., *A UV-sensitive syndrome patient with a specific CSA mutation reveals separable roles for CSA in response to UV and oxidative DNA damage.* Proc Natl Acad Sci U S A, 2009. **106**(15): p. 6209-14.

102. Horibata, K., et al., *Complete absence of Cockayne syndrome group B gene product gives rise to UV-sensitive syndrome but not Cockayne syndrome.* Proc Natl Acad Sci U S A, 2004. **101**(43): p. 15410-5.

103. Cleaver, J.E., *Photosensitivity syndrome brings to light a new transcription-coupled DNA repair cofactor.* Nat Genet, 2012. **44**(5): p. 477-8.
104. Sarasin, A., *UVSSA and USP7: new players regulating transcription-coupled nucleotide excision repair in human cells.* Genome Med, 2012. **4**(5): p. 44.
105. Wang, Y., et al., *Dysregulation of gene expression as a cause of Cockayne syndrome neurological disease.* Proc Natl Acad Sci U S A, 2014. **111**(40): p. 14454-9.
106. Proietti-De-Santis, L., P. Drane, and J.M. Egly, *Cockayne syndrome B protein regulates the transcriptional program after UV irradiation.* EMBO J, 2006. **25**(9): p. 1915-23.
107. Pascucci, B., et al., *An altered redox balance mediates the hypersensitivity of Cockayne syndrome primary fibroblasts to oxidative stress.* Aging Cell, 2012. **11**(3): p. 520-9.
108. Sakai, A., et al., *PARP and CSB modulate the processing of transcription-mediated DNA strand breaks.* Genes Genet Syst, 2012. **87**(4): p. 265-72.
109. Batenburg, N.L., et al., *Cockayne syndrome group B protein regulates DNA double-strand break repair and checkpoint activation.* EMBO J, 2015. **34**(10): p. 1399-416.
110. Aamann, M.D., et al., *Cockayne syndrome group B protein promotes mitochondrial DNA stability by supporting the DNA repair association with the mitochondrial membrane.* FASEB J, 2010. **24**(7): p. 2334-46.
111. Kamenisch, Y., et al., *Proteins of nucleotide and base excision repair pathways interact in mitochondria to protect from loss of subcutaneous fat, a hallmark of aging.* J Exp Med, 2010. **207**(2): p. 379-90.
112. Schwertman, P., W. Vermeulen, and J.A. Marteijn, *UVSSA and USP7, a new couple in transcription-coupled DNA repair.* Chromosoma, 2013. **122**(4): p. 275-84.

113. Kathe, S.D., G.P. Shen, and S.S. Wallace, *Single-stranded breaks in DNA but not oxidative DNA base damages block transcriptional elongation by RNA polymerase II in HeLa cell nuclear extracts.* J Biol Chem, 2004. **279**(18): p. 18511-20.
114. Khobta, A., et al., *8-Oxoguanine DNA glycosylase (Ogg1) causes a transcriptional inactivation of damaged DNA in the absence of functional Cockayne syndrome B (Csb) protein.* DNA Repair (Amst), 2009. **8**(3): p. 309-17.
115. Kitsera, N., et al., *8-Oxo-7,8-dihydroguanine in DNA does not constitute a barrier to transcription, but is converted into transcription-blocking damage by OGG1.* Nucleic Acids Res, 2011. **39**(14): p. 5926-34.
116. Stevnsner, T., et al., *Mitochondrial repair of 8-oxoguanine is deficient in Cockayne syndrome group B.* Oncogene, 2002. **21**(57): p. 8675-82.
117. Tuo, J., et al., *Functional crosstalk between hOgg1 and the helicase domain of Cockayne syndrome group B protein.* DNA Repair (Amst), 2002. **1**(11): p. 913-27.
118. Thorslund, T., et al., *Cooperation of the Cockayne syndrome group B protein and poly(ADP-ribose) polymerase 1 in the response to oxidative stress.* Mol Cell Biol, 2005. **25**(17): p. 7625-36.
119. Wong, H.K., et al., *Cockayne syndrome B protein stimulates apurinic endonuclease 1 activity and protects against agents that introduce base excision repair intermediates.* Nucleic Acids Res, 2007. **35**(12): p. 4103-13.
120. Menoni, H., J.H. Hoeijmakers, and W. Vermeulen, *Nucleotide excision repair-initiating proteins bind to oxidative DNA lesions in vivo.* J Cell Biol, 2012. **199**(7): p. 1037-46.
121. Iyama, T. and D.M. Wilson, 3rd, *Elements That Regulate the DNA Damage Response of Proteins Defective in Cockayne Syndrome.* J Mol Biol, 2016. **428**(1): p. 62-78.
122. Guo, J., P.C. Hanawalt, and G. Spivak, *Comet-FISH with strand-specific probes reveals transcription-coupled repair of 8-oxoGuanine in human cells.* Nucleic Acids Res, 2013. **41**(16): p. 7700-12.
123. Bohr, V.A., et al., *DNA repair in an active gene: removal of pyrimidine dimers from the DHFR gene of CHO cells is much more efficient than in the genome overall.* Cell, 1985. **40**(2): p. 359-69.

**1**

# Chapter 2

## Amplification of unscheduled DNA synthesis signal enables fluorescence-based single cell quantification of transcription-coupled nucleotide excision repair

Franziska Wienholz[1], Wim Vermeulen[1], Jurgen A. Marteijn[1*]

[1] Department of Molecular Genetics, Cancer Genomics Netherlands Erasmus MC, Wytemaweg 80, Rotterdam 3015 CN, The Netherlands

## Abstract

Nucleotide excision repair (NER) comprises two damage recognition pathways: global genome NER (GG-NER) and transcription-coupled NER (TC-NER), which remove a wide variety of helix-distorting lesions including UV-induced damage. During NER, a short stretch of single-stranded DNA containing damage is excised and the resulting gap is filled by DNA synthesis in a process called unscheduled DNA synthesis (UDS). UDS is measured by quantifying the incorporation of nucleotide analogues into repair patches to provide a measure of NER activity. However, this assay is unable to quantitatively determine TC-NER activity due to the low contribution of TC-NER to the overall NER activity. Therefore, we developed a user-friendly, fluorescence-based single-cell assay to measure TC-NER activity. We combined the UDS assay with tyramide-based signal amplification to greatly increase the UDS signal, thereby allowing UDS to be quantified at low UV doses, as well as DNA-repair synthesis of other excision-based repair mechanisms such as base excision repair and mismatch repair. Importantly, we demonstrated that the amplified UDS is sufficiently sensitive to quantify TC-NER-derived repair synthesis in GG-NER-deficient cells. This assay is important as a diagnostic tool for NER-related disorders and as a research tool for obtaining new insights into the mechanism and regulation of excision repair.

## Introduction

The integrity of DNA is threatened constantly by endogenous and exogenous DNA damaging agents, such as reactive oxygen species and ultraviolet light (UV), which severely affect DNA replication, transcription, and cell cycle progression. If they are not repaired correctly these DNA lesions may lead to cell death or mutagenesis, which can eventually result in accelerated aging or malignant transformation. Various DNA repair mechanisms have evolved to maintain genomic integrity, which each repair a subset of DNA lesions [1]. Several key repair systems remove single-stranded DNA damage via the excision of nucleotides, including nucleotide excision repair (NER) [2], base excision repair (BER) [3], and mismatch repair (MMR) [4], and use the non-damaged DNA strand as a template for gap-filling DNA synthesis [1].

NER recognizes and repairs a wide spectrum of helix-distorting DNA lesions such as those induced by UV light from the sun [5]. NER is characterized by two distinct mechanisms for damage recognition. Global genome NER (GG-NER) recognizes DNA lesions throughout the genome via the joint action of the damage sensors XPC and UV-DDB [6]. Transcription-coupled NER (TC-NER) specifically recognizes DNA lesions in actively transcribed strands. Lesion-stalled RNA polymerase 2 is recognized by the proteins CSB, CSA, and UVSSA to initiate the TC-NER pathway [7,8]. The damage recognition events in both NER pathways are followed by a shared pathway where excision of the damaged DNA is followed by gap-filling DNA synthesis, thereby completing the NER reaction [2,5].

NER deficits are linked to genetic disorders, which range from mild UV-sensitivity, to severe premature aging, or an extreme predisposition to cancer [5,9,10]. Xeroderma Pigmentosum (XP), manifested by photosensitivity and a highly increased incidence of cancer, results mainly from GG-NER deficiency, e.g., caused by mutations in XPC [9,11,12]. However, although the TC-NER linked syndromes Cockayne syndrome (CS) and UV-sensitivity syndrome (UV^SS) are characterized by a failure to restart transcription following transcription blocking damage, the phenotypes of patients vary dramatically. CS is caused by inactivating mutations in the *CSB* or *CSA* genes, which lead to severe developmental, neurological, and premature aging features [11,12]. By contrast, UV^SS caused by *UVSSA* mutations or specific mutations in *CSA* or *CSB* only has mild features, thus far solely restricted to UV-sensitivity by the skin [13]. A precise molecular mechanism that explains the divergent phenotypes of these TC-NER syndromes is still required [5,14].

Analyzing cells derived from NER-deficient patients has been crucial for the identification of most NER-related genes and they have provided important mechanistic insights into the NER reaction. NER-deficient syndromes are characterized by deficient DNA repair, which is used as an important diagnostic marker. The excision of an approximately 30 nucleotide-long patch surrounding the DNA damage is a unique property of NER, and thus the subsequent gap-filling DNA synthesis, referred to as unscheduled DNA synthesis (UDS), provides a direct measure of the damage excision and repair efficacy [15,16]. The ability to measure UDS is of great importance for diagnostic identification and classification, but it can also provide a crucial quantitative research tool for assessing the NER capacity, thereby obtaining new insights into the NER pathway and its regulation [17]. NER-derived UDS is usually monitored by measuring the incorporation of traceable nucleotide analogs after UV irradiation. Originally, pulse labeling with radioactive thymidine ($^3$H-thymidine) after UV and subsequent autoradiography was used to measure UDS [15,16]. However, pulse labeling with the thymidine analogue 5-ethynyl-2-deoxyuridine (EdU) and subsequent visualization via conjugation to a fluorescent azide has been used more often recently due to its simplicity, increased sensitivity and higher dynamic range [18,19]. GG-NER is responsible for approximately 90% of the total repair executed by NER, so the UDS signal mainly represents the GG-NER activity [18] (Fig. 1A). The remaining ~10% of TC-NER-derived UDS, which is close to the background signal levels, appears to be difficult to determine quantitatively, particularly at physiologically relevant UV doses (Fig. 1A) [18,20]. In agreement, TC-NER-deficient cells derived from CS patients are highly UV-sensitive but they have almost normal UDS levels, in contrast to cells derived from GG-NER-deficient patients, which exhibit greatly reduced and difficult to quantify UV-induced gap-filling synthesis. Hence, other techniques are currently used to measure TC-NER activity, such as strand-specific repair or recovery of RNA synthesis (RRS) for UV-induced transcription inhibition. Strand-specific repair measures the removal of cyclobutane pyrimidine dimers (CPDs), one of the most common UV-induced DNA lesions, in the transcribed strand of a specific gene by using T4 endonuclease V to incise DNA at a CPD [21]. The more sensitive comet-FISH assay uses a similar approach based on fluorescent strand-specific probes combined with single-cell gel electrophoresis to quantify TC-NER repair rates [22]. Both assays measure repair itself, but they are highly laborious and only yield information about the repair rate of the gene tested and not the average of all the transcribed genes. Therefore, TC-NER deficiency is routinely assessed using RRS, also for diagnostic purposes. The RRS assay quantifies the restart of transcription after the repair of DNA

damage is completed thereby resolving lesion-induced transcription inhibition, which indicates the completion of TC-NER [19]. However, the exact mechanism and timing of the restart of transcription following TC-NER remains unclear [23,24]. Using the RRS assay, newly synthesized RNA is visualized by pulse labeling with 5-bromouridine (BrU) or 5-ethynyluridine (EU), which is incorporated into nascent RNA [19,25]. However, this assay does not provide a direct measure of repair and it cannot discriminate between factors that are specifically involved in repair or in the restart of transcription. The ability to measure TC-NER mediated repair directly is very important because several factors have been described recently, such as HIRA (26), DOT1L [27], Spt16 [28], and ELL [20], that can uncouple TC-NER mediated repair from transcriptional restart [23,24].

To measure the TC-NER repair activity, we developed a user-friendly, highly sensitive single-cell assay. For this purpose, we amplified the EdU-mediated UDS assay in GG-NER-deficient cells by using a tyramide-based signal amplification (TSA) procedure. The TSA procedure is a widely used technique for enhancing immunofluorescence signals [29,30] with an HRP-based detection method. Briefly, using Click-chemistry, biotin-azides are coupled to EdU that are incorporated as a consequence of NER-derived DNA synthesis. Subsequently, HRP-streptadivin is bound to the biotin-azide and the oxidation of fluorescent-labeled tyramide by HRP in the presence of hydrogen peroxide generates short-lived fluorescent-labeled tyramide radicals, which are covalently coupled to local nucleophilic residues such as protein tyrosine residues [31] (Fig.1B).

The proposed amplified UDS method for obtaining sensitive measurements of excision-based DNA repair obtained a 60-fold increase in the signal compared with conventional UDS protocols. This signal amplification method allowed us to detect UDS induced by low physiologically relevant UV-C doses, but more importantly, it also allowed us to quantify DNA repair derived only from TC-NER in XPC-deficient cells. Interestingly, the DNA repair synthesis induced by oxidative and alkylating agents can also be measured using this amplified UDS method.

# Materials and methods

## Cell culture

Human hTert immortalized NER proficient VH10 fibroblasts, GG-NER deficient XP-C-fibroblasts XP186LV, XP3MA and XP20MA, NER deficient XP-A (XP25RO) and TC-NER deficient CS-B fibroblasts (CS1AN) were cultured in Ham's F10 medium (Lonza) supplemented with 15% fetal calf serum (Biowest) and 1% penicillin-streptomycin (Sigma-Aldrich) at 37°C with 5% $CO_2$ in a humidified incubator. All NER deficient cells were characterized either by complementation studies or by mutation analysis [32,33]. For transcription inhibition, cells were pretreated either with 25 μg/ml α-amanitin (Sigma-Aldrich) for 16 h or 100 μM 5,6-dichloro-1-β-D-ribofuranosylbenzimidazole (DRB, Calbiochem) for 1 h before DNA damage infliction. For inhibiting DNA polymerase ß, pamoic acid (PA, Sigma-Aldrich) dissolved in 200 mM NaCl and 20 mM Tris-HCl (pH 7) was added to the cells in a final concentration of 500 μM 16h before the experiment was started. Fresh PA was added during EdU labeling.

## DNA Damage induction

Prior to DNA damage induction, cells were washed with PBS. For global or local UV-C exposure a 254 nm germicidal lamp (Philips) was used to irradiate cells with indicated UV-C doses. Local UV irradiation was induced using isopore membranes (Millipore) with 5 μm pores [34]. Hydrogen peroxide solution (500 μM) (Sigma-Aldrich) was added freshly each hour during the 3h EdU labeling, 100 μM 1-Methly-3-nitro-1-nitroguanidine (MNNG, Tokyo Chemical Industry CO., LTD) was added to culture medium at the same moment it was started with EdU labeling for 3 h.

## EdU incorporation

Cells were cultured on 24-mm cover slips and were serum starved (0.5% fetal calf serum) for 2 days to accumulate cells in G0 phase (approx. 98%). After damage induction, cells were directly labeled with EdU for 3 h (wt cells) or 7 h (GG-NER deficient cells) using Ham's F10 supplemented with 0.5% dialyzed fetal calf serum containing 20 μM 5-ethynyl-2′-deoxyuridine (EdU, ThermoFisher Scientific). 2′-Deoxy-5-fluorouridine (1 μM) (Floxuridine, Sigma-Aldrich) was added to inhibit the thymidylate synthase to prevent the generation of endogenous thymidine. After Edu labeling, medium was changed to Ham's F10 supplemented with 0.5% dialyzed fetal calf serum containing 10 μM thymidine (Sigma-Aldrich) for 15 min to deplete unincorporated EdU in the cell. Cells were fixed by incubation with 3.6% formaldehyde (Sigma-Aldrich) in PBS

with 0.5% Triton X-100 (Sigma-Aldrich) for 15 min at room temperature. After permeabilization in 0.5% Triton for 20 min, cells were blocked with 3% BSA (Sigma-Aldrich) in PBS.

## Fluorescent-based UDS assay with incorporation of EdU

The procedure of the UDS assay was performed as described previously [19,35]. Incorporated EdU was visualized using Click-chemistry based coupling of Alexa-Fluor 488 nm azide (ThermoFisher Scientific) according to the manufactures protocol. In short, after fixation, cells were permeabilized for 20 min with 0.5% triton X-100 in PBS at room temperature and subsequently washed twice with 3% BSA in PBS. The Click-it reaction was performed by incubating cells for 30 min at room temperature with 100 µl Click-it reaction Cocktail, containing 1x Click-it reaction buffer (ThermoFisher Scientific), Copper(III)sulphate (0.1 M), Alexa Fluor 488 Azide (Click-iT EdU Imaging Kit by ThermoFisher Scientific) and 10x Reaction buffer additive (ThermoFisher Scientific). After washing the cells twice in 3% BSA in PBS and twice in PBS, cells were mounted using Vectashield (Vector Laboratories) with DAPI to stain DNA and cover slips were sealed using nail polish.

## Amplified UDS assay

After blocking, endogenous peroxidases were quenched to reduce non-specific activation of tyramide using 3% hydrogen peroxide solution (Sigma-Aldrich) in PBS for 1 h. Subsequently, DNA was denatured using freshly prepared 0.07 M NaOH in PBS for 5 min at room temperature, after which samples were incubated with PBS containing 0.5% BSA and 0.15% Glycine for 1 h. The Click-it reaction was performed using 100 µl of the Click it reaction cocktail containing Azide-PEG3-Biotin Conjugate (20 µM in DMSO, Jena Bioscience), 1x Click-it reaction buffer (ThermoFisher Scientific), Copper(III)sulphate (0.1 M), and 10x Reaction buffer additive (ThermoFisher Scientific). Subsequently, for tyramide-based amplification, samples were incubated with 100 µl HRP-Streptavidin conjugate (500 µg/ml) in 1% BSA for 1 h. Subsequently, samples were incubated for 10 min at room temperature with 100 µl amplification buffer containing 0.0015% $H_2O_2$ and 1:100 dilution of Alexa-Fluor 488 nm labeled tyramide, which was dissolved in 150 µl DMSO (ThermoFisher Scientific). The addition of 0.0015% $H_2O_2$ is required for the HRP-mediated oxidation and consecutive activation of tyramide. After each incubation step, samples were washed three times with PBS. Finally, samples were rinsed twice in PBS containing 0.5% BSA and 0.15% Glycine, then three times shortly and two times for 10 min with 0.1% Triton X-100 in PBS. If an additional CPD staining was needed, cover slips were incubated

with anti-CPD antibody (1:1,000; TDM-2 clone; COSMO BIO CO, LTD) for 1 h at room temperature. After washing five times with 0.1% triton X-100, of which the last 2 were washed for 10 min, and once with PBS containing 0.15% glycine and 0.5% BSA, cover slips were incubated for 1 h with the antibody donkey anti mouse Alexa-Fluor 594 nm (ThermoFisher Scientific). After washing the cover slips with 0.1% Triton X-100 in PBS, cover slips were embedded in DAPI containing Vectashield mounting medium (VectorLaboratories) and sealed using nail polish.

## Western blotting

For Immunoblotting, cells lysed in 100 µl 2x Laemmli sample buffer were boiled for 5 min prior to protein size-fractionation by SDS–PAGE and subsequent electro-transfer to a PVDF membrane (0.45 µm) as described [35]. Membranes were blocked in 3% BSA in PBS for 1 h at room temperature and after washing 3 times with PBS containing 0.05% Tween the membranes were subsequently incubated with primary antibodies against CSB (E-18, sc-10459, Santa Cruz Biotechnology, Inc.) and Tubulin (B512, Sigma-Aldrich) that were used in combination with Alexa-Fluor 795 donkey anti-goat (SAB4600375, Sigma-Aldrich) or Alexa-Fluor 795 goat anti-mouse (SAB4600214, Sigma-Aldrich) respectively. Western blots were analyzed and quantified using the Odyssey CLx Infrared Imaging System (LI-COR Biosciences).

## RNA interference

siRNA was transfected using RNAiMax (ThermoFisher Scientific) 2 days before the experiment according to manufacturer's protocol. siRNAs used in this study were purchased from Thermo Scientific Dharmacon. CTRL: siGENOME Non_ Targeting siRNA#5 5'- UGGUUUACAUGUCGACUAA -3' (D-001210-05), CSB: ON-Target plus Human ERCC6 (CSB) A) 5'- GCAUGUGUCUUACGAGAUA -3' (J-004888-10), B) 5'- CAAACAGAGUUGUCAUCUA -3' (J-004888-09)).

## Image acquisition

Images were obtained using a LSM700 microscope equipped with a 40x oil Plan-Apochromat 40 0.6-1.3 numerical aperture (NA) oil immersion lens (Carl Zeiss Micro imaging Inc.). The ImageJ software (Version 1.48) [36] was used for quantification purposes and to identify cell nuclei using the DAPI staining in combination with the particle analysis tool. An average signal outside nuclei was determined for each field and was used for background correction. At least 10 fields for each condition were measured. S-phase cells were identified by the very strong and distinct S-phase specific patterns of the 488 nm fluorescent

signal and were excluded from the analysis. All experiments were conducted twice and data points of the two independent experiments were pooled, unless stated otherwise. The background corrected total Alexa 488 nm fluorescence signal (nuclear fluorescence) in the nucleus was determined of each cell. The mean nuclear fluorescence is the average of the relative nuclear fluorescence of all cells measured across the independent experiments. The standard error of the mean was calculated using n = the total number of cells across the independent experiments as indicated in the figure legends. All figures show the mean nuclear fluorescence signal ± standard error of the mean. Statistical analysis was performed by a two-way analysis of variance (ANOVA) and the multiple post hoc Bonferroni-corrected t tests to compare differences between the various treatments. In all cases, a level of 5% was considered statistically significant (p < 0.05).

# Results

## Tyramide-based signal amplification combined with conventional UDS

Previously, UDS was not sufficiently sensitive to quantify TC-NER-derived gap filling synthesis (Fig.1A). To overcome this technical limitation, we combined TSA with the Click-chemistry-based UDS protocol (Fig. 1B) [19]. Tyramide can be activated nonspecifically by endogenous peroxidases, thereby yielding nonspecific fluorescent signals throughout the cell. This nonspecific tyramide activation was inhibited successfully by quenching the activity of endogenous peroxidases with 3% hydrogen peroxide (Supplementary Fig. 1A). The addition of 3% hydrogen peroxide after cell fixation did not induce DNA damage-induced DNA synthesis (Supplementary Fig. 1B). Furthermore, when the amplified-UDS signal was quantified after treatment with NaOH (0.07 M for 5 min), which is required for staining DNA damage with α-CPD antibodies, a pronounced increase in the amplified UDS signal was observed (Supplementary Fig. 1C). Therefore, all of the amplified UDS experiments were executed with successive hydrogen peroxide and NaOH incubation steps. A flowchart illustrating the different steps in the amplified UDS assay is shown in Supplementary Fig. 1D.

To quantify the amplification levels of the tyramide-based signal amplification, we compared the standard UDS signal with the amplified UDS signal in NER-proficient cells after irradiation with 10 J/m² UV-C. We measured enhanced amplification of the UDS signal by at least 60-fold (Fig. 1C), which agreed with

the previously described 30-fold amplification of the signal obtained by the TSA procedure [31]. However, the actual signal amplification levels might have been underestimated due to limitations on the dynamic range of the photomultiplier employed. The signals measured in non-irradiated samples probably represented background signals because similar signal levels were obtained when essential components of the TSA or Click-chemistry-based UDS reaction were excluded (Fig. 1D). In contrast to the UV-induced samples, the background signal detected in non-irradiated samples was amplified by less than threefold using the TSA procedure (Supplementary Fig. 1E). Overall, these results indicate that the UDS signal can be amplified specifically by the tyramide-based amplification.

## Quantitative measurements of NER at low UV-C doses

Next, we tested the UV doses at which the amplified UDS assay procedure could be used in a quantitative manner to measure gap-filling DNA synthesis. A dose-dependent amplified UDS signal was observed for UV-C doses up to 10 J/$m^2$, after which the signal plateaued (Fig. 2A). This leveling off might have been caused by a limitation imposed by the tyramide concentration at greater UV doses because higher UDS signals were observed as the tyramide concentration increased (Supplementary Fig. 1E). More importantly, these results suggest that this amplification procedure can detect UDS at low physiologically relevant UV doses. Indeed, the amplified UDS signal obtained with UV-C doses ranging from 0.5–6 J/$m^2$ exhibited a quantitative dose-dependent relationship (Fig. 2B), thereby indicating that this amplified UDS procedure is capable of detecting gap-filling synthesis at UV-C doses as low as 1 J/$m^2$ in a reproducible manner. This amplified UDS assay is also suitable for detecting UDS signals at sites of UV-induced DNA damage in a sub-nuclear region (local UV damage) in a dose-dependent manner (Fig. 2C). The detection of local UV damage using α-CPD staining indicates that the amplified UDS procedure is compatible with immunofluorescence procedures. It should be noted that at a relatively low dose of 10 J/$m^2$, a distinct UDS signal was observed with a concomitant barely visible CPD-derived signal, which clearly illustrates the sensitivity of this amplification procedure.

## TC-NER can be measured quantitatively by the amplified UDS assay

The greatly increased sensitivity of the amplified UDS procedure might facilitate the detection of TC-NER-mediated DNA repair synthesis using this assay. To test this, we employed noncycling XP-C cells, which are defective for GG-NER. In these XP-C cells, the complete NER activity, and thus gap-filling DNA synthesis, can be assigned specifically to TC-NER [2,5]. Using the amplified UDS
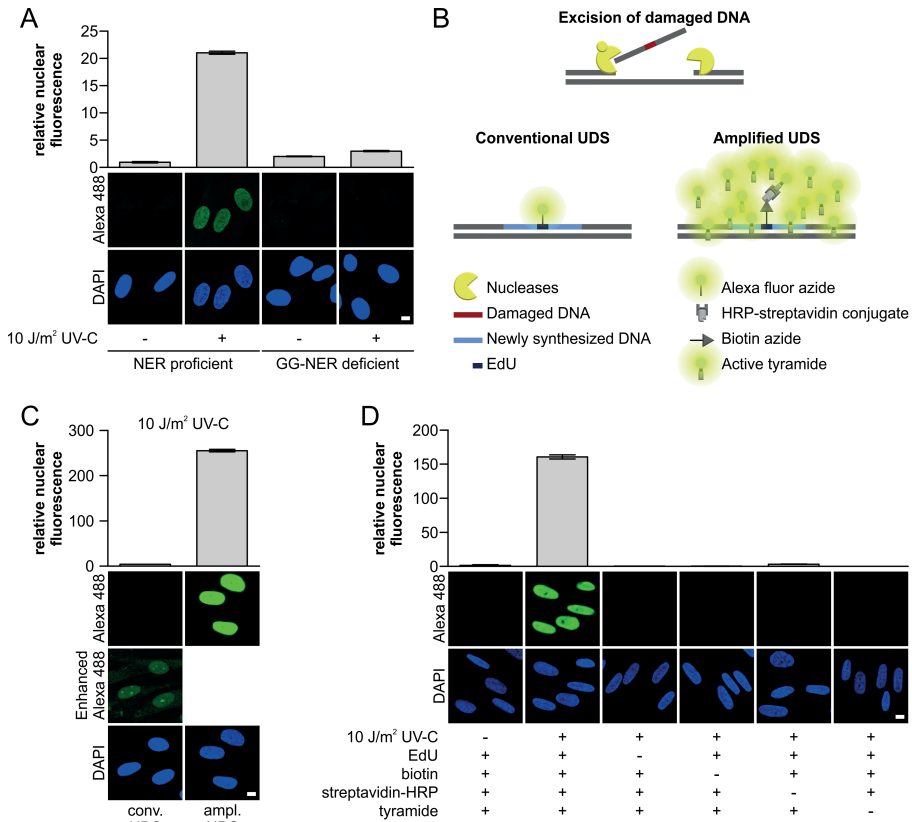
**Figure 1**

**TSA-mediated amplification of UDS signals. (A)** VH10 (NER-proficient) or XP186LV (XPC-deficient) cells grown on cover slips were irradiated with UV-C (10 J/m$^2$) or mock-treated as indicated, and subsequently labeled for 3 h with EdU. The UDS signal (n>300 cells per condition, three independent experiments) was quantified (upper panel) by confocal microscopy measurement of the total nuclear fluorescence (Alexa-Fluor 488 nm) and expressed as relative nuclear fluorescence. Representative images are shown (lower panel). Gap-filling synthesis measured by EdU-based UDS without signal amplification was only observed in GG-NER-proficient cells (VH10), whereas no TC-NER specific signal could be measured in XP-C cells (XP186LV). **(B)** Schematic overview of the different labeling approaches used by conventional and amplified UDS. The key difference is the number of fluorophores per incorporated nucleotide, where one fluorophore binds to one incorporated EdU in conventional UDS, multiple fluorophores can be bound in the proximity of 1 EdU in the amplified UDS, which is mediated by HRP activation of tyramide-labeled Alexa 488. **(C)** VH10 cells grown on a coverslip were UV-irradiated (10 J/m$^2$) or left untreated (Supplementary Fig. 1E), and subsequently labeled for 3 h with EdU. UV-induced gap-filling synthesis was measured by conventional or amplified UDS (tyramide-based signal amplification). UDS signals were quantified based on the total signal intensity of Alexa-Fluor 488 nm per nucleus. Comparing the amplified UDS assay with the conventional UDS indicated amplification of the UDS signal by >60 times (n>380 cells per condition, two independent experiments). Representative images are shown (lower panel). To visualize the UDS signal in the conventional UDS assay, the fluorescent signal was digitally amplified for the image labeled as "Enhanced Alexa 488". **(D)** Quantification of the amplified UDS signal in VH10 cells (n>250 cells per condition, two independent experiments) where essential components of the EdU-based Click-it chemistry reaction and TSA amplification were omitted as indicated by (-). Representative images are shown (lower panel). Nuclei were visualized using the DNA marker DAPI. SEM is shown. Scale bar: 10 μm
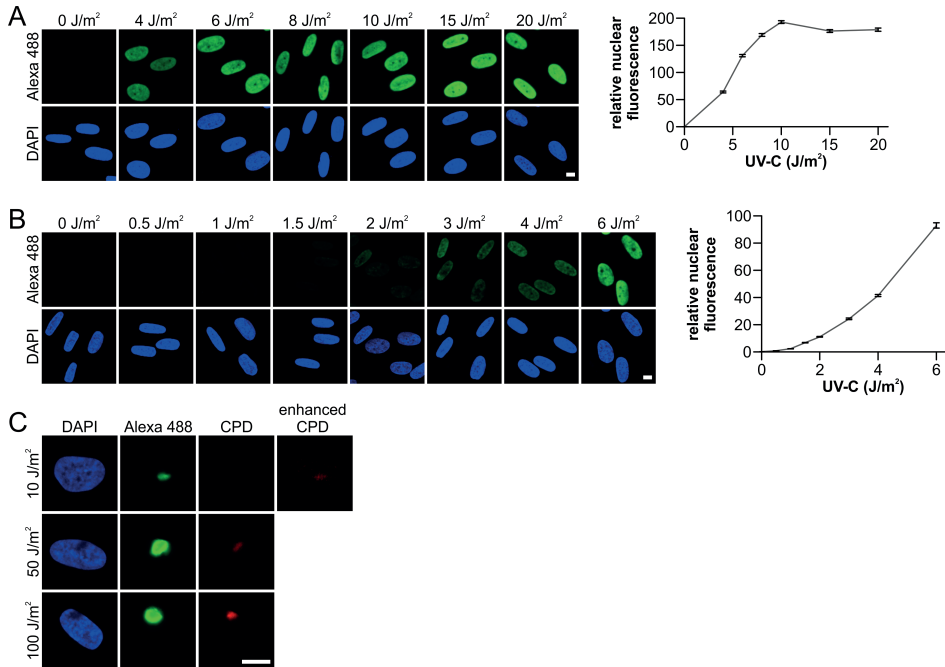
**Figure 2**

**Amplified UDS assay facilitates quantitative measurement of NER. (A)** and **(B)** Representative images (left) and quantification (right) of amplified UDS signals, as measured by fluorescence (Alexa-Fluor 488 nm, relative total signal intensity per nucleus) in VH10 cells (n>340 cells per data point, two independent experiments) irradiated with the indicated UV-C dose and labeled for 3 h with EdU. **(C)** Representative images of the amplified UDS assay in cells irradiated locally with the indicated UV-C doses and subsequently labeled for 3 h with EdU. Sub-nuclear UV-damaged regions were identified by antibody staining for cyclobutane pyrimidine dimers (CPDs). To visualize the CPD signal in samples irradiated with 10 J/m² UV-C, the fluorescent signal was digitally amplified using the image labeled as "enhanced CPD". Nuclei were visualized using the DNA marker DAPI. SEM is shown. Scale bar: 10 μm

procedure, we detected a clear UV-induced and TC-NER-derived UDS signal in XPC-deficient cells (Fig. 3A). The specificity of the TC-NER-dependent amplified UDS signal was demonstrated by the omission of essential components of the amplified UDS assay, which resulted in the complete absence of the signal (Supplementary Fig. 2A). Importantly, we also performed this assay in the presence of transcription inhibitors to confirm that the detected UDS signal was indeed attributable to TC-NER-mediated repair of the transcribed DNA strand. Following treatment with α-amanitin (an RNA polymerase II inhibitor, 16 h) or DRB (a CDK9 inhibitor, 1 h) [37] prior to UV-C-induced DNA damage, the UDS signals were comparable to those from non-irradiated samples (Fig. 3A), indicating that the amplified UDS signal was completely dependent on active transcription. In addition, siRNA-mediated knockdown of the essential TC-NER

protein CSB using two different siRNAs (Supplementary Fig. 2B), showed that the UV-induced gap filling synthesis measured in these XPC-deficient cells was dependent on active TC-NER (Fig. 3B).

In order to exclude cell-type specific effects, we irradiated different XP-C patient cell lines with UV-C and obtained comparable amplified UDS signals in the cell lines using the amplified UDS procedure (Fig. 3C). As expected, those signals were reduced to background signal levels when cells were irradiated in the presence of the transcription inhibitor α-amanitin, and when we used XP-A cells deficient in both GG-NER and TC-NER (Fig. 3C and Supplementary Fig. 2C).

Moreover, TC-NER-mediated repair could be measured by the amplified UDS procedure in a dose-dependent manner below 6 J/m² UV-C (Fig. 3D). Furthermore, we detected dose-dependent TC-NER-induced gap-filling synthesis at ³10 J/m² after local UV-C damage induction (Fig. 3E). As expected, this local amplified UDS signal was lost completely when prior to DNA damage infliction transcription was inhibited by α-amanitin. These results clearly indicate that tyramide-based UDS amplification in GG-NER-deficient cells is a highly sensitive quantitative assay for measuring TC-NER at the single-cell level.

## DNA repair induced by various types of damage can be detected using the amplified UDS method

In addition to NER, base-excision repair (BER) and mismatch repair (MMR) are DNA repair pathways based on the excision of damaged DNA fragments. The great increase in the sensitivity of the amplified UDS assay prompted us to test whether excision repair initiated by BER and MMR could also be detected. After inducing damage with oxidative (hydrogen peroxide, 500 μM) or alkylating (MNNG, 100 μM) agents, we could detect amplified UDS signals (Fig. 4A), thereby suggesting that the induced damage was removed by excision repair. BER is known to be involved in the repair of oxidized DNA bases [38]. During BER, a damaged base is removed by specific glycosylases to create apurinic/apyrimidinic (AP) sites, which are incised by AP-endonuclease. The resulting 5-deoxyribose phosphate (dRP) is removed by DNA polymerase β, which also catalyzes DNA synthesis to fill the single nucleotide gap [39]. To verify that we could actually measure BER-mediated DNA synthesis using the amplified UDS assay, we added a DNA polymerase β inhibitor (pamoic acid, PA) [40,41]. The amplified UDS signals in samples treated with $H_2O_2$ were decreased greatly after PA treatment (Fig. 4B), thereby indicating that the majority of the UDS signal after $H_2O_2$ treatment was indeed dependent on BER. Interestingly, it is
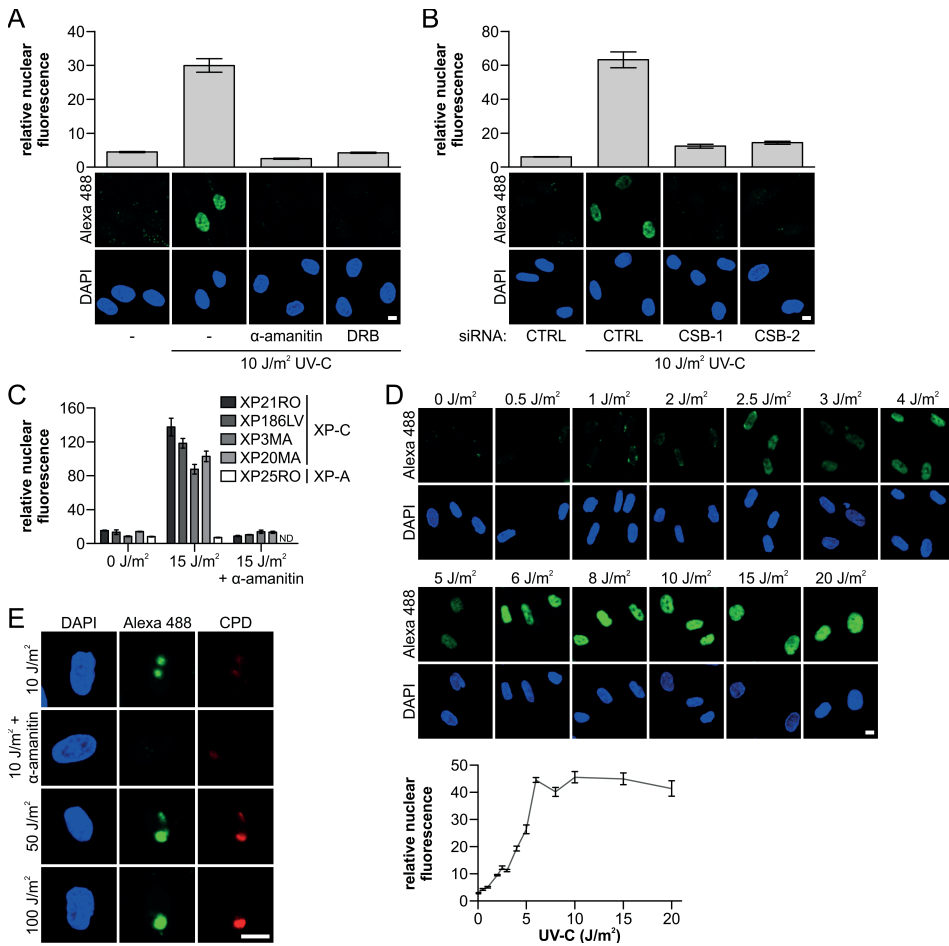
**Figure 3**

**Gap-filling activity of TC-NER can be measured quantitatively with amplified UDS. (A)** GG-NER-deficient XP186LV (XP-C) cells were treated with transcription inhibitors (α-amanitin: 25 μg/ml; 16 h before UV-C treatment, DRB: 100 μM; 1 h before UV-C treatment) or mock treated; or **(B)** transfected with non-targeting control siRNA (CTRL) and two independent siRNAs that targeting CSB (CSB-1 and -2), as indicated. Cells were labeled directly with EdU for 7 h after irradiation with UV-C (10 J/m$^2$), as indicated. **(A and B)** Amplified UDS signals were quantified (upper panel) by measuring the total nuclear fluorescence (Alexa-Fluor 488 nm, n>80 cells for each condition, two independent experiments) and representative images (lower panel) are shown. **(C)** Quantification of the amplified UDS signal measured by the total nuclear Alexa-Fluor 488 nm fluorescence in the indicated XP-C cells (n > 50 cells per condition). The TC-NER specificity of the signal was shown by the loss of signal after transcription inhibition with α-amanitin (25 μg/ml, added 16 h prior to EdU labeling for 7 h) or when amplified UDS signals were measured in an NER-deficient XP-A cell line (XP25RO). ND indicates not determined. Representative images are shown in Supplementary Fig. 2C. **(D)** Representative images (upper panel) of XP-C (XP186LV) cells (n>170 cells per condition, two independent experiments) irradiated with indicated UV-C doses. Amplified UDS signals were quantified (lower panel) based on total nuclear fluorescence (Alexa-Fluor 488 nm) after EdU labeling for 7 h and they exhibit dose-dependent UDS signals. **(E)** Representative images of XPC-deficient XP186LV cells where UV-C damage was induced locally with the indicated UV-C doses. Transcription was inhibited by 25 μg/ml α-amanitin at 16 h prior to UV-C damage and during labeling with EdU for 7 h. Sub-nuclear UV-exposed regions were identified by α-CPD staining. Nuclei were identified by DAPI staining. SEM is shown. Scale bar: 10 μM
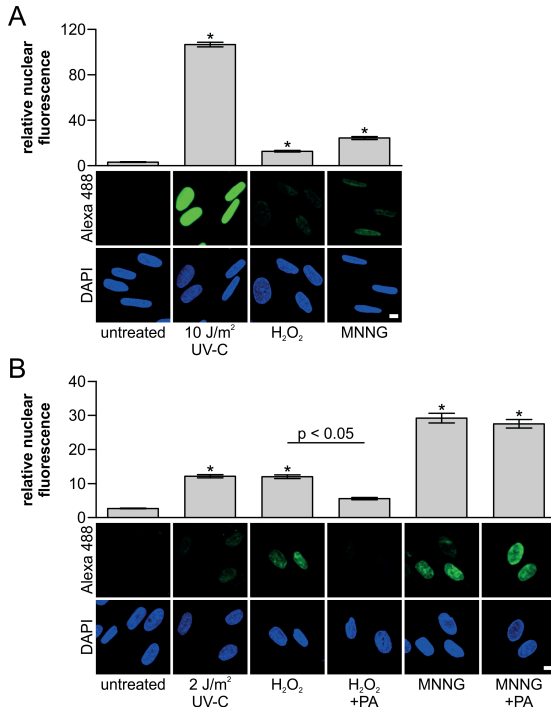
**Figure 4**

**Amplified UDS enables the measurement of excision repair. (A and B)** Representative images of the amplified UDS assay (lower panel) and quantification (upper panel) of VH10 cells (n>420 cell per condition, two independent experiments) after DNA damage. **(A)** DNA damage was inflicted with UV-C (10 J/m$^2$), H$_2$O$_2$ (500 µM), or MNNG (100 µM), or cells were mock-treated, before EdU labeling for 3 h (n>420 cells per condition, two independent experiments). **(B)** DNA damage was inflicted with UV-C (2 J/m$^2$), H$_2$O$_2$ (500 µM), or MNNG (100 µM), or cells were mock-treated, before EdU labeling for 3 h (n>180 cells per condition, two independent experiments, except for 2 J/m$^2$: one experiment, n=81 cells). At 16 h prior to and during EdU labeling, 500 µM pamoic Acid (PA, a DNA polymerase β inhibitor) was added to samples treated with H$_2$O$_2$ or MNNG, as indicated. Nuclei were identified by DAPI staining. SEM is shown, * indicates $p < 0.05$ compared with untreated samples. Scale bar: 10 µM

**2**

assumed that the DNA damage induced by MNNG is a target for BER [42], but the amplified UDS signal measured after DNA damage induction by MNNG could not be decreased using PA (Fig. 4B). This indicates that the UDS signal due to alkylated DNA damage induced by MNNG was probably caused by the activity of MMR in these noncycling cells [43,44]. Previously, MNNG-induced UDS was also observed using the classical 3H-TdR procedure [45], but quantifying the UDS signal is much more laborious and less reproducible with this approach. Overall, these results show that combining the tyramide signal amplification procedure with the UDS assay greatly increases its sensitivity and allows quantification of repair by TC-NER and other excision repair pathways in a user-friendly, single-cell assay.

# Discussion

For about four decades, UV-induced UDS has been employed successfully for monitoring the cellular NER activity using radio-labeled thymidine followed by autoradiography [15,17]. This procedure provides sensitive and reproducible information regarding NER performance, but the dependence on non-user-friendly tritiated thymidine and the fact that the assay is laborious and requires long autoradiographic exposure times, means that its application was limited to only a few laboratories worldwide. The recent replacement of radioactive labeled thymidine with EdU, which can be labeled using simple *in situ* Click-chemistry with azide-coupled fluorescent dyes of choice, makes the assay much more accessible, faster, and easier to quantify using fluorescence microscopy [19,46]. In the present study, we developed an amplified UDS assay by combining the EdU-based UDS assay with a tyramide signal amplification. This combination resulted in a signal amplification by at least 60-fold-specific signal amplification. This facilitates a more easy visualization and quantification of NER-mediated repair at more relevant, low physiological UV doses (1 J/m$^2$). Previously, conventional fluorescent UDS was generally performed with UV-C doses ranging from 16 J/m$^2$ [28] to 20 J/m$^2$ [18,46]. The use of much lower UV doses might be crucial for identifying the more subtle effects of novel regulators of the NER reaction based on its repair activity, which can only be identified at more physiologically relevant UV doses. Furthermore, the amplified UDS assay allows us to measure the gap-filling synthesis induced by DNA-damaging agents such as hydrogen peroxide and MNNG. The UDS signals measured after exposure to these genotoxic agents, which are not recognized by NER, are probably attributable to the excision activity of BER [47] or MMR [44], respectively. This indicates that the amplified UDS assay can be employed to measure the repair activity of excision-based DNA repair pathways, for which no user-friendly cellular gap-filling synthesis assays are available at this moment.

Importantly, the amplified UDS method can be applied as a quantitative, single-cell assay to measure the TC-NER-induced repair activity at relatively low doses using GG-NER-deficient cells. The induced signal is TC-NER-specific because the detected UV-induced repair signal is dependent completely on the crucial TC-NER protein CSB and active transcription. Interestingly, we observed a leveling off of the TC-NER-induced amplified UDS signal for UV-C doses above 6 J/m$^2$ (Fig. 3D). It is unlikely that this was caused by limitations of compounds used in either the tyramide-based signal amplification or Click-it chemistry because in GG-NER proficient cells, which have much higher UDS levels, the signal could be

measured quantitatively for UV-doses up to 10 J/m$^2$ before the signal plateaued (Fig. 2A). The plateauing of the amplified UDS signal for TC-NER suggests that a maximum number of lesions can be processed by TC-NER within the given time of a UDS experiment. Further research should be conducted to understand the underlying mechanism involved. Together this shows that the amplified UDS assay can obtain important new molecular, mechanistic, and/or kinetic information about TC-NER.

Our TC-NER assay based on the amplified UDS method has several key advantages compared with other TC-NER assays. Strand-specific repair assays [21], including the novel comet-FISH method [22], measure TC-NER-mediated repair by quantifying the specific removal of CPDs from the transcribed strand and by comparing this repair rate with the non-transcribed strand. The disadvantage of these elegantly designed strand-specific repair assays is that they are highly laborious and they can only study repair in one or a few specific gene(s) at a time. However, due to specific transcriptional programs or differences in the chromatin environment, the repair rate of specific genes might not be representative for the overall TC-NER activity [5,48]. By contrast, our amplified UDS-based TC-NER assay determines the average repair activity in all actively transcribed genes in a quantitative manner using single cells. Furthermore, unlike our amplified UDS method, the routinely employed RRS assay provides an indirect measure of the TC-NER dependent repair activity because it only determines the restart of transcription [25]. The exact mechanism of transcription restart after the removal of transcription blocking lesions by TC-NER is currently unknown. However, recent research has shown that several factors are specifically required to restart transcription, although they are not considered to be involved in TC-NER-mediated repair itself, including ELL [20], HIRA [26], Spt16 [28], and DOT1L1 [27]. This indicates that a specific group of proteins might be involved in facilitating transcription recovery after genotoxic stress and that transcription restart is a specific form of transcription that has not been extensively studied [23,24]. Our single cell, fluorescence-based, amplified UDS TC-NER assay can be applied easily to high content screening approaches using genomic libraries (shRNA and sgRNA) to identify factors that are involved directly in TC-NER activity. By comparing amplified UDS data with previously obtained RRS data from TC-NER screening [49], or even simultaneously conducting amplified UDS and RRS assays, it may be possible to discriminate between proteins involved in repair and those involved specifically in the transcription restart process. This approach will be important for understanding the transcription restart process after genotoxic stress.

Furthermore, this user-friendly single-cell assay facilitates quantitative analyses of TC-NER repair capacity, which is crucial for identifying TC-NER mutants, chromatin remodelers, or chemotherapeutics that might affect TC-NER. In conclusion, we describe an important improvement to the conventional UDS assay by using tyramide-based signal amplification, thereby allowing the measurement of GG-NER-mediated gap-filling synthesis at low physiologically relevant UV doses, as well as the detection of TC-NER-mediated repair in a quantitative manner. In addition, we showed that this amplified form of UDS can be used to measure other excision-based DNA repair pathways induced by other types of damage than UV-C [50].

## Funding

*Conflict of interest statement.*
None declared.

## Acknowledgements

# References

1.  Hoeijmakers, J.H. (2001) Genome maintenance mechanisms for preventing cancer. *Nature*, **411**, 366-374.
2.  Scharer, O.D. (2013) Nucleotide excision repair in eukaryotes. *Cold Spring Harb Perspect Biol*, **5**, a012609.
3.  Kim, Y.J. and Wilson, D.M., 3rd. (2012) Overview of base excision repair biochemistry. *Curr Mol Pharmacol*, **5**, 3-13.
4.  Groothuizen, F.S. and Sixma, T.K. (2016) The conserved molecular machinery in DNA mismatch repair enzyme structures. *DNA Repair (Amst)*, **38**, 14-23.
5.  Marteijn, J.A., Lans, H., Vermeulen, W. and Hoeijmakers, J.H. (2014) Understanding nucleotide excision repair and its roles in cancer and ageing. *Nat Rev Mol Cell Biol*, **15**, 465-481.
6.  Gillet, L.C. and Scharer, O.D. (2006) Molecular mechanisms of mammalian global genome nucleotide excision repair. *Chem Rev*, **106**, 253-276.
7.  Vermeulen, W. and Fousteri, M. (2013) Mammalian transcription-coupled excision repair. *Cold Spring Harb Perspect Biol*, **5**, a012625.
8.  Hanawalt, P.C. and Spivak, G. (2008) Transcription-coupled DNA repair: two decades of progress and surprises. *Nat Rev Mol Cell Biol*, **9**, 958-970.
9.  Kraemer, K.H., Patronas, N.J., Schiffmann, R., Brooks, B.P., Tamura, D. and DiGiovanna, J.J. (2007) Xeroderma pigmentosum, trichothiodystrophy and Cockayne syndrome: a complex genotype-phenotype relationship. *Neuroscience*, **145**, 1388-1396.
10. Nouspikel, T. (2009) DNA repair in mammalian cells : Nucleotide excision repair: variations on versatility. *Cell Mol Life Sci*, **66**, 994-1009.
11. de Boer, J. and Hoeijmakers, J.H. (2000) Nucleotide excision repair and human syndromes. *Carcinogenesis*, **21**, 453-460.
12. Lehmann, A.R. (2003) DNA repair-deficient diseases, xeroderma pigmentosum, Cockayne syndrome and trichothiodystrophy. *Biochimie*, **85**, 1101-1111.
13. Spivak, G. (2005) UV-sensitive syndrome. *Mutation Research/Fundamental and Molecular Mechanisms of Mutagenesis*, **577**, 162-169.
14. Schwertman, P., Vermeulen, W. and Marteijn, J.A. (2013) UVSSA and USP7, a new couple in transcription-coupled DNA repair. *Chromosoma*, **122**, 275-284.
15. Cleaver, J.E. (1968) Defective repair replication of DNA in xeroderma pigmentosum. *Nature*, **218**, 652-656.
16. Friedberg, E.C. (2004) The discovery that xeroderma pigmentosum (XP) results from defective nucleotide excision repair. *DNA Repair*, **3**, 183-195.
17. Latimer, J.J. and Kelly, C.M. (2014) Unscheduled DNA synthesis: the clinical and functional assay for global genomic DNA nucleotide excision repair. *Methods Mol Biol*, **1105**, 511-532.
18. Limsirichaikul, S., Niimi, A., Fawcett, H., Lehmann, A., Yamashita, S. and Ogi, T. (2009) A rapid non-radioactive technique for measurement of repair synthesis in primary human fibroblasts by incorporation of ethynyl deoxyuridine (EdU). *Nucleic Acids Res*, **37**, e31.
19. Nakazawa, Y., Yamashita, S., Lehmann, A.R. and Ogi, T. (2010) A semi-automated non-radioactive system for measuring recovery of RNA synthesis and unscheduled DNA synthesis using ethynyluracil derivatives. *DNA Repair*, **9**, 506-516.
20. Mourgues, S., Gautier, V., Lagarou, A., Bordier, C., Mourcet, A., Slingerland, J., Kaddoum, L., Coin, F., Vermeulen, W., Gonzales de Peredo, A. *et al.* (2013) ELL, a novel TFIIH partner, is involved in transcription restart after DNA repair. *Proc Natl Acad Sci U S A*, **110**, 17927-17932.
21. Bohr, V.A., Smith, C.A., Okumoto, D.S. and Hanawalt, P.C. (1985) DNA repair in an active gene: removal of pyrimidine dimers from the DHFR gene of CHO cells is much more efficient than in the genome overall. *Cell*, **40**, 359-369.
22. Guo, J., Hanawalt, P.C. and Spivak, G. (2013) Comet-FISH with strand-specific probes reveals transcription-coupled repair of 8-oxoGuanine in human cells. *Nucleic Acids Res*, **41**, 7700-7712.
23. Mandemaker, I.K., Vermeulen, W. and Marteijn, J.A. (2014) Gearing up chromatin: A role for chromatin remodeling during the transcriptional restart upon DNA damage. *Nucleus (Austin, Tex.)*, **5**, 203-210.

24. Adam, S. and Polo, S.E. (2014) Blurring the line between the DNA damage response and transcription: the importance of chromatin dynamics. *Exp Cell Res*, **329**, 148-153.

25. Mayne, L.V. and Lehmann, A.R. (1982) Failure of RNA synthesis to recover after UV irradiation: an early defect in cells from individuals with Cockayne's syndrome and xeroderma pigmentosum. *Cancer Res*, **42**, 1473-1478.

26. Adam, S., Polo, S.E. and Almouzni, G. (2013) Transcription recovery after DNA damage requires chromatin priming by the H3.3 histone chaperone HIRA. *Cell*, **155**, 94-106.

27. Oksenych, V., Zhovmer, A., Ziani, S., Mari, P.-O., Eberova, J., Nardo, T., Stefanini, M., Giglia-Mari, G., Egly, J.-M. and Coin, F. (2013) Histone Methyltransferase DOT1L Drives Recovery of Gene Expression after a Genotoxic Attack. *PLoS Genet*, **9**, e1003611.

28. Dinant, C., Ampatziadis-Michailidis, G., Lans, H., Tresini, M., Lagarou, A., Grosbart, M., Theil, Arjan F., van Cappellen, Wiggert A., Kimura, H., Bartek, J. *et al.* (2013) Enhanced Chromatin Dynamics by FACT Promotes Transcriptional Restart after UV-Induced DNA Damage. *Molecular Cell*, **51**, 469-479.

29. Stack, E.C., Wang, C., Roman, K.A. and Hoyt, C.C. (2014) Multiplexed immunohistochemistry, imaging, and quantitation: a review, with an assessment of Tyramide signal amplification, multispectral imaging and multiplex analysis. *Methods*, **70**, 46-58.

30. Faget, L. and Hnasko, T.S. (2015) Tyramide Signal Amplification for Immunofluorescent Enhancement. *Methods Mol Biol*, **1318**, 161-172.

31. Clutter, M.R., Heffner, G.C., Krutzik, P.O., Sachen, K.L. and Nolan, G.P. (2010) Tyramide signal amplification for analysis of kinase activity by intracellular flow cytometry. *Cytometry A*, **77**, 1020-1031.

32. Klein, B., Pastink, A., Odijk, H., Westerveld, A. and van der Eb, A.J. (1990) Transformation and immortalization of diploid xeroderma pigmentosum fibroblasts. *Exp Cell Res*, **191**, 256-262.

33. Troelstra, C., van Gool, A., de Wit, J., Vermeulen, W., Bootsma, D. and Hoeijmakers, J.H. (1992) ERCC6, a member of a subfamily of putative helicases, is involved in Cockayne's syndrome and preferential repair of active genes. *Cell*, **71**, 939-953.

34. Marteijn, J.A., Bekker-Jensen, S., Mailand, N., Lans, H., Schwertman, P., Gourdin, A.M., Dantuma, N.P., Lukas, J. and Vermeulen, W. (2009) Nucleotide excision repair-induced H2A ubiquitination is dependent on MDC1 and RNF8 and reveals a universal DNA damage response. *J Cell Biol*, **186**, 835-847.

35. van Cuijk, L., van Belle, G.J., Turkyilmaz, Y., Poulsen, S.L., Janssens, R.C., Theil, A.F., Sabatella, M., Lans, H., Mailand, N., Houtsmuller, A.B. *et al.* (2015) SUMO and ubiquitin-dependent XPC exchange drives nucleotide excision repair. *Nat Commun*, **6**, 7499.

36. Schindelin, J., Arganda-Carreras, I., Frise, E., Kaynig, V., Longair, M., Pietzsch, T., Preibisch, S., Rueden, C., Saalfeld, S., Schmid, B. *et al.* (2012) Fiji: an open-source platform for biological-image analysis. *Nat Methods*, **9**, 676-682.

37. Bensaude, O. (2011) Inhibiting eukaryotic transcription: Which compound to choose? How to evaluate its activity? *Transcription*, **2**, 103-108.

38. David, S.S., O'Shea, V.L. and Kundu, S. (2007) Base-excision repair of oxidative DNA damage. *Nature*, **447**, 941-950.

39. Beard, W.A. and Wilson, S.H. (2006) Structure and mechanism of DNA polymerase Beta. *Chem Rev*, **106**, 361-382.

40. Hazan, C., Boudsocq, F., Gervais, V., Saurel, O., Ciais, M., Cazaux, C., Czaplicki, J. and Milon, A. (2008) Structural insights on the pamoic acid and the 8 kDa domain of DNA polymerase beta complex: towards the design of higher-affinity inhibitors. *BMC Struct Biol*, **8**, 22.

41. Hu, H.Y., Horton, J.K., Gryk, M.R., Prasad, R., Naron, J.M., Sun, D.A., Hecht, S.M., Wilson, S.H. and Mullen, G.P. (2004) Identification of small molecule synthetic inhibitors of DNA polymerase beta by NMR chemical shift mapping. *J Biol Chem*, **279**, 39736-39744.

42. Wyatt, M.D. and Pittman, D.L. (2006) Methylating agents and DNA repair responses: Methylated bases and sources of strand breaks. *Chem Res Toxicol*, **19**, 1580-1594.

43. Chen, X., Zhao, Y., Li, G.M. and Guo, L. (2013) Proteomic analysis of mismatch repair-mediated alkylating agent-induced DNA damage response. *Cell Biosci*, **3**, 37.

44. Pena-Diaz, J., Bregenhorn, S., Ghodgaonkar, M., Follonier, C., Artola-Boran, M., Castor, D., Lopes, M., Sartori, A.A. and Jiricny, J. (2012) Noncanonical mismatch repair as a source of genomic instability in human cells. *Mol Cell*, **47**, 669-680.

45.  Molinete, M., Vermeulen, W., Burkle, A., Menissier-de Murcia, J., Kupper, J.H., Hoeijmakers, J.H. and de Murcia, G. (1993) Overproduction of the poly(ADP-ribose) polymerase DNA-binding domain blocks alkylation-induced DNA repair synthesis in mammalian cells. *Embo J*, **12**, 2109-2117.
46.  Jia, N., Nakazawa, Y., Guo, C., Shimada, M., Sethi, M., Takahashi, Y., Ueda, H., Nagayama, Y. and Ogi, T. (2015) A rapid, comprehensive system for assaying DNA repair activity and cytotoxic effects of DNA-damaging reagents. *Nat Protoc*, **10**, 12-24.
47.  Bauer, N.C., Corbett, A.H. and Doetsch, P.W. (2015) The current state of eukaryotic DNA base damage and repair. *Nucleic Acids Res*, **43**, 10083-10101.
48.  Lans, H., Marteijn, J.A. and Vermeulen, W. (2012) ATP-dependent chromatin remodeling in the DNA-damage response. *Epigenetics Chromatin*, **5**, 4.
49.  Boeing, S., Williamson, L., Encheva, V., Gori, I., Saunders, R.E., Instrell, R., Aygun, O., Rodriguez-Martinez, M., Weems, J.C., Kelly, G.P. *et al.* (2016) Multiomic Analysis of the UV-Induced DNA Damage Response. *Cell Rep*, **15**, 1597–1610.
50.  Newman, J.C., Bailey, A.D., Fan, H.-Y., Pavelitz, T. and Weiner, A.M. (2008) An Abundant Evolutionarily Conserved CSB-PiggyBac Fusion Protein Expressed in Cockayne Syndrome. *PLoS Genet*, **4**, e1000031.

**2**
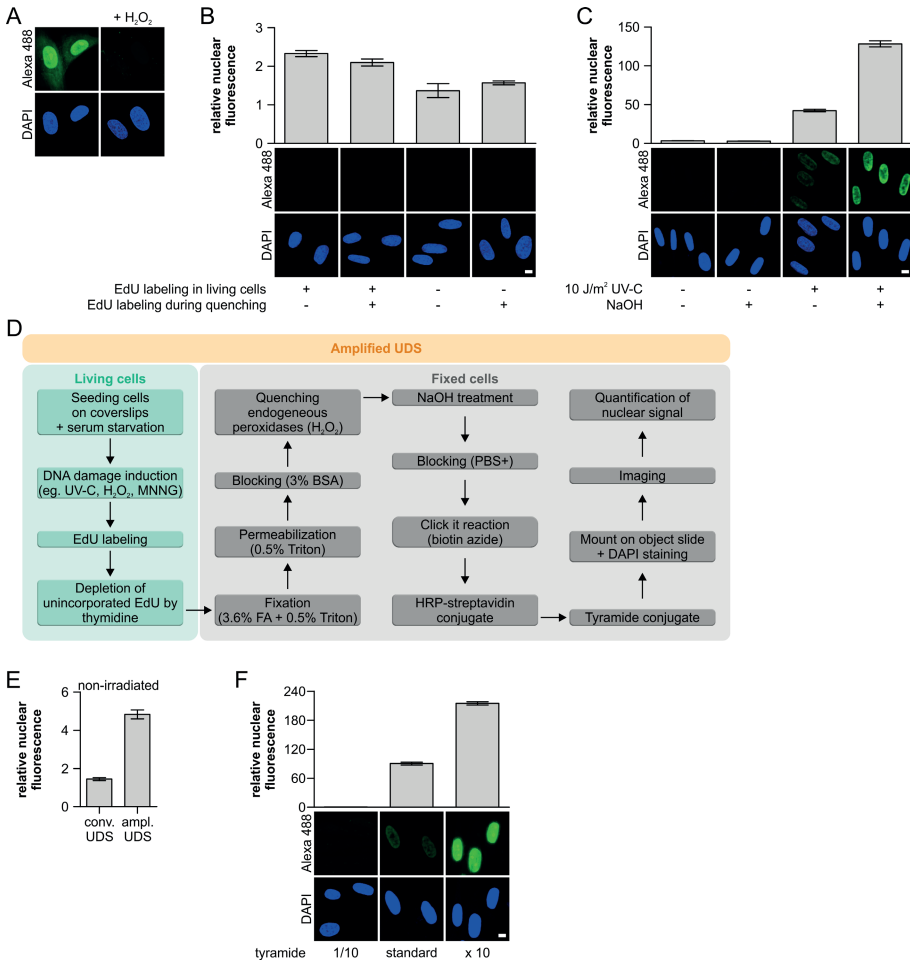
**Supplementary Figure 1**

**(A)** VH10 cells were labeled for 3 h with EdU. Fixed cells were mock treated or incubated with 3% hydrogen peroxide for 1 h, as indicated. Representative images are shown and indicate that quenching of endogenous peroxidases by hydrogen peroxide is essential to prevent unspecific activation of the tyramide. **(B)** Non-proliferating VH10 (NER-proficient) cells grown on cover slips were labeled for 3 h with EdU or were mock treated. Subsequently, the amplified UDS protocol was followed, but for samples marked with 'EdU labelling during quenching', additional EdU was added during the quenching step. The UDS signal (n > 100 cells per condition) was quantified by confocal microscopy measurement of the total nuclear fluorescence (Alexa-Fluor 488 nm) and expressed as relative nuclear fluorescence. No additional gap-filling synthesis was measured in samples that were incubated with EdU during quenching. **(C)** VH10 cells, irradiated with UV-C (10 J/m²) and EdU labeled for 3 h, were incubated with 0.07 M sodium hydroxide after fixation or were left untreated (n > 180 cells per condition, 1 experiment). The amplified UDS signal measured by the total nuclear fluorescence (Alexa-Fluor 488 nm) was quantified (upper panel) and representative images (lower panel) are shown. **(D)** Flowchart representing the different steps to accomplish the amplified UDS assay. **(E)** VH10 cells grown on a

coverslip (non-irradiated) were labeled for 3 h with EdU. Background EdU incorporation was either measured by conventional or amplified UDS (tyramide based signal amplification) procedures. Signals were quantified by means of Alexa-Fluor 488 nm total signal intensity per nucleus (n > 380cells per condition, 2 independent experiments). Quantification of VH10 cells irradiated with 10 J/m² UV-C are shown in Fig. 1C. **(F)** Quantification of VH10 cells (n > 320 cells for each condition, 2 independent experiments) incubated with different tyramide concentrations (top panel) and representative images (lower panel) that were UV-C irradiated (8 J/m²). The DNA marker DAPI was used for visualizing nuclei. SEM is shown. Scale bar: 10 µM.
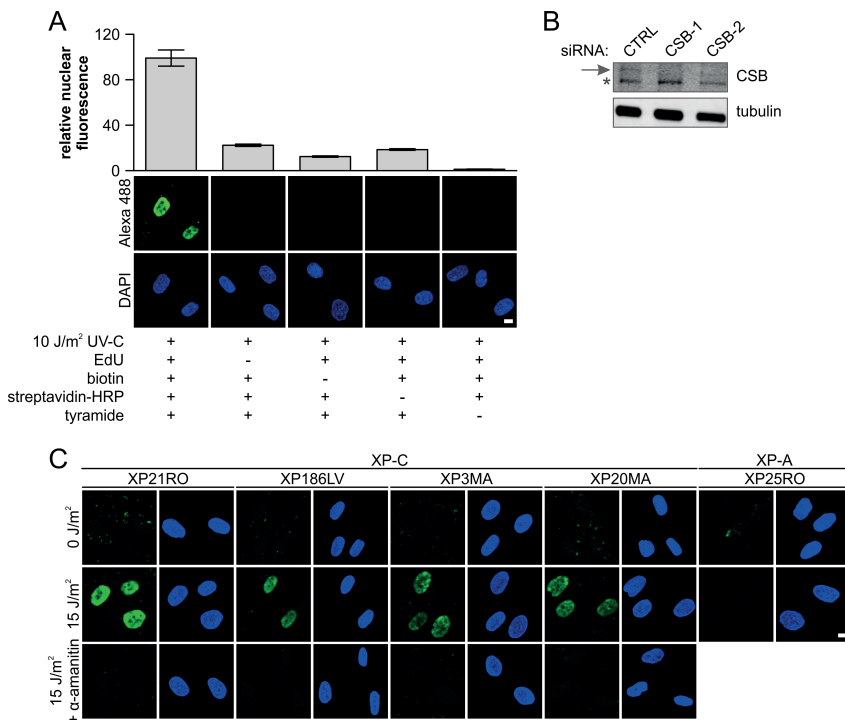


**Supplementary Figure 2**

**(A)** Representative images of XP186LV (XP-C) cells (lower panel), in which the specificity of the amplified UDS signal was tested by omitting essential components of the EdU based Click-it chemistry and TSA amplification as indicated by (-). The amplified UDS signal (upper panel), after 7 h EdU labeling in XP186LV cells, is quantified (n > 46 cells for each condition) by measuring the total nuclear fluorescence (Alexa-Fluor 488 nm). **(B)** Western blot is used for evaluating the efficacy of the CSB knockdown by two different siRNAs (CSB-1 and CSB-2) in XP186LV cells. 48 h after siRNA transfection, cells were lysed in 2x Laemmli Sample buffer. * indicates the CSB-PiggyBac fusion protein (50) that is not targeted by the used siRNA sequences. **(C)** Representative images of amplified UDS signals of different types of XP-C (XP21RO, XP186LV, XP3MA, XP20MA) and XP-A cells (XP25RO). Quantification of the signal is shown in Figure 3C. Cells were irradiated with UV-C (10 J/m²) and treated with the transcription inhibitor α-Amanitin (25 µg/ml) as indicated. The DNA marker DAPI was used for visualizing nuclei. SEM is shown. Scale bar: 10 µM.

# Chapter 3

## FACT subunit Spt16 controls UVSSA recruitment to lesion-stalled RNA Pol II and stimulates TC-NER

Franziska Wienholz[1], Yasemin Turkyilmaz[1], Di Zhou[1], Petra Schwertman[1], Maria Tresini[1], Alex Pines[1], Karel Bezstarosti[2], Jeroen A. Demmers[2] and Jurgen A. Marteijn[1]

[1] Department of Molecular Genetics, Oncode Institute, Erasmus MC, Wytemaweg 80, 3015 CN Rotterdam, The Netherlands
[2] Proteomics Centre, Erasmus University Medical Center, P.O. Box 1738, 3000 DR, Rotterdam, the Netherlands

## Abstract

Transcription-coupled Nucleotide Excision Repair (TC-NER) is a dedicated DNA repair pathway that removes Transcription-blocking DNA lesions (TBLs). TC-NER is initiated by the recognition of lesion-stalled RNA Polymerase II (Pol II) by the joint action of the TC-NER factors CSA, CSB and UVSSA. However, the exact recruitment mechanism of these factors towards TBLs remains elusive. Here, we study the recruitment mechanism of UVSSA using live-cell imaging and show that UVSSA accumulates at TBLs independent of CSA and CSB. Furthermore, using UVSSA deletion mutants, we could separate the CSA interaction function of UVSSA from its DNA damage recruitment activity, which is mediated by the UVSSA VHS and DUF2043 domain, respectively. Quantitative interaction proteomics showed that the Spt16 subunit of the histone chaperone FACT interacts with UVSSA, mediated by the DUF2043 domain. Spt16 is recruited to TBLs, independently of UVSSA, to stimulate UVSSA recruitment and TC-NER mediated repair. Spt16 specifically affects UVSSA, as Spt16 depletion did not affect CSB recruitment, highlighting that different chromatin-modulating factors regulate different reaction steps of the highly orchestrated TC-NER pathway.

## Introduction

Eukaryotic gene transcription by RNA Polymerase II (Pol II) is crucial for proper cell function. However, different types of DNA lesions can damage the Pol II template, thereby severely impeding or even stalling the progression of elongating Pol II. These transcription blocking DNA lesions (TBLs) can originate from endogenous or exogenous sources, for example metabolic byproducts may induce oxidative DNA damage, or UV-light induces helix-distorting lesions like CPDs [1-3]. TBLs pose a direct problem for cellular homeostasis due to a lack of newly synthesised RNA or may result in the appearance mutant RNA molecules. In addition, prolonged stalling of Pol II may result in collisions with advancing replication forks and may induces R-loop formation [4]. TBLs can therefore cause genome instability, severe cellular dysfunction, premature cell death and senescence, which finally may result in DNA-damage induced, accelerated ageing [5-7].

To overcome these cytotoxic TBLs, cells are endowed with transcription-coupled nucleotide excision repair (TC-NER). TC-NER is a dedicated branch of the nucleotide excision repair pathway that specifically repairs TBLs in the transcribed strand of active genes, thereby resolving lesion that stall RNA PolII and subsequently allowing transcription to restart [4, 8]. The importance of TC-NER is best shown by its causative link with the Cockayne Syndrome (CS) and the UV-sensitivity syndrome (UV$^S$S) [6, 9, 10]. CS is caused by mutations in *CSA* and *CSB* [11, 12], while mutations in *UVSSA* give rise to UV$^S$S [13-15]. Despite a similar deficiency in the repair of UV-induced TBLs, the CS and UV$^S$S phenotypes are strikingly different [6, 9, 10]. CS is characterized by photosensitivity, growth failure, progressive neurodevelopmental defects and premature aging [10, 16], while UV$^S$S has a far less severe phenotype, which is restricted to cutaneous photosensitivity, such as freckling and pigmentation abnormalities [9].

The recognition of lesion-stalled Pol II by Cockayne Syndrome protein B (CSB) is assumed to be the initiating signal for TC-NER [17-19]. In unperturbed conditions, the transcription elongation factor CSB transiently interacts with elongating Pol II, however, this interaction becomes more stable when Pol II is stalled at a TBL [18, 20]. In line with this, recent cryo-EM studies of Rad26, the yeast homolog of CSB, show that it binds DNA upstream of Pol II, where it has a key role in lesion recognition [19]. Mediated by its ATPase activity, Rad26 facilitates forward translocating of Pol II over naturally occurring pause sites or less bulky lesions. However, Rad26 cannot translocate Pol II over bulky, transcription-blocking DNA

lesions [19]. This prolonged binding of CSB to lesion stalled Pol II is thought to be one of the first steps in the assembly of the TC-NER complex, as for example shown by the CSB-dependent CSA translocation to the nuclear matrix following UV-induced DNA damage [21]. CSA forms an E3-ubiquitin ligase complex with DDB1, Cul4A, ROC1/Rbx1 [22, 23], and is involved in the ubiquitylation and subsequent degradation of CSB, upon UV-irradiation [24]. The UV-induced degradation of CSB is counteracted by the de-ubiquitylating enzyme USP7, which is recruited by the TC-NER factor UV Stimulated Scaffold Protein A (UVSSA) [13, 14]. Furthermore, UVSSA plays a role in the restoration of the hypo-phosphorylated form of Pol II (Pol IIa) [13] and in UV-induced ubiquitin modifications of Pol II [15], but both effects might be indirect. Recently it was suggested that UVSSA also plays an important role in the recruitment of transcription factor II H (TFIIH), via a direct interaction with P62 [15, 25]. TFIIH subsequently unwinds a stretch of approximately 30 nucleotides surrounding the damage site and is, in combination with XPA and RPA, responsible for damage-verification and the orientation of the XPF/ERCC1 and XPG endonucleases. Following excision of the damaged DNA, the resulting single-stranded gap is filled by DNA synthesis and sealed by DNA ligases [6].

Despite significant advances, the regulation and recruitment mechanisms of TC-NER factors to lesion stalled Pol II is thus far not fully understood and such understanding is required for proper comprehension of the TC-NER mechanism and its disease etiology. For example, the exact recruitment mechanism of UVSSA remains under debate. Like CSB, UVSSA has affinity for Pol II in unperturbed conditions [14, 18, 26], and it has been suggested that, this interaction is stabilized following DNA damage [13]. Although UVSSA interacts with CSA [27], UVSSA accumulation at sites of UV-induced DNA damage is a CSA and CSB independent process [14]. In contrast, the UV-induced UVSSA translocation to chromatin observed in cell fractionation assays was shown to depend on CSA [27].

To increase our understanding of the spatio-temporal build-up of the TC-NER complex and its molecular mechanism, we compared accumulation kinetics of different TC-NER factors in living cells and studied the UVSSA recruitment in TC-NER deficient cells in a quantitative manner. Our analysis showed that UVSSA recruitment to DNA damage occurs in a CSA and CSB independent manner. In addition, UVSSA deletion mutants showed that UVSSA binding to CSA and recruitment to TBLs, are mediated by distinct domains; the Vps/Hrs/STAM (VHS) domain and the domain of unknown function 2043 (DUF2043), respectively. Using these separation of function mutants of UVSSA, in combination with quantitative interaction proteomics, we identified the Spt16 subunit of the

H2A/H2B chaperone FACT to be involved in the UVSSA recruitment. Spt16 is recruited early in the TC-NER reaction in a UVSSA independent manner, thereby stimulating excision of the TBLs and subsequent transcription restart after DNA damage removal. Our work establishes Spt16 as an important regulator of TC-NER-mediated repair and provides new insights into the different mechanisms involved in the recognition of lesion-stalled Pol II and how the remodeling of chromatin fine-tunes the regulation of the different stages of TC-NER.

## Materials and Methods

### Plasmid constructs
GFP-tagged UVSSA deletion mutants of the DUF2043 (ΔDUF) and VHS (ΔVHS) domain were made by PCR amplification on pLenti CMV Hygro vector [28], containing either full length C1-UVSSA construct or N2-UVSSA construct, with Phusion High-Fidelity DNA polymerase (M0530, New England Biosciences) using the following primers: ΔDUF Forward 5'-CACCATGGTGAGCAAGGGCGAG-3' ΔDUF Reverse 5'-CTATGCTGCCAGCT-TCTGGGCCTC-3' ΔVHS Forward 5'-CACCATGTTTCAAGACACGAATGCTC-GGAGT-3' ΔVHS Reverse 5'-TTACTTGTA-CAGCTCGTCCAT-3'. PCR products were subcloned into pENTR™/D-TOPO® vector using pENTR™ directional TOPO® Cloning kit (Invitrogen). Recombination into the pLenti CMV Hygro destination vector (Addgene, plasmid ID: #17454) was performed using the Gateway LR Clonase II Enzyme Mix (Invitrogen).

### Cell line generation
Full length GFP-UVSSA [14] or UVSSA deletion mutants (GFP-UVSSA ΔDUF and UVSSA ΔVHS-GFP) expressing cell lines were generated by lentiviral transduction of the indicated constructs. To that end, third-generation lentiviruses were made in HEK293T cells and were used to transduce UV$^S$S-A (TA24) SV40-immortalized cells. Fibroblasts originating from NER patients (SV40 transformed) were complemented with the respective deficient NER protein as described: GFP-CSB in CS-B (CS1AN) [18], CSA-Flag-GFP in CS-A (CS3BE) [29], XPC-GFP in XP-C (XP4PA) [30], GFP-XPA in XP-A (XP20S) [31], GFP-XPB in XP-B (XPCS2BA) [32]. Vh10 (hTert) cells stably expressing GFP-DDB2 were described before [33]. The generation of U2OS cells stably expressing GFP-tagged Spt16 or SSRP1 was described before [34], UV$^S$S-A (TA24) cells expressing GFP-tagged Spt16 were generated in a similar approach. TA24 GFP-Spt16 cells were complemented with FLAG-tagged UVSSA by lentiviral transduction. Gateway

LR Clonase (Invitrogen) was used to recombine UVSSA-Flag from pENTR4 no ccDB (686-1, Addgene, plasmid ID: #17424) [14] to pLenti CMV Puro Dest (w118-1, Addgene, plasmid ID: #17452). The generated, rescued cell line was subjected to a combination of selection by Puromycin (2.5 µg/ml) for UVSSA-Flag and Hygromycin (5µg/ml) for Spt16-GFP. GFP-H2A [34] was stably expressed in HeLa cells [34] or in UV$^S$S-A (TA24) cells by transfection using X-treme Gene HP (Roche) according to the manufactures protocol. Cells stably expressing GFP-H2A were selected using 0.5 mg/ml G418 and FACS sorting.

## Cell culture

TA24 (UV$^S$S-A), CS1AN (CS-B), CS3BE (CS-A), XP4PA (XP-C), XP20S (XP-A), XPCS2BA (XP-B), HeLa, Vh10 and U2OS cell lines were cultured in a 1:1 ratio of DMEM and Ham's F10 (Invitrogen) containing 10 % fetal calf serum (FCS, Biowest) and antibiotics at 37 °C and 5 % $CO_2$. For SILAC labelling, cells were cultured for 2 weeks in DMEM without lysine, arginine or leucine (AthenaES) supplemented with antibiotics, 10 % dialyzed FCS (Invitrogen) and 105 µg/ml leucine (Sigma) and either 73 µg/ml light [$^{12}C_6$]-lysine and 42 µg/ml [$^{12}C_6,^{14}N_4$]-arginine (Sigma) or with heavy [$^{13}C_6$]-lysine and [$^{13}C_6,^{15}N_4$]-arginine (Cambridge Isotope Laboratories) at 37°C and 5% $CO_2$.

## RNA interference

Transient siRNA-mediated knock-down was achieved using Lipofectamine RNAiMAX (Invitrogen) transfection, according to the manufacturer's instruction. The siRNA oligonucleotides used, (Thermo Fisher Scientific) were as follows: CTRL (D-001210-05-20) 5'-UGGUUUACAUGUCGACUAA-3', Spt16 (L-009517-00) 5'-AGUCUAAUGUGUCCUAUAA-3', 5'-GCAUAUACCAUCGCUGUAA-3', 5'-ACACGGAUGUGCAGUUCUA-3', 5'-GUACAGCAAUUGGCGGAAA-3', SSRP1 (L-011783-00), 5'-GCUCUGGGCCAUGGACUUA-3', 5'-GGAGUUCAACGACGUC-UAU-3', 5'-CGAUGAAUAUGCUGACUCU-3', 5'-AAGAAGAACUAGCCAGUAC-3', UVSSA (J-0243197-23-0002) 5'-GCUCGUGGAUCCAGCGCUU-3', Nap1L1 (L-017274-01-0005), 5'-UAACCAUAGUUCAUCGAAAUU-3', 5'-GCGUAUAAU-CCCAAGAUCAUU-3', 5'-GUUAAGGCAUAUUGAGUUAUU-3', 5'-GGAACGAGAU-GCUAUACU-3'

## Clonogenic survival assay

Cells were seeded in triplicate in 6-well plates (300 cells/well) and treated with a single dose of the indicated UV-C dose (254 nm; Philips TUV lamp) 1 day after seeding. After 1 week, colonies were fixed and stained in 50 % methanol, 7 % acetic acid and 0.1 % Coomassie blue and subsequently counted with the

Gelcount (Oxford Optronix, Software Version 1.1.2.0). The survival was plotted as the mean percentage of colonies detected following the indicated UV-C dose compared to the mean number of colonies from the non-irradiated samples.

## Live-cell confocal laser-scanning microscopy

Confocal laser-scanning microscopy images were obtained with a Leica SP5 confocal microscope using a 100x quartz objective for local UV-damage induction. Local DNA damage infliction for kinetic studies of GFP-tagged protein accumulation was performed using a 266 nm UV-C (2 mW pulsed (7.8 kHz) diode pumped solid-state laser (Rapp OptoElectronic, Hamburg) as described previously [14, 35]. Briefly, cells were grown on quartz cover slips and were imaged and irradiated through a 100 x 1.2 NA Ultrafluar quartz objective. During microscopy, cells were kept at 37°C and 5% $CO_2$. Images were acquired using the LAS AF software (Leica) and the fluorescence intensity at the damage area was recorded over time, background corrected and normalized to pre-damage fluorescence levels to quantify aaccumulation kinetics. H2A exchange on UV-C induced DNA damage was performed as described previously [34]. In short, half of the nucleus was photobleached by a 488nm laser and local UV-C damage was subsequently induced in the bleached area. The recovery of fluorescence, representing histone exchange, on the UV-C damaged area and non-damaged area was quantified. Fluorescence intensities were background corrected and the fluorescence on the UV-C damaged area was normalised to the fluorescence for the non-damaged area. The indicated number of cells originate from at least 2 experiments and the results were pooled and plotted as the mean fluorescence intensity ± SEM.

## Immunofluorescence

Cells were grown on 24-mm coverslips and fixed using 2% paraformaldehyde supplemented with triton X-100. Subsequently cells were permeabilized with PBS containing 0.1% triton X-100. Coverslips were washed with PBS containing 0.15% glycine and 0.5% BSA and incubated with primary antibody, FLAG M2 (1:1000) for 1–2 h at room temperature. Cells were washed three times and two times for 10 min with 0.1% triton X-100 and once with PBS containing 0.15% glycine and 0.5% BSA. To visualize primary antibodies, coverslips were incubated for 1 h with secondary antibodies labelled with ALEXA fluorochrome 594 (Invitrogen). Again cells were washed with 0.1% Triton X-100 and PBS+. Subsequently coverslips were embeddedin Dapi-containing Vectashield mounting medium (Vector Laboratories). Images were obtained using a Zeiss LSM700 microscope equipped with a 63 × oil Plan-apochromat 1.4 NA oil immersion lens (Carl Zeiss Microimaging Inc.).

## TC-NER specific Unscheduled DNA Synthesis (UDS)

The amplified UDS assay was performed as described [36]. Briefly, XP186LV, XPC-deficient cells, seeded on 24-mm coverslips 4 days prior to the experiment were transfected with siRNA 2 days later. 1 day following transfection the medium was replaced by low-serum containing medium (Ham's F10 supplemented with 0.5 % FCS) to reduce the number of cells in S-phase. For global UV-C irradiation (8 J/m$^2$), a 254 nm germicidal lamp (Philips) was used. Following irradiation, cells were labelled with medium (Ham's F10 supplemented with 0.5% dialyzed FCS) containing 5-ethynyl,2'-deoxyuridine (EdU, 20 μM, ThermoFisher Scientific) and 2'-Deoxy-5-fluorouridine (Floxuridine, 1 μM, Sigma-Aldrich) for 7 h. Subsequently, cells were fixed in 3.6 % formaldehyde (Sigma-Aldrich) in PBS with 0.5% Triton X-100 (Sigma-Aldrich). EdU incorporation was visualized using a combination of the Click-iT reaction (Invitrogen) and Tyramide Signal Amplification (ThermoFisher Scientific). The Click-it reaction was performed as described in the manufactures protocol using Azide-PEG3-Biotin Conjugate (20 μM in DMSO, Jena Bioscience), 1x Click-it reaction buffer (ThermoFisher Scientific), Copper(III)sulphate (0.1 M), and 10x Reaction buffer additive (ThermoFisher Scientific). The tyramide-based amplification was conducted as described in the manufactures protocol by using the HRP-Streptavidin conjugate (500 μg/ml, ThermoFisher Scientific) and Alexa-Fluor 488 nm labeled tyramide (ThermoFisher Scientific). Cover slips were embedded in DAPI containing Vectashield mounting medium (VectorLaboratories) and sealed using nail polish, and visualizedusing a Zeiss LSM700 microscope equipped with a 40x oil Plan-Apochromat 40 0.6-1.3 numerical aperture (NA) oil immersion lens (Carl Zeiss Micro imaging Inc.). TCR-UDS signal was quantified by analyzing at least 6 fields for each condition Mean nuclear fluorescence signals were quantified using ImageJ software (Version 1.48) [37]. Sample analysis was performed as described [36]. The mean nuclear fluorescence signal ± standard error of the mean is shown.

## *In vivo* cross-linking and immunoprecipitation

The cross-linked immunoprecipitation procedure has been described previously [14, 34]. Briefly, *in vivo* cross-linking was performed by adding 1 % formaldehyde to the culture medium for 10 min at 4 °C. Cross-linked cells were scrapped and chromatin was purified. Finally, the nuclear suspension was sonicated using the Bioruptor Sonicator (Diagenode) with 6 cycles of 30 s on and 60 s off. For immunoprecipitations, equal amounts of crosslinked chromatin from all samples were incubated in RIPA buffer with 30 μl GFP-Trap-A agarose bead slurry (ChromoTek), overnight at 4 °C. Beads were collected by centrifugation,

washed 5 times with RIPA buffer and GFP-tagged proteins were de-crosslinked and eluted and by incubation at 95 °C for 30 min in 2x Laemlie SDS sample buffer. Samples were analysed by western blot and loaded to 4–15% Mini-PROTEAN TGX™ Precast Protein Gels (BioRad). Gels were fixed and stained by Roti-blue (Carl Roth GmbH) according to the manufacturer's protocol.

## Western blot and Antibodies

Lysates were separated by SDS–PAGE and transferred to a PVDF membrane (0.45 μm). Membranes were blocked with 5% milk in PBS for 1 h at room temperature and incubated with primary antibodies raised against GFP (Roche, 11814460001), CSA/ERCC8 (Abcam, ab137033), USP7 (Bethyl, A300-033A), Spt16, SSRP1 (Santa Cruz Biotechnology, sc-28734 and sc-74536, respectively), Spt16 (Abcam, Ab56855) or Tubulin (Sigma Aldrich, clone B-5-1-2). Secondary antibodies coupled to IRDyes (LI-COR) were used to visualize proteins using an Odyssey CLx infrared scanner (LiCor).

## Mass spectrometry

SDS-PAGE gel lanes were cut into 2-mm slices and subjected to in-gel reduction with dithiothreitol, alkylation with iodoacetamide and digestion with trypsin (sequencing grade; Promega), as described previously [14]. Nanoflow liquid chromatography tandem mass spectrometry (nLC-MS/MS) was performed on an EASY-nLC coupled to a Q Exactive mass spectrometer (Thermo) or to an Orbitrap Fusion Tribid mass spectrometer (Thermo), both operating in positive mode. Peptide mixtures were trapped on a ReproSil C18 reversed phase column (Dr Maisch; 1.5 cm × 100 μm) at a rate of 8 μl/min. Peptides were separated on a ReproSil-C18 reversed-phase column (Dr Maisch; 15 cm × 50 μm) using a linear gradient of 0–80% acetonitrile (in 0.1% formic acid) for 170 min at a rate of 200 nl/min. The elution was directly sprayed into the electrospray ionization (ESI) source of the mass spectrometer. Spectra were acquired in continuum mode; fragmentation of the peptides was performed in data-dependent mode by HCD (Q Exactive) or CID (Orbitrap Fusion).

Raw mass spectrometry data were analyzed using the MaxQuant software suite (version 1.4.1.2) [38]. A false discovery rate of 0.01 for proteins and peptides and a minimum peptide length of 7 amino acids were set. The Andromeda search engine was used to search the MS/MS spectra against the Uniprot database (taxonomy: *Homo sapiens*, release June 2013). A maximum of two missed cleavages was allowed. The peptide tolerance was set to 10 ppm and the fragment ion tolerance was set to 20 mmu for HCD spectra (Q Exactive) or to 0.6

Da for CID spectra (Orbitrap Fusion). The enzyme specificity was set to "trypsin", and cysteine carbamidomethylation was set as a fixed modification. SILAC protein ratios were calculated as the median of all peptide ratios assigned to the protein. In addition, a posterior error probability for each MS/MS spectrum below or equal to 0.1 was required. In case the identified peptides of two proteins were the same or the identified peptides of one protein included all peptides of another protein, these proteins were combined by MaxQuant and reported as one protein group. Before further statistical analysis, known contaminants and reverse hits were removed.

## Results

### UVSSA accumulates independently of CSA and CSB on UV-C induced DNA damage

To acquire more insights in the recruitment mechanism of UVSSA, we first quantified its accumulation at sites of DNA damage and compared this to the recruitment kinetics of the other TC-NER initiating factors, CSA and CSB. For this purpose, we used TC-NER deficient patient cell lines that are mutated in either CSA, CSB or UVSSA and are functionally complemented by stable expression of GFP-tagged versions of the respective TC-NER factor [14, 18, 29] (Supplemental Figure 1 A). Accumulation kinetics of these TC-NER factors at sites of local UV-C laser (266 nm) induced DNA damage were determined using quantitative live-cell confocal imaging [35]. GFP-UVSSA and GFP-CSB recruitment at site of locally UV-induced DNA damage (LUD) was clearly visible and showed a similar, swift, 2-fold accumulation (Figure 1A and B). Interestingly, despite the fact that CSA is a crucial TC-NER factor [5] and that CSA has been shown to directly interact with both UVSSA and CSB [13, 24, 27] (Figure 2C), its accumulation at sites of sites of LUD was barely was barely detectable (Figure 1A and B). This might be explained by a transient binding of CSA to the TC-NER complex. Furthermore, the almost complete absence of CSA at LUD makes it unlikely that UVSSA recruitment to the TC-NER complex is mediated via a direct protein-protein interaction with CSA. In line with this assumption, we have previously shown that UVSSA accumulation can still be detected at sites of UV-C induced DNA damage in the absence of functional CSA and CSB [14]. However, as these experiments do not rule out that CSA or CSB might have more subtle effects on UVSSA recruitment kinetics, e.g. reduced accumulating rates or levels, we determined the accumulation of GFP-UVSSA in time in a quantitative manner in CSA and CSB deficient cells and compared this to TC-NER proficient cells (complemented UV$^S$S-A patient
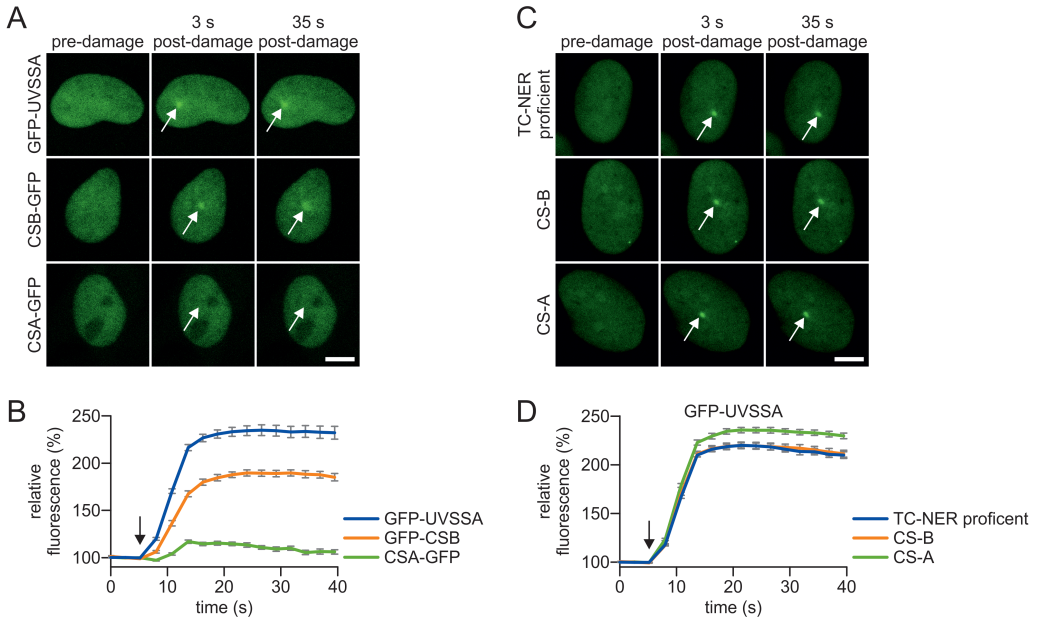
**Figure 1: Accumulation kinetics of TC-NER factors reveal a CSA independent UVSSA recruitment.** **(A)** Representative images of live cell imaging analysis of GFP-UVSSA, GFP-CSB or CSA-GFP at the indicated time points following local UV-C laser (266nm) induced damage (LUD) in a sub-nuclear region (indicated by a white arrow). Scale bar: 7.5 μm. **(B)** Relative accumulation of the indicated GFP-tagged TC-NER factors. GFP fluorescence intensity at LUD was quantified over time and normalised to pre-damage intensity set at 100 at t=0 (n = 25 cells of 2 independent experiments, mean ± SEM). The moment of damage induction is indicated with a black arrow. **(C)** Representative images of GFP-UVSSA accumulation at the indicated time points at LUD (indicated by a white arrow). GFP-UVSSA is expressed to functionally complement UV$^s$S-A cells (TC-NER proficient cells) or GFP-UVSSA expressed in CS-A and CS-B cell lines. Scale bar: 7.5 μm. **(D)** Relative accumulation of GFP-UVSSA in the indicated cell lines. GFP fluorescence intensity at LUD of was quantified over time and normalised to pre-damage intensity set at 100 at t=0 (n = 30 cells, 2 independent experiments, mean ± SEM). The moment of damage induction is indicated with a black arrow.

cell line) (Figure 1C and D). GFP-UVSSA was recruited with the same kinetics in TC-NER proficient cells as in CSA or CSB deficient cells, indicating that UVSSA accumulation is not influenced by CSA or CSB activities.

## The VHS and DUF2043 domains of UVSSA have distinct functions and are both required for TC-NER

To gain insight into the mechanism of UVVSA recruitment to TBLs, we tested which domain of UVSSA is involved in this process. Therefore, we stably expressed two GFP-tagged UVSSA deletion mutants in UVSSA deficient TA24 cells, in which either the C-terminal DUF2043 domain (ΔDUF), or the N-terminal
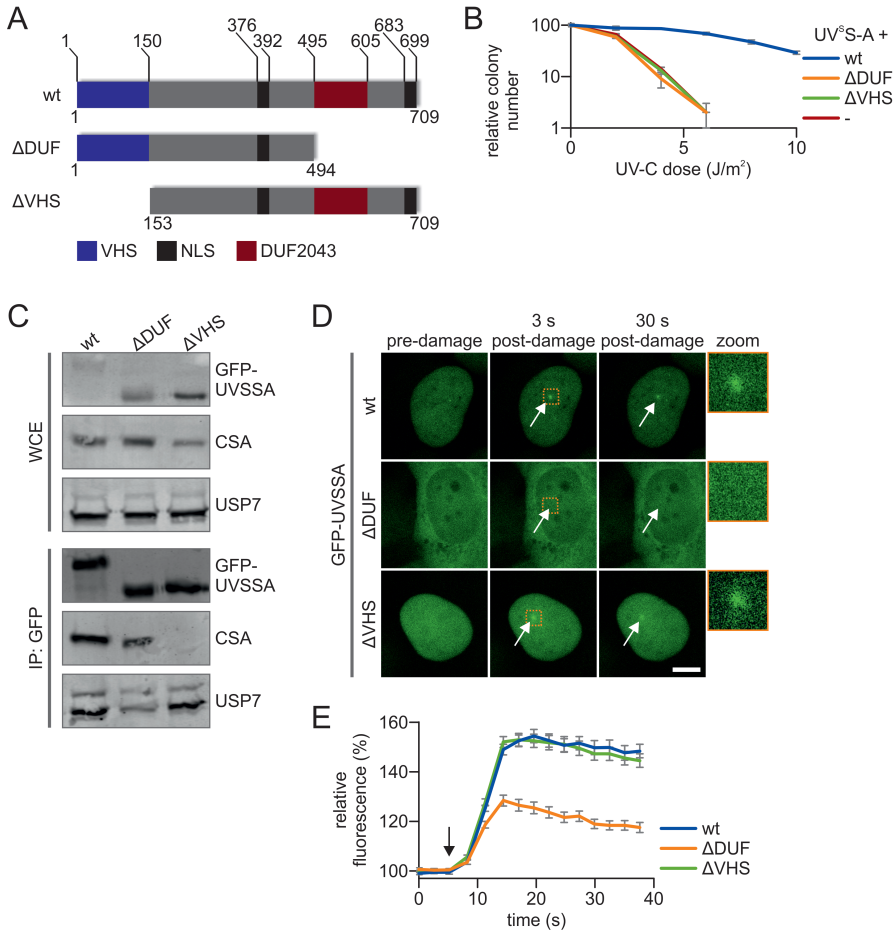
**Figure 2: CSA interaction and recruitment to DNA damage is mediated by distinct UVSSA domains.** **(A)** Schematic overview of the protein domains present in UVSSA and the used UVSSA deletion mutants that either lack the VHS domain (ΔVHS) or the DUF2043 domain (ΔDUF). NLS: nuclear localization signal. **(B)** UV sensitivity of UV$^S$S-A cells (-) and UV$^S$S-A cells complemented with GFP-UVSSA (wt), GFP-UVSSA ΔDUF (ΔDUF) or UVSSA ΔVHS-GFP (ΔVHS) was determined by their colony-forming ability, following irradiation with the indicated UV-C doses. The percentage of surviving colonies is plotted against the UV-C dose. The number of colonies counted at 0 J/m² is set as 100% survival. Data represents the experiment conducted in triplicate and error bars represent SEM. **(C)** Whole cell extracts (WCE) of the UV$^S$S-A patient cells stably expressing the indicated constructs were subjected to GFP immunoprecipitation. Western blot analysis of the immunoprecipitated proteins was performed using GFP, CSA or USP7 antibodies. WCE: whole-cell extract, IP: Immunoprecipitate. **(D)** Representative images of live cell imaging analysis of GFP-UVSSA or ΔDUF and ΔVHS mutants following local UV-C laser (266nm) induced damage (indicated by a white arrow). Scale bar: 7.5 μm. Right panel: 4x zoomed image to visualize accumulation at 3s post-damage induction. **(E)** GFP fluorescence intensity of the indicated constructs at LUD was quantified over time and normalised to pre-damage intensity set at 100 at t=0 (n = 30 cells of 2 independent experiments, mean ± SEM). The moment of damage induction is indicated with a black arrow.

VHS domain (ΔVHS) [15] were deleted (Figure 2A). In contrast to expression of full-length GFP-UVSSA (wt), cells expressing either ΔDUF or ΔVHS UVSSA mutants showed similar UV-hypersensitivity as UVSSA deficient cells (Figure 2B), indicating that both the DUF2043 and VHS domains are essential for TC-NER. In line with previous data that mapped the CSA interaction domain to the N-terminus of UVSSA [27], immunoprecipitation experiments showed that the deletion of the N-terminal ΔVHS domain resulted in the complete loss of CSA interaction, while this interaction remained unaffected in the ΔDUF mutant (Figure 2C). Of note, the ΔVHS mutant could still interact with the known UVSSA interaction partner USP7 (Figure 2C), indicating that the ΔVHS mutant is still partially functional. Like wt UVSSA, the ΔVHS mutant showed strict nuclear localization (Figure 2D). However, the ΔDUF mutant featured an additional cytoplasmic localization, which may have been caused by the deletion of the predicted C-terminal nuclear localization signal (aa 683-699) [15]. Despite its partial cytoplasmic localization, a significant fraction of the ΔDUF mutant remained present in the nucleus, in line with the retained interaction with the nuclear TC-NER factor CSA [21] (Figure 2C). Subsequently, we quantified the recruitment kinetics of these UVSSA mutants to DNA damage. While the ΔVHS mutant accumulated to the same level as wt UVSSA, the recruitment of the ΔDUF mutant at sites of local DNA damage was severely reduced (Figure 2D, E). Together our data show a clear separation of function of the UVSSA domains; the VHS domain is crucial for CSA interaction, while the DUF2043 domain plays an important role during the UVSSA recruitment to DNA damage. Importantly, in line with the unaffected UVSSA accumulation in CS-A cells, these data further show that UVSSA recruitment to TBLs is a CSA independent process.

## Identification of UVSSA interacting proteins

To identify proteins that are involved in recruiting UVSSA to DNA damage, we set out to identify UVSSA interacting proteins using SILAC-based quantitative interaction proteomics. UVSSA containing protein complexes were isolated using GFP-nanotrap pulldowns [39] in UV$^S$-A cells stably complemented with GFP-UVSSA. UV$^S$-A cells expressing free GFP were used as a control for non-specific binding proteins. All experiments were conducted in dublicates with a label swap and only proteins identified in both independent experiments (forward and reverse) with a $\log_2$ SILAC ratio of GFP-UVSSA/GFP above 0.6, were considered specific UVSSA interacting proteins. Results were visualized by plotting the $\log_2$ SILAC ratios of proteins of the two independent experiments (Figure 3A). In total, 66 specific UVSSA interactors were identified (Figure 3A, indicated in blue and orange). The bait UVSSA was identified with the highest

**A** — log$_2$ SILAC ratio GFP-UVSSA/GFP (L/H) vs log$_2$ SILAC ratio GFP-UVSSA/GFP (H/L); labeled points UVSSA, USP7, Spt16, SSRP1; dashed lines at 0.6.

**B**

| pathway ID | pathway description | GC | FDR |
|---|---|---|---|
| GO.0051276 | chromosome organization | 33 | 1.59E-24 |
| GO.0032392 | DNA geometric change | 14 | 1.38E-19 |
| GO.0032508 | DNA duplex unwinding | 12 | 3.55E-16 |
| GO.0071103 | DNA conformation change | 17 | 3.64E-16 |
| GO.0006281 | DNA repair | 19 | 7.23E-14 |
| GO.0006974 | cellular response to DNA damage stimulus | 22 | 9.85E-14 |
| GO.0006271 | DNA strand elongation involved in DNA replication | 9 | 1.29E-12 |
| GO.0006259 | DNA metabolic process | 20 | 1.71E-11 |
| GO.0006996 | organelle organization | 32 | 3.06E-09 |
| GO.0006325 | chromatin organization | 17 | 7.03E-09 |

**C** — log$_2$ SILAC ratio wt/ΔVHS (L/H) vs log$_2$ SILAC ratio wt/ΔVHS (H/L); labeled points SSRP1, USP7, Spt16.

**D** — log$_2$ SILAC ratio wt/ΔDUF (L/H) vs log$_2$ SILAC ratio wt/ΔDUF (H/L); labeled points USP7, Spt16, SSRP1.

**E** — GFP-UVSSA; lanes: -, wt, ΔDUF, ΔVHS (WCE) and -, wt, ΔDUF, ΔVHS (IP: GFP); rows: GFP, Spt16, SSRP1, USP7, CSA.

**Figure 3: Quantitative interaction proteomics reveal UVSSA interaction partners and required UVSSA-domains. (A)** Scatter plot of log$_2$ SILAC ratios of proteins isolated by GFP-pulldown in UV$^S$S-A cells stably expressing either GFP-UVSSA or GFP (non-specific binding control). The experiment was conducted in duplicate with a label swap. The log$_2$ SILAC ratios of proteins identified in the forward experiment (GFP-UVSSA versus GFP, H/L, x-axis) are plotted against the log$_2$ SILAC ratios of proteins identified in the reversed experiment (GFP-UVSSA versus GFP, L/H, y-axis). Proteins were classified as specific UVSSA interactors (marked in blue) when log$_2$ SILAC ratio > 0.6 (indicated by grey dotted line) in both replicates. **(B)** GO-term analysis of the 66 proteins identified as specific interactors of UVSSA. A selection of the top 10 enriched

biological process pathways is shown. GC: gene count, FDR: false discovery rate. **(C)** Scatter plot of $\log_2$ SILAC ratios of proteins identified in the GFP-pulldowns of wt UVSSA versus ΔVHS, only proteins that were also identified in the GFP-UVSSA versus GFP proteomics experiment are depicted. The experiment was conducted in duplicate, including a label swap. The $\log_2$ SILAC ratios of proteins identified in the forward experiment (wt versus ΔVHS, H/L, x-axis) are plotted against the $\log_2$ SILAC ratio of proteins identified in the reversed experiment (wt versus ΔVHS, L/H, y-axis). The majority of proteins have similar binding ability to the ΔVHS mutant compared to the wt ($\log_2$ SILAC ratio < 0.6, proteins marked in grey). Proteins marked in blue represent proteins whose interaction with UVSSA is decreased in the absence of the VHS domain. **(D)** Scatter plot of $\log_2$ SILAC ratios of proteins identified in the GFP-pulldowns of wt UVSSA versus ΔDUF only proteins that were also identified in the GFP-UVSSA versus GFP proteomics experiment are depicted. The experiment was conducted in duplicate, including a label swap. The $\log_2$ SILAC ratios of proteins identified in the forward experiment (wt versus ΔDUF, H/L, x-axis) are plotted against the $\log_2$ SILAC ratio of proteins identified in the reversed experiment (wt versus ΔDUF, L/H, y-axis). Proteins marked in blue have a reduced interaction with UVSSAΔDUF compared to wt (proteins are marked in blue, $\log_2$ SILAC ratio > 0.6, grey dotted line marks the threshold). **(E)** Crosslinked nuclear extracts of UV[s]S-A patient cell line (TA24), stably expressing the indicated constructs were subjected to GFP immunoprecipitation. Non-complemented UV[s]S-A patient cell line (-) was used as negative binding control. WCE: whole-cell extract, IP: Immunoprecipitate. Western blot analysis of the co-immunoprecipitated proteins was performed for GFP, Spt16, SSRP1, USP7 and CSA.

SILAC ratio followed by USP7, a known UVSSA interactor [13, 14, 40], confirming the validity of our approach. To identify biological processes associated with these UVSSA-interacting proteins, we performed a Gene Ontology (GO) enrichment analysis. As expected, the biological process of DNA repair was among the top enriched GO annotations (Figure 3B). In addition, several of the top enriched GO terms were proteins involved in chromatin remodeling, suggesting that UVSSA interactors are involved in this process. Chromatin remodeling has been shown to play an important role in TC-NER [41-43], for example by enhancing the recruitment of TC-NER factors to DNA damage [44].

To pinpoint which proteins, from the 66 identified UVSSA interactors, are involved in the recruitment of UVSSA to DNA damage, we hypothesized that these proteins would retain their interaction with the ΔVHS mutant (the mutant that can localize to DNA damage), but might have lost binding with the ΔDUF mutant (the mutant that is not recruited to damage). Therefore, we performed quantitative proteomics experiments to map which of the identified UVSSA interactors are lost in the respective UVSSA deletion mutants (Supplemental Data set 1). We compared proteins interacting with GFP-UVSSA (wt) to GFP-UVSSA ΔVHS (Figure 3C) or GFP-UVSSA (wt) to GFP-UVSSA ΔDUF (Figure 3D). $\log_2$ SILAC ratios around 0 indicate that proteins are equally bound to wt UVSSA as they are bound to the respective deletion mutant, while a positive $\log_2$ SILAC

ratio indicates that the interaction with the tested deletion mutant is reduced compared to wt UVSSA. Remarkably, only a few interactions were lost in the ΔVHS deletion mutant (Figure 3C, marked in blue), while numerous protein interactions with UVSSA were lost in the ΔDUF mutant (Figure 3D). This shows, in contrast to the interaction of the VHS domain with CSA (Figure 2C), that the majority of identified UVSSA interactors depend on the DUF2043 domain.

Of the 66 proteins identified as UVSSA interactors (Figure 3A, indicated in blue), 45 proteins were detected in all three proteomic screens. The SILAC ratio of 25 of these proteins remained unchanged (SILAC ratio < 1.2) in the ΔVHS mutant, indicating that the interactions between those proteins and UVSSA were similar for the wt UVSSA and the ΔVHS mutant. Since we hypothesized that proteins involved in the UVSSA recruitment to DNA damage would bind specifically to the DUF2043 domain (Figure 3D, indicated in blue), we sorted these remaining 25 proteins with descending wt/ΔDUF SILAC ratios (Supplemental Table 1). Interestingly, both the Spt16 and SSRP1 subunits of the histone chaperone complex FACT were identified as UVSSA interactors whose binding was lost most upon deletion of theDUF2043 domain.

## FACT complex interaction with UVSSA is mediated by the DUF2043 domain

The H2A/H2B histone chaperone FACT (facilitates chromatin transcription) is an interesting interaction partner of UVSSA, as it was originally discovered as an essential factor for productive *in vitro* Pol II transcription on chromatinized DNA [45] and plays essential roles in histone H2A/H2B exchange during DNA transcription and replication [46, 47]. Interestingly, recent studies have shown that FACT is involved in several DNA repair pathways [34, 48-53]. More specifically, Spt16 was shown to stimulate histone H2A/H2B exchange at sites of UV-induced DNA damage and to play an important role during the cellular response to TBLs, by facilitating efficient restart of transcription following DNA damage removal [34]. However, its exact mode of action, and whether Spt16 is involved in TC-NER remains thus far unknown.

To test whether the role of Spt16 in transcription restart might be mediated via its identified interaction with UVSSA, we first confirmed the interaction between the FACT complex and UVSSA. Immunoprecipitation experiments verified the interaction of the FACT complex with UVSSA and as expected, with the known UVSSA interaction-partners, CSA [27] and USP7 [13, 14, 40] (Figure 3E). In line with our proteomics data, we confirmed that FACT binding is mediated by the DUF2043

domain of UVSSA, as immunoprecipitation of the ΔDUF mutant resulted in the absence of Spt16 and SSRP1, whereas the interaction was present in the wt and ΔVHS mutant. Of note, the USP7 interaction with ΔDUF was significantly reduced, in agreement with our proteomics data (Figure 3D). However, the USP7 interaction was not completely lost, indicating that in addition to the DUF 2043 domain, also other UVSSA domains are also involved[40].

## Spt16 enables efficient UVSSA recruitment and stimulates TC-NER mediated damage excision

The identified UVSSA interaction with the FACT subunits SSRP1 and Spt16, together with the previously identified role of Spt16 in transcription restart, indicate that the FACT complex is involved in the function of UVSSA at sites of DNA damage. To test this, we quantified the UVSSA accumulation to sites of DNA damage in cells following siRNA mediated knock-down of the FACT complex. Simultaneous knock-down of both FACT subunits significantly reduced the accumulation of UVSSA at LUD (Figure 4A and B). Interestingly, while knock down of Spt16 alone resulted in a comparable reduction of UVSSA accumulation, depletion of its canonical binding partner SSRP1, did not affect the accumulation of UVSSA, even though SSRP1 was efficiently depleted following siRNA transfection (Figure 4C). To test whether Spt16 depletion specifically affects UVSSA recruitment, or whether its absence inhibits the TC-NER complex assembly in general, we tested whether Spt16 depletion has a similar effect on CSB recruitment. In contrast to UVSSA, siRNA depletion of FACT did not affect CSB accumulation on UV-induced DNA damage (Figure 4D and Supplemental Figure 1B). As CSB is recruited to lesion stalled Pol II [18], the absence of an effect of UVSSA on CSB recruitment, suggests that the effect of Spt16 on UVSSA accumulation is not caused by a general effect on transcription or chromatin state. In line with this, the depletion of another H2A/H2B chaperone, NAP1L1, did not interfere with UVSSA accumulation (Figure 4E and Supplemental Figure 1C, D), indicating that UVSSA accumulation is not influenced by histone chaperones in general.

In accordance with the SSRP1-independent role of Spt16 in UVSSA recruitment, Spt16 was also shown to be specifically involved in transcription restart [34]. This might suggest that the observed inhibition of transcription resumption is caused by a reduced UVSSA recruitment to sites of DNA damage, thereby inhibiting TC-NER efficiency and the subsequent transcription restart. To quantify TC-NER activity, we measured unscheduled DNA synthesis (UDS) by quantifying the DNA damage-induced EdU incorporation during gap-filling synthesis, which
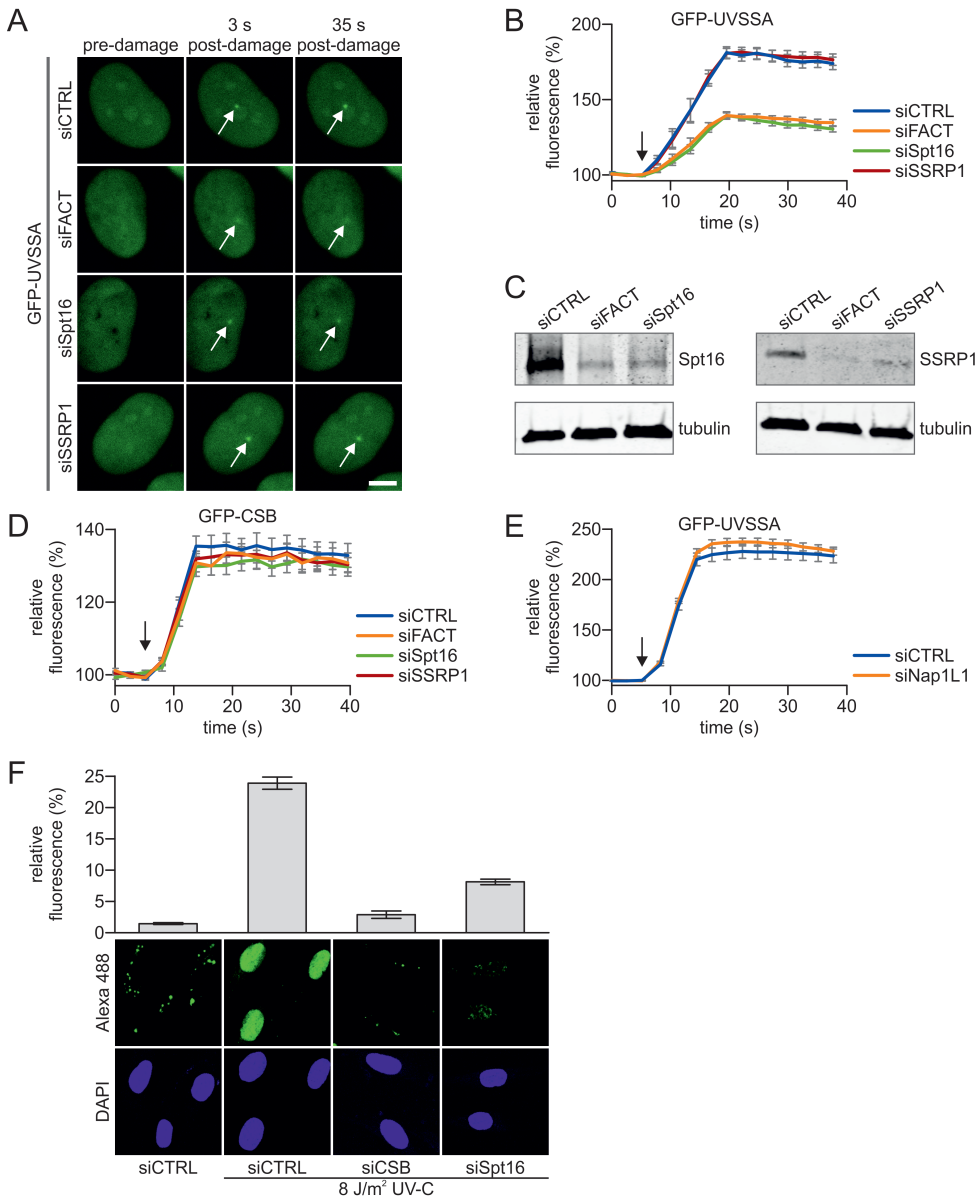
**Figure 4: Spt16 mediates UVSSA accumulation on UV-C induced DNA damage. (A)** Representative images of live-cell imaging analysis of GFP-UVSSA expressing cells transfected with the indicated siRNAs (CTRL is a non-targeting siRNA), following local UV-C laser (266nm) induced damage (indicated by a white arrow). Scale bar: 7.5 μm. **(B)** Relative GFP-UVSSA accumulation at sites of LUD in cells transfected with the indicated siRNA. GFP fluorescence intensity at LUD was measured over time using live-cell confocal imaging and normalised to pre-damage intensity set at 100 at t=0 (n = 30 cells of 2 independent, pooled experiments, mean ± SEM). The moment of damage induction is indicated with a black arrow. **(C)** siRNA transfected cells as used in the live-

cell imaging experiments (A and B) were lysed directly after the experiment. Lysates were analysed by Western blot with the indicated antibodies. Tubulin was used as loading control. **(D)** Relative GFP-CSB accumulation in CS-B (CS1AN) cells at sites of LUD in cells transfected with the indicated siRNA. GFP fluorescence intensity at LUD was measured over time using live-cell confocal imaging and normalised to pre-damage intensity set at 100 at t=0 (n > 25 cells of 2 independent experiments , mean ± SEM). The black arrow indicated the moment of damage induction. Representative images are shown in Supplemental Figure 1 B. **(E)** Relative GFP-UVSSA accumulation at sites of LUD in control and NAP1L1 depleted cells. Representative images and knock down efficacy are shown in Supplemental Figure 1C and D respectively. GFP fluorescence intensity at LUD was measured over time using live-cell confocal imaging and normalised to pre-damage intensity set at 100 at t=0 (n > 30 cells, 2 independent experiments , mean ± SEM). The black arrow indicates the moment of damage induction. **(F)** XP186LV patient cells (XP-C; GG-NER-deficient) were transfected with non-targeting control (CTRL) siRNA and siRNA against CSB and Spt16. Cells were irradiated with UV-C (8 J/m²) or mock-treated as indicated, and subsequently labelled for 7 h with EdU. The efficacy of the gap-filling synthesis was assessed by measuring the fluorescently labelled, incorporated EdU into the DNA. Amplified UDS signals were quantified (upper panel) by confocal microscopy measurement of the total nuclear fluorescence (Alexa-Fluor 488 nm, n>170 cells for each condition, two independent experiments, mean ± SEM) and representative images (lower panel) are shown.

represents the last step of NER [36]. To specifically quantify the TC-NER-mediated UDS, this assay was performed in non-cycling GG-NER deficient cells (XP-C) and combined with a signal amplification step [36]. In control siRNA transfected cells a clear UV-induced and TC-NER-specific UDS signal was observed, which was severely reduced following CSB depletion (Figure 4E). Interestingly, also upon siRNA mediated knockdown of Spt16, the TC-NER mediated UDS was significantly reduced. This indicates that Spt16 plays an important role in TC-NER by enhancing UVSSA recruitment, thereby subsequently stimulating transcription restart.

## Spt16 has a function in TC-NER

Previously, we have shown that Spt16 stimulates accelerated exchange of histones H2A/H2B at sites of UV-induced damage [34]. The identified interaction of Spt16 with UVSSA (Figure 3) together with the finding that both factors are recruited to DNA damage sites [14, 34] (Figure 4A and 5D), prompted us to test whether UVSSA is involved in damage-induced accelerated exchange of histones H2A/H2B. Hence, we compared the UV-induced histone H2A exchange in UVSSA proficient and deficient cells. Histone exchange at DNA damagewas determined in living cells by inducing local UV-C damage in a photobleached area of cells stably expressing GFP-H2A [34]. Areas in the photobleached half of the nucleus that feature a higher histone exchange rate are characterized by an increased local GFP-H2A fluorescence, due to eviction of photobleached GFP-H2A followed by incorporation of fluorescent (non-photobleached) GFP-H2A
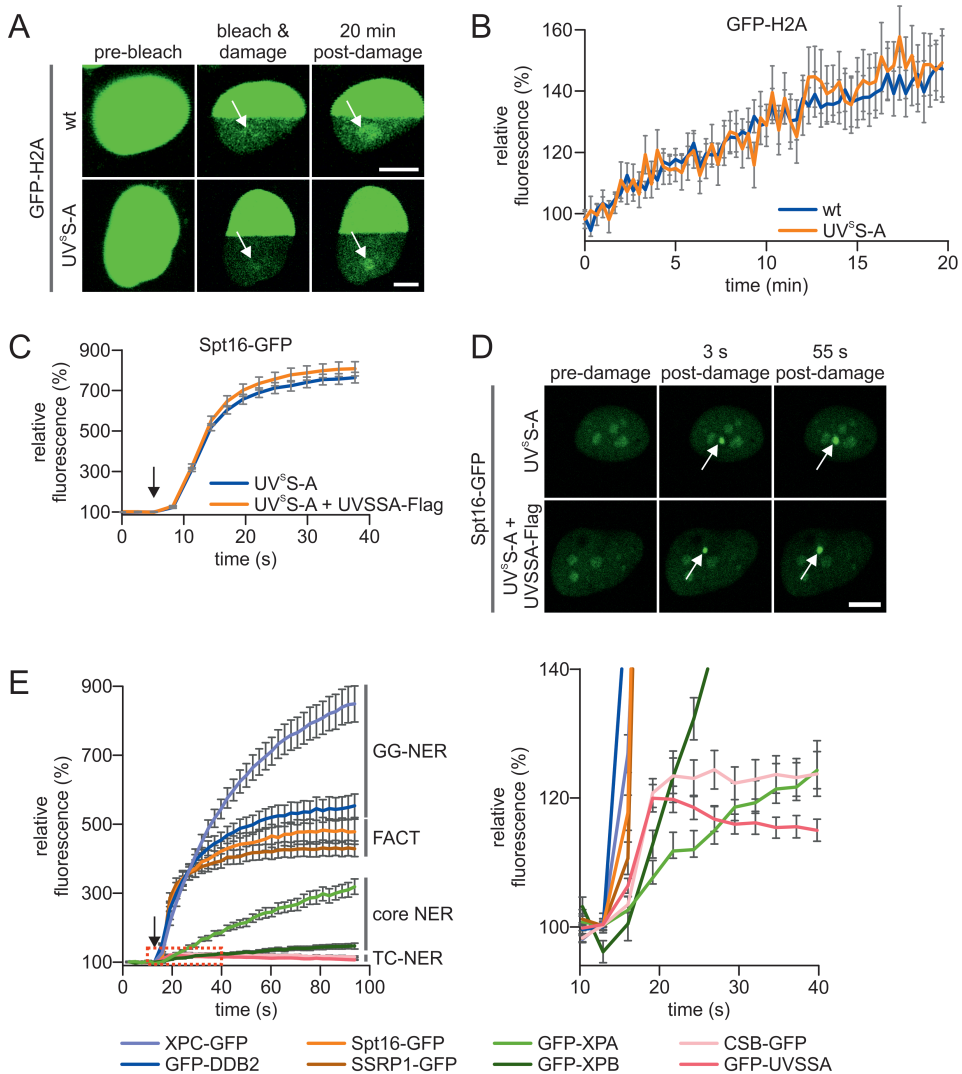
**Figure 5: Spt16 is recruited to DNA damage early during TC-NER and independent of UVSSA. (A)** Representative images of live-cell analysis of stable GFP-H2A expressing TC-NER proficient (HeLa cells, top panel) or UV$^s$S-A (TA24 cells, lower panel) cells. Left panel, unbleached cells. After photobleaching half of the nucleus, (middle panel), local UV-damage (indicated with a white arrow)was inflicted with an UV-C (266 nm) laser in the bleached half of the nucleus. H2A-GFP exchange was imaged over time. Scale bar: 7.5 μm. **(B)** The recovery of fluorescence in damaged and undamaged areas of the photobleached half of the nucleus is quantified in time. GFP-H2A exchange rate at LUD is depicted, normalized to the undamaged area (n = 15 cells from 2 independent mean ± SEM). **(C)** Relative Spt16-GFP accumulation at sites of LUD in UV$^s$S-A deficient and complemented cells. GFP fluorescence intensity at LUD was measured over time using live-cell confocal imaging and was normalised to pre-damage intensity at t=0, which was set to 100 (n = 30 cells, 2 independent experiments, mean ± SEM). The moment of damage induction is indicated with a black arrow. **(D)** Representative images of live-cell imaging analysis of Spt16-GFP expressed in either UV$^s$S-A

deficient or in UV$^S$SA complemented (UVSSA-Flag) cells (lower panel). The white arrow indicates areas of UV-C laser (266 nm) induced DNA damage. Scale bar: 7.5 μm. **(E)** Quantification of the GFP fluorescence intensity of cells stably expressing the indicated GFP-tagged NER proteins, GFP-tagged Spt16 or SSRP1. Cells subjected to local UV-C laser (266nm) induced DNA damage were imaged over time. All cells were imaged and damaged under the exact same conditions. Fluorescence at LUD was normalised to pre-damage fluorescence at t=0, which was set to 100 (n = 20 cells, 2 independent experiments,mean ± SEM). The moment of damage induction is indicated with a black arrow. Right graph shows zoomed graph of the indicated box, to clearly illustrate the kinetics of TC-NER factors. Representative images are shown in Supplemental Figure 2.

**3**

(Figure 5A). Histone exchange was quantified by comparing the recovery of GFP-H2A signal at sites of LUD with an undamaged region in the bleached part of the nucleus (Figure 5B). Both in UV$^S$S-A (TA24) and TC-NER proficient cells (HeLa), a comparable UV-induced H2A exchange was observed. This indicates that the Spt16 mediated H2A exchange at sites of DNA damage is independent of UVSSA. Together with the Spt16-dependent UVSSA accumulation, this suggests that the Spt16 recruitment acts in parallel or prior to UVSSA recruitment. To verify this, we compared the accumulation of stably expressed GFP-Spt16 to LUD in UV$^S$S-A patient cells with UV$^S$S-A complemented cells (Figure 5C and D, Supplemental Figure 1E). No difference could be observed in Spt16 accumulation. Similar results were obtained in U2OS cells stably expressing Spt16-GFP in which UVSSA was depleted using siRNA (Supplemental Figure 1F and G). The observatioin that Spt16 enhances the UVSSA accumulation to transcription blocking lesions (Figure 4B), but not vice-versa, indicates that the activity of Spt16 is needed prior to the UVSSA recruitment during TC-NER.

To test whether Spt16 is indeed a factor that is recruited at the early stages of the TC-NER reaction, we directly compared its recruitment with the accumulation kinetics of a panel of GFP-tagged NER factors that are active at different stages in the NER reaction (Figure 5E and Supplemental Figure 2). In line with previous studies [14, 54], the DNA damage recognizing GG-NER factors XPC and DDB2 showed a swift and robust accumulation (>6 fold change), while the core NER factors (XPA and XPB) involved in the more downstream damage verification step of NER featured slower accumulation kinetics with a more modest accumulation (1.5 – 3 fold change). The TC-NER specific CSB and UVSSA proteins showed a quick, but very modest accumulation (~1.2 fold change). In line with a Spt16 recruitment upstream of UVSSA recruitment, Spt16 showed a very rapid accumulation. Remarkably, Spt16 showed a more pronounced accumulation (~5 fold) than UVSSA and CSB (~1.2 fold) (Figure 5E), which might indicate a different mode of damage recruitment for Spt16 compared to TC-

NER factors. Of note, even though not essential for UVSSA recruitment, SSRP1 showed similar accumulation as Spt16 [34].

Together our data show that Spt16 functions as an early factor in the UV-DDR and plays an important role in the recruitment of UVSSA, thereby stimulating efficient transcription-coupled repair and subsequent transcription resumption.

## Discussion

Recognition of lesion-stalled Pol II is a crucial initiating step for damage removal by TC-NER and its tight regulation is expected to be critical for correct spatiotemporal formation of the TC-NER complex, remodeling of lesion-stalled Pol II and for the subsequent recruitment of downstream NER factors enabling efficient excision of TBLs [8, 55]. To gain further insight in this regulation we investigatd in detail the spatiotemporal behavior of the TC-NER initiating proteins CSA, CSB and UVSSA. We found that in living cells the accumulation kinetics of CSB and UVSSA were strikingly similar that might suggest similar modes of recruitment. Both proteins have been reported to have affinity for Pol II in unperturbed conditions, and their interaction is stabilized or their affinity is increased when bound to lesion-stalled Pol II [14, 18, 19]. Despite their highly similar recruitment kinetics, UVSSA was recruited in a CSB independent manner. Vice versa, while CSB accumulation is reduced in the absence of UVSSA [13, 14], this is most likely caused not by a direct effect of UVSSA on the initial CSB recruitment, but rather, by the stabilization of CSB via the deubiquitylating activity of the UVSSA binding partner USP7 [13, 14]. Interestingly, even though the crucial TC-NER factor CSA has been shown to directly interact with both UVSSA [27] and CSB [24], it could hardly be detected at sites of UV-induced DNA. The absence of CSA at sites of DNA damage might be explained by the fact that CSA binds transiently to the TC-NER complex. This is in line with a general highly dynamic nature of interactions of E3 ligases with their substrates. Furthermore, this suggests that, in contrast to CSB and UVSSA, CSA has no structural or scaffold-like function in the TC-NER complex. Of note, the expected short residence time of CSA on TBLs makes it unlikely that CSA is responsible for recruiting UVSSA to UV-induced DNA damage via a direct protein interaction, as previously suggested based on cellular fractionation assays [13, 27].

In this study we precisely determined the accumulation kinetics in living cells and show that UVSSA accumulation is similar in TC-NER proficient and CSA and CSB deficient cells, indicating that the recruitment of UVSSA to sites of DNA damage is not influenced by CSA or CSB. The CSA independent accumulation of UVSSA was further shown by the use of UVSSA deletion mutants lacking either the N-terminal VHS or C-terminal DUF2043 domain. Of note, deletion of either domain resulted in a severe UV-sensitivity and a reduced transcription resumption following irradiation [15]. Interestingly, while deletion of the VHS domain resulted in the complete loss of CSA interaction [27], this mutant was recruited to DNA damage with exactly the same kinetics as full length UVSSA. Conversely, deletion of the DUF2043 domain resulted in a severe reduction of UVSSA recruitment, without affecting the CSA interaction. These experiments show that the UVSSA recruitment at sites of TBLs can be separated from its interaction with CSA.

A plausible explanation for the apparent contrasting results on the role of CSA and CSB in the UVSSA recruitment [13, 14, 27, 56] could be that the initial UVSSA recruitment to lesion stalled Pol II, as determined in live-cell imaging experiments, is completely independent of CSA and CSB. However, the direct interaction between CSA and UVSSA, or another activity of CSA, might play an important role in the subsequent stabilization of the TC-NER complex. This complex stabilizing function of CSA might explain the loss of UVSSA near TBLs in the absence of CSA [13, 27], as weak or transient interactions might be lost during fractionation or immunoprecipitation assays. The CSA-independent UVSSA accumulation during live-cell experiments is also in line with previous studies. For example, the ATP-dependent chromatin remodeler SWI/SNF-related matrix-associated actin-dependent regulator of chromatin subfamily A member 5 (SMARCA5) stimulates CSB (and presumably CSA) recruitment to UV-induced DNA damage, but does not affect UVSSA recruitment [44]. Furthermore, while CSA is dispensable for the attraction of TFIIH to lesion-stalled Pol II [57], functional TFIIH is essential for the CSA translocation to damaged chromatin [58]. The recent suggestion that UVSSA recruits TFIIH [25], supports a model in which UVSSA is recruited prior and independent of CSA. This model raises an interesting question regarding the physiological fucntion of the observed CSA-UVSSA interaction that can be detected even in unperturbed conditions [13, 15, 27, 29]. A specific mutation in CSA (W361C), which abolishes the interaction with UVSSA, results in the development of UV$^S$S [27], indicating the importance of the CSA-UVSSA interaction for efficient TC-NER. It is tempting to speculate that the intrinsic affinity of UVSSA for CSA might be involved in the recruitment of

the CRL4[CSA] E3 ligase to DNA damage. Otherwise, as CSA has affinity for CSB as well [24], it may play an important role in the stabilization or proper conformation of the TC-NER complex.

To identify proteins involved in the recruitment of UVSSA we performed interaction proteomics. Among the top interacting proteins were the established UVSSA binding partners USP7 and the DDB1 and CUL4B subunits of the CRL4[CSA] complex [13, 14, 27] showing the validity of our approach (Figure 3A). To identify factors involved in UVSSA recruitment we assumed that their interaction would be dependent on the DUF2043 domain, which is crucial for its localization to TBLs. Interestingly, in addition to the loss of interaction with FACT subunits Spt16 and SSRP1, many other interactions were lost upon deletion of the DUF2043 domain, suggesting that this domain is a hotspot for interactions. For example, our MS analysis shows that the DUF2043 domain is essential for the UVSSA interaction with the U2 and U5 snRNP splicing factors SF3B1, SF3B2 and PRPF8. The interactions with these U2 and U5 snRNPs might be explained by the affinity of UVSSA for elongating Pol II in both unperturbed or DNA damage conditions [14]. These late-stage splicing factors have been shown to be displaced from the chromatin following TBL induction, thereby increasing R-Loop formation and activation of ATM signaling [59]. The identified interaction with these splicing factors might indicate a role for UVSSA in these transcription-coupled processes during the DNA damage response.

In this study we focused on the role of Spt16 in the regulation of UVSSA and TC-NER, as we have previously identified this subunit of the H2A/H2B histone chaperone FACT to be involved in the UV-induced H2A/H2B exchange and to stimulate transcription restart following DNA damage [34]. However, thus far the exact mechanism of how Spt16 regulates TC-NER remains unknown. In line with the interaction of Spt16 being dependent on the DUF2043 domain of UVSSA, we found that Spt16 is required for the recruitment of UVSSA to damged DNA. The ~50% reduction of UVSSA recruitment following SPT16 depletion, caused severe effects on the TC-NER mediated repair, as shown by a strong impediment of the TC-NER specific gap-filling synthesis. This reduced repair efficiency can explain the previously observed inhibition of transcription restart and UV-sensitivity upon Spt16 knockdown [34]. However, additional effects of Spt16 on the transcription restart process independent of repair, as shown for Dot1L [60], cannot be excluded.

The effects of Spt16 on UVSSA recruitment, as well as transcription restart and UV-sensitivity [34], are independent of SSRP1, its canonical binding partner in the FACT complex. Despite being not essential for TC-NER, SSRP1 interacts with UVSSA and has similar accumulation kinetics at DNA damage sites as Spt16. Although, it remains unknown how Spt16 and SSRP1 are recruited to sites of DNA damage, Spt16 seems to be the driving force of the FACT accumulation, as the SSRP1 accumulation at UV-induced DNA damage dependends on the presence of Spt16 [34]. Spt16 accumulation occurs early during the repair reaction and independent of other TC-NER initiating factors (Figure 5C-E) [34]. In addition, Spt16 and SSRP1 showed, in comparative DNA damage accumulation experiments, a striking pattern. Like TC-NER factors, FACT accumulated almost instantaneously following DNA damage infliction. However, while CSB and UVSSA only showed a modest ~1,2 fold accumulation, FACT subunits showed a 5 fold accumulation, almost to the same extent as the highly efficient DNA damage recognizing GG-NER factors DDB2 and XPC. This might suggest that Spt16 has, in addition to what is described for SSRP1 [50, 53], damage recognizing capabilities, either by directly recognizing the lesion, or indirectly, for example by sensing damage-induced transcription impediment. Furthermore, these differences in fold accumulation might indicate that a multitude of Spt16 molecules are present near TBLs compared to the TC-NER proteins CSB and UVSSA.

We found that H2A/H2B exchange at sites of DNA damage was independent of UVSSA. This indicates that UVSSA interaction with Spt16 is not needed to induce accelerated histone exchange at TBLs, but rather suggests that Spt16-mediated histone exchange mediates efficient UVSSA recruitment or, alternatively, that is important for the stable incorporation of UVSSA in the TC-NER complex. However, this effect is not caused by a general inhibition of histone turnover, as knockdown of Nucleosome assembly protein 1-like 1 (NAP1L1), another H2A/H2B chaperone, did not affect UVSSA recruitment (Figure 4E).

Although transcription and thus also TC-NER, occurs in a more open and therefore accessible chromatin state, several chromatin remodeling enzymes were shown to be necessary for efficient repair and transcription restart [4, 42]. For example, example, Nap1L1 stimulates the ATP-dependent chromatin remodeling activity of CSB [61]. In addition, in our UVSSA interaction screen we also identified CHD4 as putative TC-NER-involved chromatin remodeller (Supplemental table 1 ). While CHD4 has been reported to be involved in the DDR [62, 63], it is currently unknown whether it is involved in TC-NER. Thus far, the only two chromatin

modifying factors shown to influence accumulation of TC-NER factors are Spt16, which stimulates UVSSA recruitment, and the ATP dependent chromatin remodeller SMARCA5, which facilitates recruitment of CSB [44]. Interestingly, both factors act at specific TC-NER reaction steps; SMARCA5 does not affect UVSSA recruitment and Spt16 is not involved in the CSB recruitment. This suggests that the involvement of these chromatin modifiers in TC-NER is not restricted simply to making the chromatin accessible. The need for different chromatin modifying enzymes for recruitment of CSB and UVSSA strengthens our observation that, despite their similar accumulation kinetics, these TC-NER initiating factors are independently recruited [14] to damaged chromatin. Furthermore, this suggest that both SMARCA5 and Spt16 stimulate specific changes in the chromatin, e.g. nucleosome sliding or histone exchange, that are important during different TC-NER reaction steps. In line with this notion, distinct functions for CSB and UVSSA during TC-NER have been described. CSB was suggested to stimulate Pol II forward translocation, thereby discriminating between lesion-stalled Pol II and other non-forward translocating Pol II complexes, e.g Pol II stalled on naturally occurring pause sites [19]. UVSSA was shown to recruit TFIIH via a direct interaction with P62 in a similar manner as XPC recruits TFIIH in GG-NER [64]. Collectively, these observations would suggest that SMARCA5 is involved in remodeling lesion-stalled Pol II, while Spt16 either recruits or allows TFIIH to properly function during the TC-NER reaction. In summary, this study provides important new insight in the regulation of TC-NER and more specifically in the assembly of the TC-NER complex. Furthermore, these results highlight that different chromatin modulating factors regulate distinct steps of the highly orchestrated TC-NER pathway.

## Conflict of interest statement

None declared.

## Funding

**3**

## Acknowledgements

# References

1.    Brueckner, F., et al., *CPD damage recognition by transcribing RNA polymerase II.* Science, 2007. **315**(5813): p. 859-62.
2.    Shin, J.H., L. Xu, and D. Wang, *RNA polymerase II acts as a selective sensor for DNA lesions and endogenous DNA modifications.* Transcription, 2016. **7**(3): p. 57-62.
3.    Vermeij, W.P., J.H. Hoeijmakers, and J. Pothof, *Aging: not all DNA damage is equal.* Curr Opin Genet Dev, 2014. **26**: p. 124-30.
4.    Steurer, B. and J.A. Marteijn, *Traveling Rocky Roads: The Consequences of Transcription-Blocking DNA Lesions on RNA Polymerase II.* J Mol Biol, 2017. **429**(21): p. 3146-3155.
5.    Hanawalt, P.C. and G. Spivak, *Transcription-coupled DNA repair: two decades of progress and surprises.* Nat Rev Mol Cell Biol, 2008. **9**(12): p. 958-70.
6.    Marteijn, J.A., et al., *Understanding nucleotide excision repair and its roles in cancer and ageing.* Nat Rev Mol Cell Biol, 2014. **15**(7): p. 465-81.
7.    Tornaletti, S., *Transcription arrest at DNA damage sites.* Mutat Res, 2005. **577**(1-2): p. 131-45.
8.    Spivak, G., *Transcription-coupled repair: an update.* Arch Toxicol, 2016. **90**(11): p. 2583-2594.
9.    Spivak, G., *UV-sensitive syndrome.* Mutat Res, 2005. **577**(1-2): p. 162-9.
10.   Karikkineth, A.C., et al., *Cockayne syndrome: Clinical features, model systems and pathways.* Ageing Res Rev, 2017. **33**: p. 3-17.
11.   Laugel, V., *Cockayne syndrome: the expanding clinical and mutational spectrum.* Mech Ageing Dev, 2013. **134**(5-6): p. 161-70.
12.   Cleaver, J.E., E.T. Lam, and I. Revet, *Disorders of nucleotide excision repair: the genetic and molecular basis of heterogeneity.* Nat Rev Genet, 2009. **10**(11): p. 756-68.
13.   Zhang, X., et al., *Mutations in UVSSA cause UV-sensitive syndrome and destabilize ERCC6 in transcription-coupled DNA repair.* Nat Genet, 2012. **44**(5): p. 593-7.
14.   Schwertman, P., et al., *UV-sensitive syndrome protein UVSSA recruits USP7 to regulate transcription-coupled repair.* Nat Genet, 2012. **44**(5): p. 598-602.
15.   Nakazawa, Y., et al., *Mutations in UVSSA cause UV-sensitive syndrome and impair RNA polymerase IIo processing in transcription-coupled nucleotide-excision repair.* Nat Genet, 2012. **44**(5): p. 586-92.
16.   Spivak, G., *The many faces of Cockayne syndrome.* Proc Natl Acad Sci U S A, 2004. **101**(43): p. 15273-4.
17.   Selby, C.P. and A. Sancar, *Human transcription-repair coupling factor CSB/ERCC6 is a DNA-stimulated ATPase but is not a helicase and does not disrupt the ternary transcription complex of stalled RNA polymerase II.* J Biol Chem, 1997. **272**(3): p. 1885-90.
18.   van den Boom, V., et al., *DNA damage stabilizes interaction of CSB with the transcription elongation machinery.* J Cell Biol, 2004. **166**(1): p. 27-36.
19.   Xu, J., et al., *Structural basis for the initiation of eukaryotic transcription-coupled DNA repair.* Nature, 2017. **551**(7682): p. 653-657.
20.   Troelstra, C., et al., *ERCC6, a member of a subfamily of putative helicases, is involved in Cockayne's syndrome and preferential repair of active genes.* Cell, 1992. **71**(6): p. 939-53.
21.   Kamiuchi, S., et al., *Translocation of Cockayne syndrome group A protein to the nuclear matrix: possible relevance to transcription-coupled DNA repair.* Proc Natl Acad Sci U S A, 2002. **99**(1): p. 201-6.
22.   Groisman, R., et al., *The ubiquitin ligase activity in the DDB2 and CSA complexes is differentially regulated by the COP9 signalosome in response to DNA damage.* Cell, 2003. **113**(3): p. 357-67.
23.   Fischer, E.S., et al., *The molecular basis of CRL4DDB2/CSA ubiquitin ligase architecture, targeting, and activation.* Cell, 2011. **147**(5): p. 1024-39.
24.   Groisman, R., et al., *CSA-dependent degradation of CSB by the ubiquitin-proteasome pathway establishes a link between complementation factors of the Cockayne syndrome.* Genes Dev, 2006. **20**(11): p. 1429-34.
25.   Okuda, M., et al.
26.   de Boer, J. and J.H. Hoeijmakers, *Nucleotide excision repair and human syndromes.* Carcinogenesis, 2000. **21**(3): p. 453-60.
27.   Fei, J. and J. Chen, *KIAA1530 protein is recruited by Cockayne syndrome complementation group protein A (CSA) to participate in transcription-coupled repair (TCR).* J Biol Chem, 2012. **287**(42): p. 35118-26.
28.   Campeau, E., et al., *A versatile viral system for expression and depletion of proteins in mammalian cells.* PLoS One, 2009. **4**(8): p. e6529.

29.  Pines, A., et al., *TRiC controls transcription resumption after UV damage by regulating Cockayne syndrome protein A*. Nat Commun, 2018. **9**(1): p. 1040.
30.  Hoogstraten, D., et al., *Versatile DNA damage detection by the global genome nucleotide excision repair protein XPC.* J Cell Sci, 2008. **121**(Pt 17): p. 2850-9.
31.  Rademakers, S., et al., *Xeroderma pigmentosum group A protein loads as a separate factor onto DNA lesions.* Mol Cell Biol, 2003. **23**(16): p. 5755-67.
32.  Hoogstraten, D., et al., *Rapid Switching of TFIIH between RNA Polymerase I and II Transcription and DNA Repair In Vivo.* Molecular Cell, 2002. **10**(5): p. 1163-1174.
33.  Pines, A., et al., *PARP1 promotes nucleotide excision repair through DDB2 stabilization and recruitment of ALC1.* J Cell Biol, 2012. **199**(2): p. 235-49.
34.  Dinant, C., et al., *Enhanced chromatin dynamics by FACT promotes transcriptional restart after UV-induced DNA damage.* Mol Cell, 2013. **51**(4): p. 469-79.
35.  Dinant, C., et al., *Activation of multiple DNA repair pathways by sub-nuclear damage induction methods.* J Cell Sci, 2007. **120**(Pt 15): p. 2731-40.
36.  Wienholz, F., W. Vermeulen, and J.A. Marteijn, *Amplification of unscheduled DNA synthesis signal enables fluorescence-based single cell quantification of transcription-coupled nucleotide excision repair.* Nucleic Acids Res, 2017. **45**(9): p. e68.
37.  Schindelin, J., et al., *Fiji: an open-source platform for biological-image analysis.* Nat Methods, 2012. **9**(7): p. 676-82.
38.  Cox, J., et al., *Andromeda: a peptide search engine integrated into the MaxQuant environment.* J Proteome Res, 2011. **10**(4): p. 1794-805.
39.  Rothbauer, U., et al., *A versatile nanotrap for biochemical and functional studies with fluorescent fusion proteins.* Mol Cell Proteomics, 2008. **7**(2): p. 282-9.
40.  Higa, M., et al., *Stabilization of Ultraviolet (UV)-stimulated Scaffold Protein A by Interaction with Ubiquitin-specific Peptidase 7 Is Essential for Transcription-coupled Nucleotide Excision Repair.* J Biol Chem, 2016. **291**(26): p. 13771-9.
41.  Lans, H., J.A. Marteijn, and W. Vermeulen, *ATP-dependent chromatin remodeling in the DNA-damage response.* Epigenetics Chromatin, 2012. **5**: p. 4.
42.  Mandemaker, I.K., W. Vermeulen, and J.A. Marteijn, *Gearing up chromatin: A role for chromatin remodeling during the transcriptional restart upon DNA damage.* Nucleus, 2014. **5**(3): p. 203-10.
43.  Czaja, W., P. Mao, and M.J. Smerdon, *The emerging roles of ATP-dependent chromatin remodeling enzymes in nucleotide excision repair.* Int J Mol Sci, 2012. **13**(9): p. 11954-73.
44.  Aydin, O.Z., et al., *Human ISWI complexes are targeted by SMARCA5 ATPase and SLIDE domains to help resolve lesion-stalled transcription.* Nucleic Acids Res, 2014. **42**(13): p. 8473-85.
45.  Orphanides, G., et al., *FACT, a factor that facilitates transcript elongation through nucleosomes.* Cell, 1998. **92**(1): p. 105-16.
46.  Tsunaka, Y., et al., *Integrated molecular mechanism directing nucleosome reorganization by human FACT.* Genes Dev, 2016. **30**(6): p. 673-86.
47.  Winkler, D.D. and K. Luger, *The histone chaperone FACT: structural insights and mechanisms for nucleosome reorganization.* J Biol Chem, 2011. **286**(21): p. 18369-74.
48.  Gao, Y., et al., *SSRP1 Cooperates with PARP and XRCC1 to Facilitate Single-Strand DNA Break Repair by Chromatin Priming.* Cancer Res, 2017. **77**(10): p. 2674-2685.
49.  Charles Richard, J.L., et al., *FACT Assists Base Excision Repair by Boosting the Remodeling Activity of RSC.* PLoS Genet, 2016. **12**(7): p. e1006221.
50.  Yarnell, A.T., et al., *Interaction of FACT, SSRP1, and the high mobility group (HMG) domain of SSRP1 with DNA damaged by the anticancer drug cisplatin.* J Biol Chem, 2001. **276**(28): p. 25736-41.
51.  Oliveira, D.V., et al., *Histone chaperone FACT regulates homologous recombination by chromatin remodeling through interaction with RNF20.* J Cell Sci, 2014. **127**(Pt 4): p. 763-72.
52.  Keller, D.M. and H. Lu, *p53 serine 392 phosphorylation increases after UV through induction of the assembly of the CK2.hSPT16.SSRP1 complex.* J Biol Chem, 2002. **277**(51): p. 50206-13.
53.  Krohn, N.M., et al., *Protein kinase CK2 phosphorylates the high mobility group domain protein SSRP1, inducing the recognition of UV-damaged DNA.* J Biol Chem, 2003. **278**(15): p. 12710-5.
54.  Marteijn, J.A., et al., *Nucleotide excision repair-induced H2A ubiquitination is dependent on MDC1 and RNF8 and reveals a universal DNA damage response.* J Cell Biol, 2009. **186**(6): p. 835-47.

**3**

55. Marteijn, J.A., J.H. Hoeijmakers, and W. Vermeulen, *Check, Check ...Triple Check: Multi-Step DNA Lesion Identification by Nucleotide Excision Repair.* Mol Cell, 2015. **59**(6): p. 885-6.

56. Schwertman, P., W. Vermeulen, and J.A. Marteijn, *UVSSA and USP7, a new couple in transcription-coupled DNA repair.* Chromosoma, 2013. **122**(4): p. 275-84.

57. Fousteri, M. and L.H. Mullenders, *Transcription-coupled nucleotide excision repair in mammalian cells: molecular mechanisms and biological effects.* Cell Res, 2008. **18**(1): p. 73-84.

58. Saijo, M., et al., *Functional TFIIH is required for UV-induced translocation of CSA to the nuclear matrix.* Mol Cell Biol, 2007. **27**(7): p. 2538-47.

59. Tresini, M., et al., *The core spliceosome as target and effector of non-canonical ATM signalling.* Nature, 2015. **523**(7558): p. 53-8.

60. Oksenych, V., et al., *Histone methyltransferase DOT1L drives recovery of gene expression after a genotoxic attack.* PLoS Genet, 2013. **9**(7): p. e1003611.

61. Cho, I., et al., *ATP-dependent chromatin remodeling by Cockayne syndrome protein B and NAP1-like histone chaperones is required for efficient transcription-coupled DNA repair.* PLoS Genet, 2013. **9**(4): p. e1003407.

62. Burd, C.J., et al., *UV radiation regulates Mi-2 through protein translation and stability.* J Biol Chem, 2008. **283**(50): p. 34976-82.

63. O'Shaughnessy, A. and B. Hendrich, *CHD4 in the DNA-damage response and cell cycle progression: not so NuRDy now.* Biochem Soc Trans, 2013. **41**(3): p. 777-82.

64. Okuda, M., et al., *Common TFIIH recruitment mechanism in global genome and transcription-coupled repair subpathways.* Nucleic Acids Res, 2017. **45**(22): p. 13043-13055.

**3**
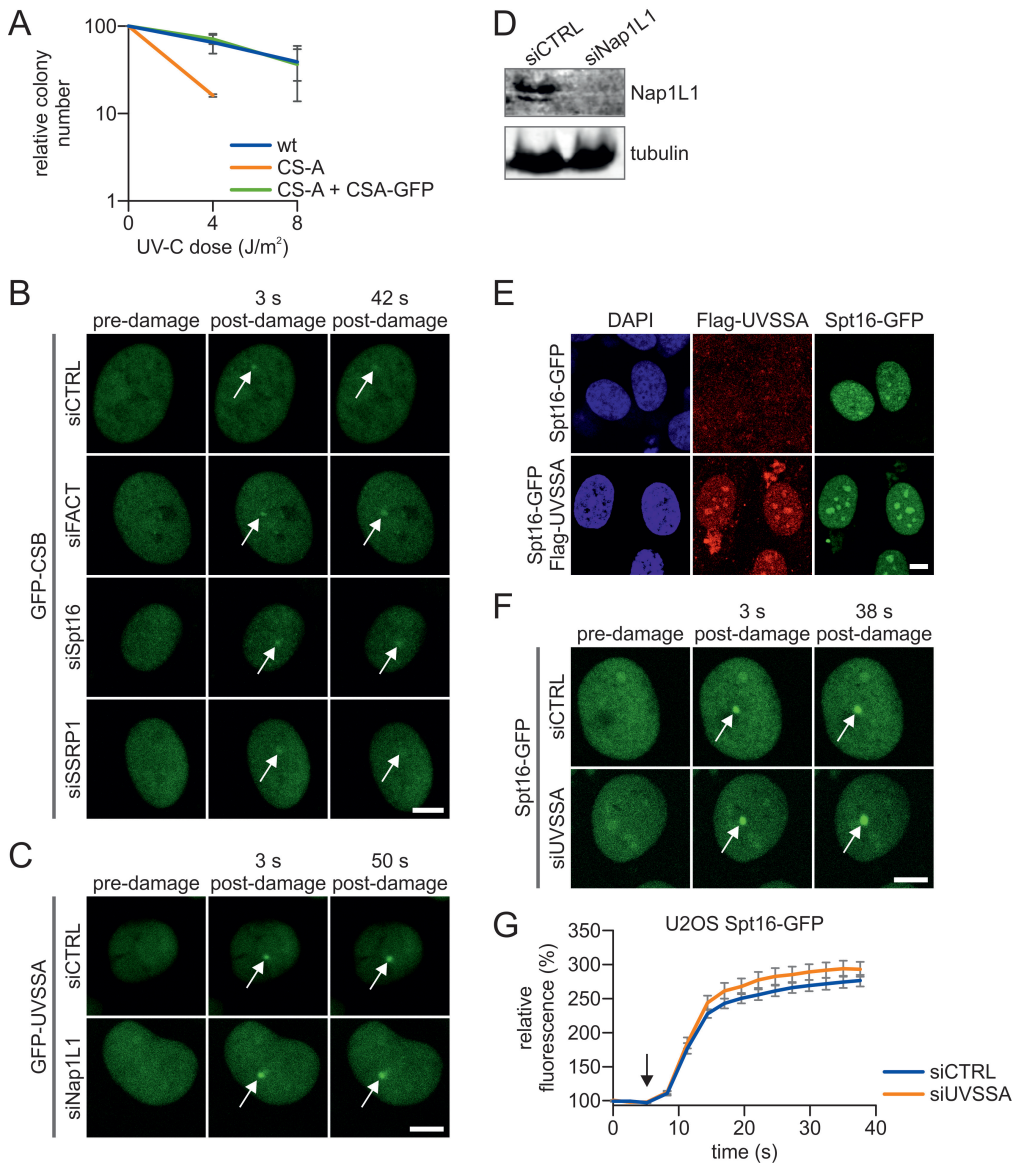
**Supplemental Figure 1: (A)** Colony survival of wt (VH10), CS-A (CS3BE) and CS-A cells complemented with CSA-GFP (CS3BE + CSA-GFP) following UV irradiation. The percentage of surviving cells, normalized to undamaged conditions is plotted against the applied UV-C (J/m²) dose. Data represent two pooled, independent experiments ± standard deviation. **(B)** Representative images of the accumulation of CSB in CS-B (CS1AN) cells upon local DNA damage induction using a UV-C (266nm) laser. Cells were transfected with the indicated siRNAs (siFACT: combination of both siSpt16 and siSSRP1. siCTRL: is a non-targeting siRNA). GFP fluorescence intensity at LUD (indicated by a white arrow) was measured over time using live-cell confocal imaging. Scale bar: 7.5 μm. **(C)** Representative images of the accumulation of UVˢS-A cells stably expressing GFP-UVSSA, transfected with CTRL or Nap1L1 siRNA. GFP fluorescence intensity was measured over time at LUD (indicated by a white arrow) using

live-cell confocal imaging. Scale bar: 7.5 µm. **(D)** Knock down efficacy of Nap1L1 was determined by Western blotting using Nap1L1 antibody, tubulin is used as loading control. **(E)** UV^{S}S-A (TA24) stably expressing Spt16-GFP (top panel) or Spt16-GFP and Flag-UVSSA (bottom panel) were subjected to immunofluorescence to determine expression of Flag-UVSSA in all cells (Alexa-Fluor 594). Nuclei were visualized by DAPI staining. **(F)** Representative images of U2OS cells stably expressing Spt16-GFP, transfected with indicated siRNA's. Spt16-GFP accumulation (indicated by a white arrow) upon local exposure to UV-C (266nm) laser-induced DNA damage was measured by monitoring GFP fluorescence intensity over time using live-cell confocal imaging. Scale bar: 7.5 µm. **(G)** Quantification of the GFP fluorescence intensity at LUD was normalised to pre-damage fluorescence at t=0, which was set to 100 (n = 30 cells of 2 independent experiments were pooled, mean ± SEM). The moment of damage induction is indicated with a black arrow.

3
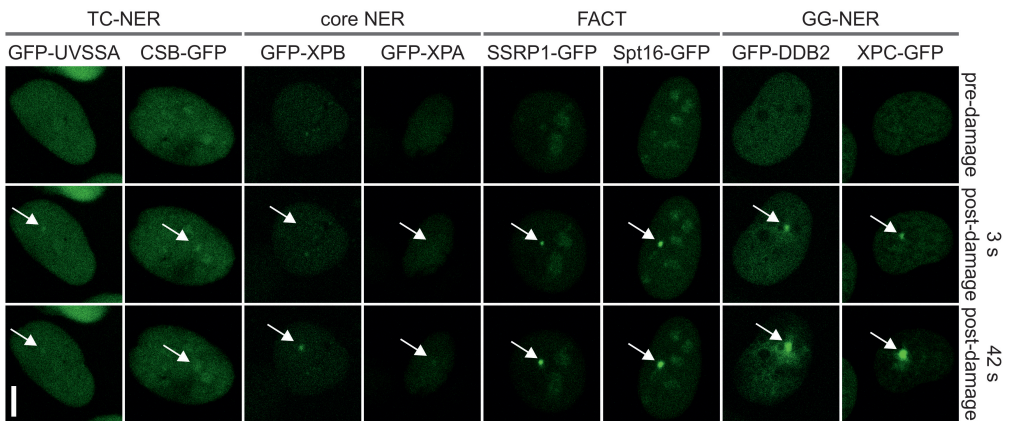


**Supplemental Figure 2:** Representative images of quantification plotted in Figure 5E. Cells stably expressing the indicated GFP-tagged NER proteins were followed over time after UV-C laser (266nm) induced DNA damage (indicated by a white arrow). All cells expressing fluorescent protein tagged-NER factors, Spt16-GFP or SSRP1-GFP were imaged and damaged under the exact same conditions. Scale bar: 7.5 µm.

**Supplemental Table 1:** Proteins identified with increased normalised SILAC ratios in the GFP vs GFP-UVSSA and wt vs ΔDUF mass spectrometry screen and with non-responding normalised SILAC ratios in the wt vs ΔVHS mass spectrometry screen. Proteins are sorted based on the SILAC ratios in the wt vs ΔDUF screen in a descending manner.

| Gene names | GFP vs GFP-UVSSA | | | wtvsΔDUF | | | wt vs ΔVHS | | |
|---|---|---|---|---|---|---|---|---|---|
| | Ratio F | Ratio R | Average | Ratio F | Ratio R | Average | Ratio F | Ratio R | Average |
| SUPT16H* | 1.90 | 4.29 | 3.09 | 8.29 | 2.96 | 5.63 | 1.09 | 0.78 | 0.94 |
| SNRNP200 | 1.65 | 6.72 | 4.18 | 8.04 | 2.55 | 5.30 | 1.39 | 1.02 | 1.20 |
| CHD4 | 1.96 | 4.63 | 3.29 | 6.81 | 3.70 | 5.26 | 1.25 | 0.86 | 1.06 |
| KIF4A;KIF4B | 1.87 | 6.04 | 3.96 | 7.51 | 2.89 | 5.20 | 1.39 | 0.90 | 1.14 |
| SF3B2 | 2.30 | 4.65 | 3.48 | 6.96 | 3.07 | 5.01 | 1.11 | 1.07 | 1.09 |
| SMARCC2 | 1.58 | 5.44 | 3.51 | 6.56 | 3.33 | 4.95 | 1.22 | 1.00 | 1.11 |
| SF3B1 | 1.55 | 3.40 | 2.47 | 6.90 | 2.81 | 4.85 | 1.16 | 1.02 | 1.09 |
| PRPF8 | 1.97 | 4.05 | 3.01 | 6.61 | 2.41 | 4.51 | 1.30 | 0.94 | 1.12 |
| MCM5 | 1.87 | 2.91 | 2.39 | 6.21 | 2.15 | 4.18 | 1.06 | 0.85 | 0.96 |
| SSRP1 | 1.56 | 3.17 | 2.37 | 5.97 | 2.19 | 4.08 | 0.99 | 0.90 | 0.94 |
| XRCC5 | 2.19 | 3.50 | 2.84 | 5.99 | 2.16 | 4.07 | 1.28 | 0.99 | 1.14 |
| MCM6 | 1.94 | 2.36 | 2.15 | 5.88 | 2.22 | 4.05 | 0.97 | 0.85 | 0.91 |
| MCM3 | 1.90 | 2.23 | 2.07 | 5.72 | 2.20 | 3.96 | 1.06 | 0.83 | 0.95 |
| FEN1 | 2.09 | 3.29 | 2.69 | 5.87 | 2.02 | 3.94 | 1.05 | 0.79 | 0.92 |
| RBM12 | 1.76 | 3.26 | 2.51 | 5.42 | 2.46 | 3.94 | 1.10 | 1.04 | 1.07 |
| XRCC6 | 2.20 | 3.22 | 2.71 | 5.78 | 1.90 | 3.84 | 1.24 | 0.94 | 1.09 |
| MCM7 | 1.96 | 3.29 | 2.62 | 5.34 | 2.27 | 3.81 | 0.97 | 0.79 | 0.88 |
| MCM4 | 2.26 | 2.85 | 2.55 | 5.43 | 2.08 | 3.76 | 1.00 | 0.84 | 0.92 |
| MCM2 | 2.36 | 2.22 | 2.29 | 5.64 | 1.81 | 3.72 | 1.01 | 0.81 | 0.91 |
| TOP2A | 1.93 | 5.05 | 3.49 | 5.22 | 2.17 | 3.70 | 1.06 | 0.88 | 0.97 |
| RBBP4 | 1.52 | 3.46 | 2.49 | 4.90 | 2.07 | 3.48 | 1.19 | 1.00 | 1.10 |
| IPO5 | 8.86 | 6.84 | 7.85 | 3.34 | 3.51 | 3.43 | 0.54 | 0.71 | 0.63 |
| DDB1 | 3.20 | 3.91 | 3.55 | 4.64 | 2.07 | 3.36 | 1.13 | 1.14 | 1.13 |
| HCFC1 | 1.58 | 2.83 | 2.20 | 4.96 | 1.74 | 3.35 | 1.21 | 1.09 | 1.15 |
| DEK | 1.62 | 3.81 | 2.71 | 3.88 | 2.48 | 3.18 | 1.13 | 1.10 | 1.12 |
| SSB | 1.74 | 3.08 | 2.41 | 4.55 | 1.68 | 3.12 | 1.09 | 0.92 | 1.01 |
| GMPS | 2.33 | 2.07 | 2.20 | 3.61 | 1.94 | 2.77 | 1.23 | 0.96 | 1.09 |

* SUPT16H is the gene name for the protein Spt16

**Supplemental Table 2:** Proteins identified in the GFP vs GFP-UVSSA mass spectrometry screen. Proteins are sorted based on the averaged log2 SILAC ratio (> 0.5)

¤  Interaction increased for GFP-UVSSA

•  Interaction equal between GFP and GFP-UVSSA

| Gene names | Forward | | | Reverse | | | Ratio normalized Average | log2 ratio Average |
|---|---|---|---|---|---|---|---|---|
| | Ratio normalized | log2 ratio | Peptide count | Ratio normalized | log2 ratio | Peptide count | | |
| ¤  UVSSA | 17.28 | 4.11 | 74 | 30.41 | 4.93 | 82 | 23.85 | 4.52 |
| ¤  IPO5 | 8.86 | 3.15 | 22 | 6.84 | 2.77 | 19 | 7.85 | 2.96 |
| ¤  USP7 | 4.40 | 2.14 | 6 | 8.25 | 3.04 | 7 | 6.32 | 2.59 |
| ¤  TKT | 4.32 | 2.11 | 18 | 4.61 | 2.20 | 21 | 4.46 | 2.16 |
| ¤  MSH2 | 3.06 | 1.61 | 2 | 5.63 | 2.49 | 6 | 4.34 | 2.05 |
| ¤  SART3 | 2.68 | 1.42 | 3 | 6.38 | 2.67 | 2 | 4.53 | 2.05 |
| ¤  TRIM28 | 2.44 | 1.28 | 26 | 5.92 | 2.57 | 25 | 4.18 | 1.93 |
| ¤  TP53 | 1.64 | 0.71 | 10 | 8.39 | 3.07 | 7 | 5.02 | 1.89 |
| ¤  DDB1 | 3.20 | 1.68 | 9 | 3.91 | 1.97 | 7 | 3.55 | 1.82 |
| ¤  RECQL | 2.16 | 1.11 | 11 | 5.43 | 2.44 | 7 | 3.80 | 1.78 |
| ¤  KIF4A;KIF4B | 1.87 | 0.91 | 7 | 6.04 | 2.59 | 6 | 3.96 | 1.75 |
| ¤  PRKDC | 2.25 | 1.17 | 44 | 5.00 | 2.32 | 43 | 3.63 | 1.75 |
| ¤  PARP1 | 2.48 | 1.31 | 6 | 4.47 | 2.16 | 11 | 3.47 | 1.74 |
| ¤  SNRNP200 | 1.65 | 0.72 | 6 | 6.72 | 2.75 | 8 | 4.18 | 1.74 |
| ¤  RNF40 | 1.68 | 0.75 | 6 | 6.52 | 2.71 | 2 | 4.10 | 1.73 |
| ¤  SF3B2 | 2.30 | 1.20 | 4 | 4.65 | 2.22 | 4 | 3.48 | 1.71 |
| ¤  GTF2I | 1.87 | 0.90 | 7 | 5.72 | 2.52 | 6 | 3.79 | 1.71 |
| ¤  CUL4B | 2.36 | 1.24 | 4 | 4.25 | 2.09 | 7 | 3.31 | 1.66 |
| ¤  PSMC3 | 5.77 | 2.53 | 2 | 1.71 | 0.78 | 2 | 3.74 | 1.65 |
| ¤  TOP2A | 1.93 | 0.95 | 5 | 5.05 | 2.34 | 5 | 3.49 | 1.64 |
| ¤  SLFN11 | 2.29 | 1.20 | 5 | 4.16 | 2.06 | 3 | 3.23 | 1.63 |
| ¤  CHD4 | 1.96 | 0.97 | 3 | 4.63 | 2.21 | 3 | 3.29 | 1.59 |
| ¤  SMARCC2 | 1.58 | 0.66 | 3 | 5.44 | 2.44 | 2 | 3.51 | 1.55 |
| ¤  ANXA1 | 1.59 | 0.67 | 7 | 5.26 | 2.39 | 16 | 3.42 | 1.53 |
| ¤  SUPT16H | 1.90 | 0.92 | 5 | 4.29 | 2.10 | 10 | 3.09 | 1.51 |
| ¤  PRPF8 | 1.97 | 0.98 | 5 | 4.05 | 2.02 | 2 | 3.01 | 1.50 |
| ¤  FN1 | 2.61 | 1.38 | 11 | 2.98 | 1.58 | 31 | 2.79 | 1.48 |
| ¤  XRCC5 | 2.19 | 1.13 | 11 | 3.50 | 1.81 | 19 | 2.84 | 1.47 |
| ¤  RPA1 | 2.19 | 1.13 | 3 | 3.44 | 1.78 | 9 | 2.81 | 1.46 |
| ¤  IFI16 | 1.59 | 0.67 | 4 | 4.68 | 2.23 | 4 | 3.13 | 1.45 |
| ¤  XRCC6 | 2.20 | 1.14 | 19 | 3.22 | 1.69 | 33 | 2.71 | 1.41 |
| ¤  FEN1 | 2.09 | 1.06 | 11 | 3.29 | 1.72 | 9 | 2.69 | 1.39 |
| ¤  ACAT2 | 3.95 | 1.98 | 7 | 1.69 | 0.76 | 6 | 2.82 | 1.37 |
| ¤  SUMO2 | 1.56 | 0.64 | 8 | 4.16 | 2.06 | 7 | 2.86 | 1.35 |
| ¤  MCM4 | 2.26 | 1.18 | 5 | 2.85 | 1.51 | 7 | 2.55 | 1.34 |
| ¤  MCM7 | 1.96 | 0.97 | 11 | 3.29 | 1.72 | 4 | 2.62 | 1.34 |
| ¤  DEK | 1.62 | 0.69 | 7 | 3.81 | 1.93 | 4 | 2.71 | 1.31 |

**3**

| | | | | | | | | | |
|---|---|---|---|---|---|---|---|---|---|
| ¤ | RBM12 | 1.76 | 0.81 | 2 | 3.26 | 1.70 | 2 | 2.51 | 1.26 |
| ¤ | TMPO | 1.61 | 0.69 | 6 | 3.53 | 1.82 | 10 | 2.57 | 1.26 |
| ¤ | FASN | 2.77 | 1.47 | 193 | 2.01 | 1.01 | 182 | 2.39 | 1.24 |
| ¤ | MCM5 | 1.87 | 0.90 | 2 | 2.91 | 1.54 | 2 | 2.39 | 1.22 |
| ¤ | SSB | 1.74 | 0.80 | 3 | 3.08 | 1.62 | 2 | 2.41 | 1.21 |
| ¤ | SF3B1 | 1.55 | 0.63 | 7 | 3.40 | 1.76 | 6 | 2.47 | 1.20 |
| ¤ | RBBP4 | 1.52 | 0.61 | 10 | 3.46 | 1.79 | 9 | 2.49 | 1.20 |
| ¤ | MCM2 | 2.36 | 1.24 | 5 | 2.22 | 1.15 | 8 | 2.29 | 1.20 |
| ¤ | HMGB2 | 1.94 | 0.95 | 3 | 2.66 | 1.41 | 5 | 2.30 | 1.18 |
| ¤ | CBX5 | 2.27 | 1.18 | 3 | 2.21 | 1.14 | 5 | 2.24 | 1.16 |
| ¤ | SSRP1 | 1.56 | 0.64 | 6 | 3.17 | 1.67 | 8 | 2.37 | 1.15 |
| ¤ | GMPS | 2.33 | 1.22 | 5 | 2.07 | 1.05 | 8 | 2.20 | 1.14 |
| ¤ | NCBP1 | 1.82 | 0.86 | 3 | 2.61 | 1.38 | 4 | 2.21 | 1.12 |
| ¤ | ACLY | 2.85 | 1.51 | 31 | 1.61 | 0.69 | 35 | 2.23 | 1.10 |
| ¤ | MCM6 | 1.94 | 0.95 | 12 | 2.36 | 1.24 | 9 | 2.15 | 1.09 |
| ¤ | CSE1L | 2.14 | 1.10 | 9 | 2.10 | 1.07 | 9 | 2.12 | 1.08 |
| ¤ | HCFC1 | 1.58 | 0.66 | 3 | 2.83 | 1.50 | 2 | 2.20 | 1.08 |
| ¤ | RFC4 | 1.72 | 0.78 | 4 | 2.55 | 1.35 | 5 | 2.14 | 1.07 |
| ¤ | MCM3 | 1.90 | 0.93 | 9 | 2.23 | 1.16 | 19 | 2.07 | 1.04 |
| ¤ | G6PD | 2.35 | 1.23 | 7 | 1.73 | 0.79 | 5 | 2.04 | 1.01 |
| ¤ | FAM129B | 1.52 | 0.60 | 2 | 2.48 | 1.31 | 2 | 2.00 | 0.96 |
| ¤ | TXNRD1 | 1.91 | 0.94 | 2 | 1.89 | 0.92 | 2 | 1.90 | 0.93 |
| ¤ | RRM2 | 1.84 | 0.88 | 3 | 1.83 | 0.87 | 3 | 1.83 | 0.88 |
| ¤ | HMGB1;HMGB1P1 | 1.77 | 0.82 | 11 | 1.88 | 0.91 | 7 | 1.82 | 0.87 |
| ¤ | COPS2 | 1.87 | 0.90 | 3 | 1.74 | 0.80 | 5 | 1.80 | 0.85 |
| ¤ | DNAJA1 | 1.86 | 0.89 | 8 | 1.65 | 0.72 | 7 | 1.75 | 0.81 |
| ¤ | SMS | 1.52 | 0.60 | 4 | 1.88 | 0.91 | 2 | 1.70 | 0.76 |
| ¤ | WDR82 | 1.57 | 0.65 | 3 | 1.82 | 0.86 | 3 | 1.69 | 0.76 |
| ¤ | CDK1 | 1.68 | 0.75 | 4 | 1.63 | 0.70 | 5 | 1.65 | 0.72 |
| ¤ | CAND1 | 1.62 | 0.69 | 8 | 1.54 | 0.62 | 9 | 1.58 | 0.66 |
| ● | SFN | 1.35 | 0.44 | 2 | 15.00 | 3.91 | 4 | 8.17 | 2.17 |
| ● | RALY | 1.15 | 0.21 | 3 | 8.20 | 3.04 | 7 | 4.68 | 1.62 |
| ● | SMC1A | 1.35 | 0.43 | 15 | 4.61 | 2.20 | 9 | 2.98 | 1.32 |
| ● | SRRT | 1.49 | 0.57 | 2 | 4.04 | 2.01 | 4 | 2.76 | 1.29 |
| ● | MATR3 | 1.01 | 0.02 | 3 | 5.71 | 2.51 | 5 | 3.36 | 1.26 |
| ● | CDC5L | 1.25 | 0.32 | 2 | 4.53 | 2.18 | 5 | 2.89 | 1.25 |
| ● | HIST2H3A;HIST3H | 1.21 | 0.28 | 5 | 4.58 | 2.20 | 7 | 2.90 | 1.24 |
| ● | THRAP3 | 1.33 | 0.41 | 6 | 4.13 | 2.05 | 4 | 2.73 | 1.23 |
| ● | WDHD1 | 1.46 | 0.55 | 3 | 3.54 | 1.83 | 2 | 2.50 | 1.19 |
| ● | MTA2;DKFZp686F | 1.23 | 0.30 | 3 | 4.14 | 2.05 | 8 | 2.68 | 1.17 |
| ● | SFPQ | 1.27 | 0.34 | 18 | 3.75 | 1.91 | 10 | 2.51 | 1.12 |
| ● | HNRNPC;HNRNPC | 0.81 | -0.31 | 22 | 5.80 | 2.54 | 15 | 3.31 | 1.11 |
| ● | HNRNPU | 1.25 | 0.32 | 15 | 3.75 | 1.91 | 13 | 2.50 | 1.11 |
| ● | SNRPD2 | 1.43 | 0.51 | 5 | 3.23 | 1.69 | 6 | 2.33 | 1.10 |
| ● | NUMA1 | 0.97 | -0.05 | 9 | 4.76 | 2.25 | 10 | 2.86 | 1.10 |
| ● | H2AFV;H2AFZ | 1.21 | 0.27 | 4 | 3.80 | 1.93 | 4 | 2.51 | 1.10 |
| ● | HNRNPM | 1.04 | 0.06 | 18 | 4.33 | 2.11 | 15 | 2.68 | 1.09 |
| ● | RBMX | 0.82 | -0.29 | 4 | 5.44 | 2.44 | 5 | 3.13 | 1.07 |

| | | | | | | | | |
|---|---|---|---|---|---|---|---|---|
| ● | DHX9 | 1.32 | 0.40 | 11 | 3.35 | 1.75 | 9 | 2.34 | 1.07 |
| ● | POLD1 | 1.22 | 0.29 | 2 | 3.41 | 1.77 | 2 | 2.32 | 1.03 |
| ● | DDX5 | 1.24 | 0.31 | 11 | 3.31 | 1.73 | 14 | 2.28 | 1.02 |
| ● | HIST1H4A | 1.06 | 0.09 | 33 | 3.84 | 1.94 | 34 | 2.45 | 1.02 |
| ● | EIF4A3 | 1.27 | 0.34 | 5 | 3.21 | 1.68 | 8 | 2.24 | 1.01 |
| ● | HIST1H2BL;HIST1H | 1.11 | 0.15 | 20 | 3.62 | 1.85 | 23 | 2.37 | 1.00 |
| ● | HIST1H2AJ;HIST1H | 1.10 | 0.13 | 7 | 3.66 | 1.87 | 9 | 2.38 | 1.00 |
| ● | PRPF19 | 1.10 | 0.13 | 7 | 3.65 | 1.87 | 4 | 2.37 | 1.00 |
| ● | HIST2H2BE;HIST1H | 1.18 | 0.24 | 2 | 3.34 | 1.74 | 3 | 2.26 | 0.99 |
| ● | DDX17 | 1.47 | 0.56 | 8 | 2.67 | 1.42 | 9 | 2.07 | 0.99 |
| ● | NONO | 1.24 | 0.31 | 12 | 3.15 | 1.66 | 16 | 2.20 | 0.98 |
| ● | SF3A1 | 1.26 | 0.33 | 3 | 3.11 | 1.64 | 3 | 2.18 | 0.98 |
| ● | ATP5A1 | 2.59 | 1.37 | 5 | 1.47 | 0.56 | 4 | 2.03 | 0.97 |
| ● | DSP | 0.25 | -2.02 | 6 | 14.90 | 3.90 | 8 | 7.57 | 0.94 |
| ● | ILF2 | 0.95 | -0.08 | 5 | 3.86 | 1.95 | 2 | 2.40 | 0.94 |
| ● | HNRNPA2B1 | 0.94 | -0.09 | 20 | 3.84 | 1.94 | 27 | 2.39 | 0.92 |
| ● | HNRNPD | 1.15 | 0.20 | 9 | 3.11 | 1.63 | 15 | 2.13 | 0.92 |
| ● | PSMC4 | 2.35 | 1.23 | 3 | 1.51 | 0.59 | 4 | 1.93 | 0.91 |
| ● | DHX15 | 1.46 | 0.55 | 5 | 2.39 | 1.26 | 9 | 1.93 | 0.90 |
| ● | SMARCA5 | 1.12 | 0.17 | 6 | 3.08 | 1.62 | 4 | 2.10 | 0.90 |
| ● | HNRNPAB | 0.98 | -0.03 | 5 | 3.50 | 1.81 | 4 | 2.24 | 0.89 |
| ● | SNRPB2 | 1.25 | 0.33 | 2 | 2.73 | 1.45 | 2 | 1.99 | 0.89 |
| ● | ALYREF | 1.05 | 0.06 | 2 | 3.20 | 1.68 | 2 | 2.12 | 0.87 |
| ● | LMNA | 0.94 | -0.09 | 49 | 3.54 | 1.83 | 49 | 2.24 | 0.87 |
| ● | MIF | 2.95 | 1.56 | 3 | 1.09 | 0.13 | 4 | 2.02 | 0.84 |
| ● | WBP2 | 2.67 | 1.42 | 3 | 1.20 | 0.26 | 3 | 1.93 | 0.84 |
| ● | MAT2B | 2.27 | 1.18 | 2 | 1.41 | 0.50 | 2 | 1.84 | 0.84 |
| ● | SNRNP40 | 0.94 | -0.09 | 3 | 3.40 | 1.77 | 2 | 2.17 | 0.84 |
| ● | HNRNPA0 | 0.99 | -0.02 | 4 | 3.24 | 1.70 | 3 | 2.11 | 0.84 |
| ● | HNRNPA1;HNRNP | 0.92 | -0.11 | 14 | 3.44 | 1.78 | 18 | 2.18 | 0.83 |
| ● | SF3A3 | 1.15 | 0.20 | 3 | 2.75 | 1.46 | 3 | 1.95 | 0.83 |
| ● | SNRPN;SNRPB | 1.22 | 0.28 | 2 | 2.57 | 1.36 | 3 | 1.89 | 0.82 |
| ● | PSMD6 | 2.16 | 1.11 | 6 | 1.43 | 0.51 | 5 | 1.79 | 0.81 |
| ● | RAD50 | 0.85 | -0.24 | 7 | 3.64 | 1.87 | 10 | 2.24 | 0.81 |
| ● | PSMD3 | 2.10 | 1.07 | 7 | 1.47 | 0.55 | 11 | 1.78 | 0.81 |
| ● | TCEA1 | 1.38 | 0.46 | 7 | 2.23 | 1.16 | 9 | 1.80 | 0.81 |
| ● | PSMA3 | 2.10 | 1.07 | 4 | 1.46 | 0.54 | 3 | 1.78 | 0.81 |
| ● | CDK2 | 1.46 | 0.55 | 2 | 2.08 | 1.06 | 2 | 1.77 | 0.80 |
| ● | PSMD13 | 2.13 | 1.09 | 4 | 1.43 | 0.51 | 6 | 1.78 | 0.80 |
| ● | PSMA7 | 2.13 | 1.09 | 4 | 1.42 | 0.51 | 2 | 1.78 | 0.80 |
| ● | RPS27A;UBB;UBA5 | 1.39 | 0.48 | 25 | 2.17 | 1.12 | 20 | 1.78 | 0.80 |
| ● | PSMC2 | 1.99 | 1.00 | 9 | 1.51 | 0.60 | 7 | 1.75 | 0.80 |
| ● | PSMC1 | 2.02 | 1.02 | 3 | 1.46 | 0.54 | 3 | 1.74 | 0.78 |
| ● | LRPPRC | 1.36 | 0.44 | 2 | 2.15 | 1.10 | 7 | 1.75 | 0.77 |
| ● | HIST1H1B | 0.97 | -0.05 | 13 | 2.99 | 1.58 | 13 | 1.98 | 0.77 |
| ● | PRMT1 | 1.36 | 0.45 | 17 | 2.10 | 1.07 | 16 | 1.73 | 0.76 |
| ● | PSMD12 | 1.94 | 0.96 | 2 | 1.46 | 0.55 | 4 | 1.70 | 0.75 |
| ● | H1FX | 0.98 | -0.03 | 2 | 2.81 | 1.49 | 3 | 1.89 | 0.73 |

| | | | | | | | | | |
|---|---|---|---|---|---|---|---|---|---|
| ● | SRSF6 | 0.90 | -0.15 | 3 | 3.05 | 1.61 | 4 | 1.97 | 0.73 |
| ● | ILF3 | 0.78 | -0.35 | 11 | 3.49 | 1.80 | 8 | 2.14 | 0.73 |
| ● | PCNA | 1.85 | 0.89 | 5 | 1.47 | 0.55 | 7 | 1.66 | 0.72 |
| ● | HNRNPH1 | 1.17 | 0.22 | 12 | 2.33 | 1.22 | 15 | 1.75 | 0.72 |
| ● | NCL | 1.01 | 0.02 | 12 | 2.68 | 1.42 | 14 | 1.85 | 0.72 |
| ● | DSTN | 2.46 | 1.30 | 12 | 1.09 | 0.13 | 13 | 1.78 | 0.71 |
| ● | SF3B3 | 1.20 | 0.26 | 3 | 2.24 | 1.16 | 6 | 1.72 | 0.71 |
| ● | P4HB | 1.91 | 0.93 | 3 | 1.40 | 0.48 | 8 | 1.65 | 0.71 |
| ● | PSMC5 | 1.98 | 0.99 | 2 | 1.34 | 0.43 | 4 | 1.66 | 0.71 |
| ● | HIST1H1D | 1.05 | 0.07 | 19 | 2.54 | 1.34 | 20 | 1.79 | 0.71 |
| ● | SMC3 | 0.97 | -0.04 | 10 | 2.72 | 1.44 | 11 | 1.84 | 0.70 |
| ● | UBA1 | 1.84 | 0.88 | 3 | 1.43 | 0.52 | 3 | 1.64 | 0.70 |
| ● | KATNAL2 | 2.03 | 1.02 | 2 | 1.30 | 0.37 | 2 | 1.66 | 0.70 |
| ● | PSMD8 | 2.07 | 1.05 | 5 | 1.27 | 0.35 | 3 | 1.67 | 0.70 |
| ● | MAPK1 | 2.23 | 1.15 | 19 | 1.18 | 0.23 | 24 | 1.70 | 0.69 |
| ● | MAGOHB;MAGOH | 1.21 | 0.28 | 2 | 2.15 | 1.11 | 2 | 1.68 | 0.69 |
| ● | PRPF4 | 1.13 | 0.18 | 4 | 2.29 | 1.20 | 3 | 1.71 | 0.69 |
| ● | PSMD7 | 1.92 | 0.94 | 10 | 1.35 | 0.43 | 8 | 1.63 | 0.69 |
| ● | HNRNPA3 | 0.77 | -0.37 | 2 | 3.36 | 1.75 | 5 | 2.06 | 0.69 |
| ● | PSMB5 | 1.90 | 0.93 | 5 | 1.35 | 0.43 | 6 | 1.62 | 0.68 |
| ● | CPPED1 | 2.45 | 1.29 | 2 | 1.04 | 0.06 | 4 | 1.75 | 0.67 |
| ● | XPO1 | 1.37 | 0.46 | 9 | 1.85 | 0.88 | 11 | 1.61 | 0.67 |
| ● | SRSF1 | 0.89 | -0.17 | 4 | 2.85 | 1.51 | 4 | 1.87 | 0.67 |
| ● | KIF2A | 0.90 | -0.15 | 2 | 2.78 | 1.47 | 4 | 1.84 | 0.66 |
| ● | TOP1 | 0.82 | -0.29 | 2 | 3.04 | 1.60 | 2 | 1.93 | 0.66 |
| ● | NHP2L1 | 0.91 | -0.13 | 3 | 2.71 | 1.44 | 2 | 1.81 | 0.65 |
| ● | ERP44 | 2.55 | 1.35 | 14 | 0.97 | -0.05 | 15 | 1.76 | 0.65 |
| ● | PSMB6 | 2.17 | 1.12 | 2 | 1.13 | 0.18 | 2 | 1.65 | 0.65 |
| ● | CIP29;SARNP | 1.28 | 0.35 | 2 | 1.91 | 0.93 | 2 | 1.59 | 0.64 |
| ● | PSMD2 | 1.70 | 0.77 | 11 | 1.43 | 0.51 | 11 | 1.57 | 0.64 |
| ● | VCP | 1.82 | 0.86 | 14 | 1.33 | 0.41 | 17 | 1.57 | 0.64 |
| ● | PLS3 | 1.62 | 0.70 | 4 | 1.48 | 0.56 | 8 | 1.55 | 0.63 |
| ● | PSMA1 | 1.88 | 0.91 | 8 | 1.27 | 0.35 | 4 | 1.57 | 0.63 |
| ● | CTBP2 | 1.05 | 0.07 | 5 | 2.26 | 1.17 | 6 | 1.65 | 0.62 |
| ● | NQO1 | 1.70 | 0.76 | 4 | 1.39 | 0.47 | 3 | 1.54 | 0.62 |
| ● | PSMD11 | 1.74 | 0.80 | 8 | 1.35 | 0.43 | 10 | 1.55 | 0.62 |
| ● | HDAC2 | 1.18 | 0.24 | 2 | 1.99 | 0.99 | 2 | 1.58 | 0.62 |
| ● | H1F0 | 0.69 | -0.54 | 2 | 3.41 | 1.77 | 2 | 2.05 | 0.61 |
| ● | TARDBP | 1.07 | 0.09 | 5 | 2.19 | 1.13 | 5 | 1.63 | 0.61 |
| ● | U2AF2 | 0.88 | -0.18 | 3 | 2.61 | 1.39 | 2 | 1.75 | 0.60 |
| ● | IPO7 | 1.51 | 0.60 | 2 | 1.47 | 0.56 | 2 | 1.49 | 0.58 |
| ● | PFN2 | 2.40 | 1.26 | 2 | 0.93 | -0.11 | 4 | 1.66 | 0.58 |
| ● | MRE11A | 0.76 | -0.40 | 3 | 2.93 | 1.55 | 2 | 1.84 | 0.57 |
| ● | GALK1 | 1.26 | 0.34 | 2 | 1.75 | 0.81 | 2 | 1.51 | 0.57 |
| ● | NPEPPS | 1.48 | 0.57 | 2 | 1.48 | 0.56 | 2 | 1.48 | 0.56 |
| ● | PSMD14 | 1.54 | 0.63 | 2 | 1.38 | 0.47 | 2 | 1.46 | 0.55 |
| ● | CPNE3 | 1.28 | 0.35 | 4 | 1.67 | 0.74 | 4 | 1.47 | 0.54 |
| ● | BUB3 | 1.24 | 0.31 | 6 | 1.71 | 0.77 | 8 | 1.47 | 0.54 |

| | | | | | | | | | |
|---|---|---|---|---|---|---|---|---|---|
| ● | GBE1 | 1.53 | 0.61 | 5 | 1.38 | 0.46 | 3 | 1.45 | 0.54 |
| ● | DNAJA2 | 1.30 | 0.38 | 3 | 1.61 | 0.69 | 4 | 1.46 | 0.53 |
| ● | ACTL6A | 0.87 | -0.20 | 2 | 2.36 | 1.24 | 3 | 1.61 | 0.52 |
| ● | NUDT21 | 0.99 | -0.01 | 2 | 2.07 | 1.05 | 2 | 1.53 | 0.52 |
| ● | FN3KRP | 2.13 | 1.09 | 9 | 0.95 | -0.07 | 7 | 1.54 | 0.51 |
| ● | PTRF | 1.24 | 0.31 | 7 | 1.62 | 0.69 | 9 | 1.43 | 0.50 |
| ● | VIM | 0.90 | -0.14 | 142 | 2.20 | 1.14 | 158 | 1.55 | 0.50 |
| ● | KHDRBS1;KHDRBS | 1.21 | 0.28 | 5 | 1.64 | 0.72 | 7 | 1.43 | 0.50 |

3

# Chapter 5

## The transcription-coupled DNA repair-initiating protein CSB promotes XRCC1 recruitment to oxidative DNA damage

Hervé Menoni[1,2,3]*, Franziska Wienholz[1,2], Arjan F. Theil[2], Roel C. Janssens[2], Hannes Lans[2], Anna Campalans[4,5], J. Pablo Radicella[4,5], Jurgen A. Marteijn[2], Wim Vermeulen[2]*

[1]   These authors contributed equally to this work.

[2]   Department of Molecular Genetics, Oncode Institute, Cancer Genomics Netherlands, Erasmus MC, Dr. Molewaterplein 40, 3015 GD Rotterdam, The Netherlands

[3]   Current address: Laboratoire de Biologie et Modélisation de la Cellule (LBMC) CNRS/ENSL/UCBL UMR 5239, Université de Lyon, Ecole Normale Supérieure de Lyon, 69007 Lyon, France; Université de Grenoble Alpes/INSERM U1209/CNRS UMR 5309, 38042 Grenoble Cedex 9, France.

[4]   CEA, Institute of Cellular and Molecular Radiobiology, F-96265 Fontenay aux Roses, France

[5]   UMR967 CEA/INSERM/Universités Paris-Diderot et Paris-Sud, F-92265 Fontenay aux Roses, France

## Abstract

Transcription-coupled nucleotide excision repair factor Cockayne syndrome protein B (CSB) was suggested to function in the repair of oxidative DNA damage. However thus far, no clear role for CSB in base excision repair (BER), the dedicated pathway to remove abundant oxidative DNA damage, could be established. Using live cell imaging with a laser-assisted procedure to locally induce 8-oxo-7,8-dihydroguanine (8-oxoG) lesions, we previously showed that CSB is recruited to these lesions in a transcription-dependent but NER-independent fashion. Here we showed that recruitment of the preferred 8-oxoG-glycosylase 1 (OGG1) is independent of CSB or active transcription. In contrast, recruitment of the BER-scaffolding protein, X-ray repair cross-complementing protein 1 (XRCC1), to 8-oxoG lesions is stimulated by CSB and transcription. Remarkably, recruitment of XRCC1 to BER-unrelated single strand breaks (SSBs) does not require CSB or transcription. Together, our results suggest a specific transcription-dependent role for CSB in recruiting XRCC1 to BER-generated SSBs, whereas XRCC1 recruitment to SSBs generated independently of BER relies predominantly on PARP activation. Based on our results, we propose a model in which CSB plays a role in facilitating BER progression at transcribed genes, probably to allow XRCC1 recruitment to BER-intermediates masked by RNA polymerase II complexes stalled at these intermediates.

## Introduction

Our genome is constantly challenged by a large number of DNA damaging agents leading to various types of DNA lesions. DNA damage contributes to genome instability and is associated with serious consequences for human health, including cancer, neurodegeneration and ageing [1,2]. Reactive oxygen species (ROS) are undesirable byproducts of cells' oxygen consumption and a major source of unavoidable endogenously produced DNA damage. Among the various different types of oxidative DNA lesions, the highly mutagenic 8-oxo-7,8-dihydroguanine (8-oxoG) is one of the most abundant [3,4]. In eukaryotic cells, the bifunctional glycosylase 8-oxoG-glycosylase 1 (OGG1) specifically recognizes and excises the 8-oxoG from the sugar backbone leaving an abasic site [5]. The DNA chain at this abasic site is subsequently cleaved by either OGG1's intrinsic AP lyase activity that creates 3'α,β-unsaturated aldehyde and 5'-phosphate termini [5] or by AP endonuclease 1 (APE1) which produces 3'-OH and 5'-ribose-phosphate termini. The X-ray repair cross-complementing protein 1 (XRCC1) protein stimulates the APE1 activity to allow efficient processing of the intermediates left by OGG1 [6,7]. This proposed complex cascade of events is currently difficult to address in vivo partly due to redundant factors that deal with 8-oxoG.

Most of the BER factors downstream of the glycosylases are essential for cell viability [2,8]. The 70-kDa XRCC1 protein was initially thought to be mainly required for coordinating single-strand DNA break repair (SSBR), by functioning as a non-enzymatic scaffold protein to which several factors involved in sealing the DNA nick are recruited [9,10]. Single-strand breaks induce the production of poly ADP-ribose (PAR) chains, catalyzed by the Poly ADP-ribose polymerases 1 or 2 (PARP-1 or PARP-2) enzymes, which are required for recruiting XRCC1 to DNA breaks [11,12]. While neither XRCC1 nor parylation are required for BER of 8-oxoG to proceed *in vitro* [13], biochemical studies on DNA with uracil suggested that XRCC1 could direct BER towards the short-patch gap-filling branch [14]. *In vitro* experiments on chromatinized templates showed that BER efficiency is not only supported by chromatin remodelers and specific histones chaperons [15,16], but also by XRCC1, which possibly further disrupts or translocates inhibiting nucleosomes [17]. With the use of live cell microscopy and locally induced oxidative DNA damage we have previously shown that while XRCC1 recruitment to direct SSBs is dependent on parylation, its relocalization to BER complexes does not require this post-translational modification [18]. Moreover, several studies showed that XRCC1 is directly recruited to BER through its interaction

with the glycosylases that recognize the damage [7,9,19-21]. It is thus likely that for its important function in coordinating BER, XRCC1 is recruited to SSBs originating from BER-intermediates through direct protein-protein interactions rather than only parylated substrates.

In addition, we previously showed that the Cockayne syndrome B protein (CSB) is quickly recruited to oxidative base damage in a transcription-dependent manner, with almost similar kinetics as the OGG1 glycosylase [18,22]. CSB is essential for transcription-coupled nucleotide excision repair (TC-NER), a dedicated sub-branch of NER to resolve transcription-blocking DNA lesions [23]. Since cells from Cockayne Syndrome (CS) patients were found to be hyper-sensitive to oxidative DNA damage, a role for the CS proteins in the response to oxidized bases has been proposed [24-27]. However, whether a dedicated transcription-coupled BER (TC-BER) pathway, analogous to TC-NER, exists has been subject to controversy. The notion that 8-oxoG lesions, which only cause minor helix-distortions [28], do not block RNA polymerase II (RNAPII) elongation unless processed by its specific glycosylase 8-Oxoguanine glycosylase (OGG1) [29-31], suggests that if indeed TC-BER exists it is not directly triggered by stalled RNAPII on the oxidative lesions itself as in TC-NER. Further support for transcription-associated processing of BER lesions comes from recent data showing the involvement of the histone-chaperone FACT (facilitates chromatin transcription) in BER [32], which is in line with a previously established role of FACT in TC-NER [33].

To investigate the existence of a transcription-associated BER process, we exploited our recently developed tool to locally inflict different types of DNA lesions and to monitor the subsequent recruitment kinetics of repair factors in living cells. To that aim, we used isogenic cells, which either express CSB or have the *CSB* gene disrupted by CRISPR/Cas9-mediated genome editing. The stable expression of fluorescently tagged BER proteins in those isogenic cells allowed us to directly assess the impact of CSB on the behavior of BER proteins.

## Materials and methods

### Cell lines, constructs and transfection

The CRISPR/Cas9 genome editing approach was applied to obtain CSB knock out cells. Specific single guide RNA (sgRNA) sequences, targeting intron 2 and 3 of the CSB gene respectively, were cloned in a LentiCRISPRv2 plasmid. The LentiCRISPRv2 plasmid was a gift from Feng Zhang (Addgene plasmid #52961, [34]).

The guide sequences are as follows: 5'-GCGAGGGCTGAACGGGATGG-3' and 5'- GCTTTGGAAAACTTAAGGGT-3'. To clone these constructs, annealed complementary oligo's with 5' overhangs were ligated in the BsmB1 digested backbone of the LentiCRISPRv2 plasmid. The correct insert was verified by sequencing. Sv40 immortalized MRC-5 cells were transiently co-transfected with 1 μg of each of the two indicated LentiCRISPRv2 plasmids at 70% cell density on a single well of a 6-well cultured plate using Polyplus JetPei transfection reagent (Westburg). Transfection was carried out according to the manufactures protocol. Transfected cells were selected using 3 μg/ml puromycin for several days. Subsequently, single cells were seeded on a 96-well plate to obtain pure clones and tested for knock out by genotyping and Western blot analysis.

Plasmids pEGFP-N1 and pEYFP-N1 (Clonetech) containing XRCC1-YFP, XRCC1[L360D]-YFP or OGG1-GFP were described in [18]. Fluorescent cDNA fusions were amplified by PCR and subsequently cloned into pLenti CMV Puro (Addgene plasmid #17452; [35]). Third-generation lentiviruses, generated in HEK293T cells, were used to transduce Sv40 immortalized MRC-5 cells and it's isogenic Sv40 immortalized MRC-5 CSB knock-out cells. We further used the Sv40 immortalized human fibroblasts CS1AN (Cockayne syndrome group B-deficient [CS-B]) and HeLa cells. The following constructs were used for transient or stable expression of fluorescently tagged proteins: pOGG1-DsRed, pmCherry-CSB, pXRCC1-EYFP and pXRCC1[L360D]-EYFP [18]. Transient transfections were performed with Fugene6 reagent (Roche), according to the manufacturer's instructions. Stably expressing cells were obtained by using puromycin for 1 week to select for resistant cells. Prior to experiments, all cells were grown in a 1:1 mixture of Ham's F10 and DMEM (Gibco), supplemented with penicillin/streptomycin and 10% FCS at 37°C, in a 5% $CO_2$ humidified incubator.

## Western blot
Cells were lysed in 2x Laemmli sample buffer and were boiled for 5 min. Protein size-fractionation by a 6% SDS–PAGE gel and subsequent electro-transfer to a PVDF membrane (0.45 μm) was accomplished as described [36]. Blotting was performed overnight at 4°C, 75mA in 2x Blot-buffer (50mM Tris, 384mM Glycin, 0.02% SDS) without methanol. Blocking of the membranes was accomplished with 3% BSA in PBS for 1 h at room temperature. Membranes were then washed 3 times with PBS containing 0.05% Tween and were subsequently incubated with primary antibodies against CSB (E-18, sc-10459, Santa Cruz Biotechnology, Inc., 1:250 in PBS 3% BSA), Tubulin (B512, Sigma-Aldrich, 1:5000 in PBS 3% BSA), or OGG1 (ab12474, Abcam, 1:1000 in PBS 3% BSA) or SFPQ (ab177149, Abcam,

1:2000 in PBS 3% BSA) in combination with Odyssey-compatible secondary antibodies. Western blots were analyzed using the Odyssey CLx Infrared Imaging System (LI-COR Biosciences).

## Gentoyping

PCR amplification was used for verifying the deletion of exon 3 in the endogenous CSB gene. 100 ng DNA of each sample was used per PCR reaction. Taq DNA polymerase was purchased from Invitrogen and used according to the manufacturer's instructions. PCR conditions were as follows: 95°C for 3 min, 35x [95°C for 45s, 60°C for 30 s, 72°C for 2min], 72°C for 10 min. The primer sequences used are as follows: forward primer: 5'-ggcagtgtcaggtaagcaag-3', reverse primer: 5'-agttgggatggcagaactga-3'. PCR products were run on an agarose gel containing ethidium bromide. The expected PCR products are: 2.1 Kbp for exon 3 containing (wild-type CSB) and 210 bp for exon 3 deleted (CSB KO).

## Colony survival

MRC-5 and MRC-5 CSB-deficient cells were seeded in triplicate in 6-well plates (300 cells/well) and treated with a single dose of UV-C (0–6 J/m$^2$; 254 nm; Philips TUV lamp) or with a single dose of Potassium Bromide (KBrO$_3$, 0-10 mM) 1 d after seeding. After 7 days, colonies were fixed and stained in 50% methanol, 7% acetic acid and 0.1% Coomassie blue and subsequently analyzed with the Gelcount by Oxford Optronix and appertaining Software (version 1.1.2.0.). The survival was plotted after pooling three (UV-C) or two (KBrO$_3$) independent experiments as the mean percentage of colonies detected 1 week after damage treatment compared to the mean number of colonies from the non-treated samples.

## Silencing and cell treatments

Small interfering RNAs against CSB (ON-TARGETplus SMART-pool; L-004888-00-0020, Human ERCC6, NM_000124; Dharmacon), targeting OGG1 (On-TARGETplus SMARTpool; L-005147-00, Human OGG1; Dharmacon) or non-targeting (siGENOME NonTargeting D-001210-05-20, Dharmacon) were transfected to cells using Lipofectamine 2000 reagent (Invitrogen), according to the manufacturer's instructions. Silencing in HeLa OGG1-DsRed cell lines with indicated small interfering RNAs was performed using Lipofectamine RNAiMAX reagent (Invitrogen) according to the manufacturer's instructions. Silencing efficiency was determined using Western blotting. PARP activity was inhibited with N-(6-oxo-5,6-dihydro-henanthridin-2-yl)-N,N-dimethylacetamide HCl hydrochloride hydrate (PJ-34) purchased from Sigma–Aldrich and used at a

concentration of 15 µM (37). Transcription was inhibited with the RNAPII inhibitor 5,6-Dichlorobenzimidazole 1-β-D-ribofuranoside (DRB, 100 µM, Sigma-Aldrich) added 2 h prior to the experiment or Actinomycin D (1µg/ml, Sigma-Aldrich) added 2 h prior to experiment [38].

## Microscopic settings, damage induction and FRAP

Images were recorded with different confocal microscopes; Nikon A1, Leica TCS SP5 microscope (with Leica Application Suite), and LSM 510 (Carl Zeiss), all equipped with a 63× Plan-APO (1.4 NA) oil immersion lens. Two days prior to microscopy experiments cells were seeded to full confluency on sterile glass coverslips. During microscopy, cells were examined in normal culture medium maintained at 37°C and 5% $CO_2$ within a large chamber included in the microscope. Imaging of eGFP, eYFP and DsRed were performed using respectively 488 nm, 514 nm and 561 nm laser light to excite the chromophores; emitted light was recorded with the respective filters BP505-550, BP530-600 and LP585. Local base damage in a subnuclear area of 2 x 2 µm was induced, as previously described [22]. For the induction of direct SSBs a single (1 frame; 2.58 sec/frame) 405 nm laser-pulse (corresponding to approximately 1 mW) was used. For the induction of oxidative base damage, cells were incubated for 10 minutes with 10 µM photosensitizer Ro 19-08022 (a kind gift from F. Hoffmann-La Roche, Ltd) and irradiated as described above. Accumulation of DNA repair factors at locally damaged sites was determined by measuring the fluorescent intensity in the damaged area and compared to non-damaged areas of the same size. The measured fluorescence on the damaged area was corrected for background and monitor bleaching, normalized for pre-damage values and averaged. It should be noted that for all the quantitative experiments we have carefully selected cells with comparable expression levels.

Fluorescence recovery after photo-bleaching (FRAP) experiments were performed as previously described [22]. In short, the pre-defined damaged and non-damaged subnuclear areas of 2 x 2 µm were illuminated with the respective laser set to 100% laser power for 6 frames (0.032 sec/frame) to bleach fluorescent proteins of interest. The subsequent fluorescence recovery was recorded before (100 frames) and after (750 frames) photobleaching, normalized to pre-bleaching values and expressed as mean relative fluorescence intensity.

**5**

# Results

## CSB has no effect on OGG1 immediate recruitment and retention at oxidative DNA damage

We previously established a procedure to measure the recruitment kinetics of OGG1 to locally generated oxidative DNA damage [22]. Using that approach we showed that CSB was recruited to these sites in a transcription-dependent manner. Interestingly, the absence of co-recruitment of downstream NER factors suggested that not a full TC-NER reaction was activated at these sites [22]. To further explore a possible role of CSB in BER, we measured the recruitment kinetics of OGG1 to local oxidative DNA damage in the presence and absence of CSB. To that aim we stably expressed OGG1 tagged with GFP in Sv40-immortalized MRC-5 cells. We applied CRISPR/Cas9-mediated genome editing to obtain an isogenic CSB knock-out cell line, in which the absence of CSB was confirmed by PCR and Western-blotting (Fig. S1A, B). As expected, those cells have an increased sensitivity to UV-C light exposure (Fig. S1C) and to oxidative
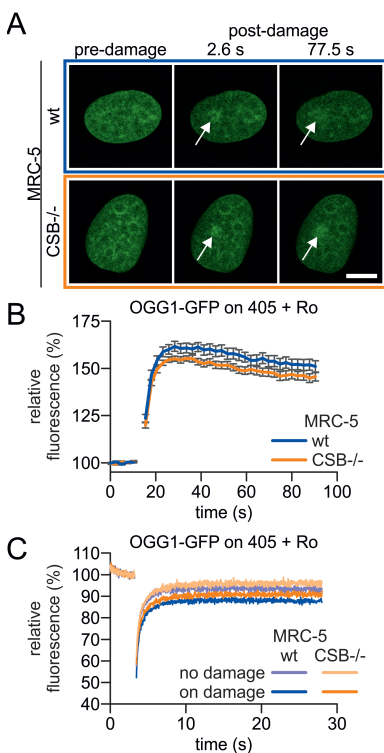


**Figure 1**

**CSB does not affect the recruitment of OGG1 to oxidative DNA damage. (A)** Representative stills of time-lapse imaging to determine accumulation kinetics of OGG1-GFP in CSB-proficient (upper panel) or CSB-deficient (lower panel) MRC-5 cells at micro-irradiated (405 nm) subnuclear regions, indicated by arrows, in the presence of 10 μM Ro 19-8022 photosensitizer. Scale bar: 7.5 μm. **(B)** Accumulation kinetics of OGG1-GFP at micro-irradiated areas (as shown in A). The mean relative fluorescence intensity is plotted against time in seconds. **(C)** FRAP analysis of OGG1-GFP expressed in CSB-proficient and deficient MRC-5 cells at locally damaged areas (on damage) or at a similar sized area without DNA damage (no damage). For (B) and (C), error bars indicate the SEM of 20 cells of 2 independent, pooled experiments.

damage (Fig. S1D). We observed an immediate and fast recruitment of OGG1 to local oxidative DNA damage containing sites in wild-type (wt) cells (Fig. 1A, B) in accordance with earlier reports [18]. Surprisingly however, the recruitment kinetics of OGG1 in wt and CSB-deficient cells were identical (Fig. 1A, B), indicating that CSB is not involved in the immediate glycosylase recruitment. Comparable results were obtained in HeLa cells stably expressing OGG1 fused to DsRed that were depleted for CSB via RNA silencing (Fig. S1E, G). Together, these data indicate that in different human cells the rapid recruitment of OGG1 to oxidative damage (8-oxoG) is independent of CSB.

We previously reported a faster disappearance of OGG1 accumulation to local oxidative damage in CSB-deficient cells [22]. This may suggest that although CSB is not required for the initial OGG1 recruitment, it might be involved in retaining OGG1 at the site of damage. To test this hypothesis, we performed fluorescence recovery after photobleaching (FRAP) experiments on locally induced oxidative damage. In a non-damaged area of wt or CSB-deficient cells, the fluorescent signal quickly recovered after bleaching (Fig. 1C), indicative for a freely diffusing protein. The fluorescence recovery was however incomplete when photobleaching was performed at sites of induced oxidative damage in both wt and CSB-deficient cells (Fig. 1C), suggesting that a fraction of OGG1 is immobilized (bound) at these sites. We did however not observe a difference in the amount of lesion-bound OGG1 in the absence or presence of CSB. Similar results were obtained in HeLa cells stably expressing OGG1-DsRed in which CSB is knocked down by siRNA (Fig. S1F, G). Despite the notion that a slower repair of 8-oxoG was observed in CSB-deficient mouse embryonic fibroblasts (MEFs) compared to wild-type littermates MEFs [25], we were not able to unveil differences in the *in vivo* OGG1 binding properties early after damage induction. Since the full repair of 8-oxoG lesions requires several hours [39], it is possible that CSB influences OGG1 binding to a subset of 'difficult-to-repair' oxidative DNA lesions. For example, the immediate targeting of glycosylases to lesions may be impaired due to sequence context, chromatin status or lesions located in close vicinity of each other. However, within our experimental conditions it was not possible, to reveal these subtle differences and to measure binding kinetics at later stages after damage induction. We conclude that OGG1 is rapidly recruited to sites of damage in a CSB-independent manner. This implies that 8-oxoG lesions can efficiently be removed in the absence of CSB and that the formed AP-site is most likely rapidly processed to a SSB in a BER-dependent manner either by the AP-lyase activity of the glycosylase or by APE1.

A



B

XRCC1-YFP on 405



C



D

XRCC1-YFP on 405 + PARPi + Ro



E



F

XRCC1$^{L360D}$-YFP on 405
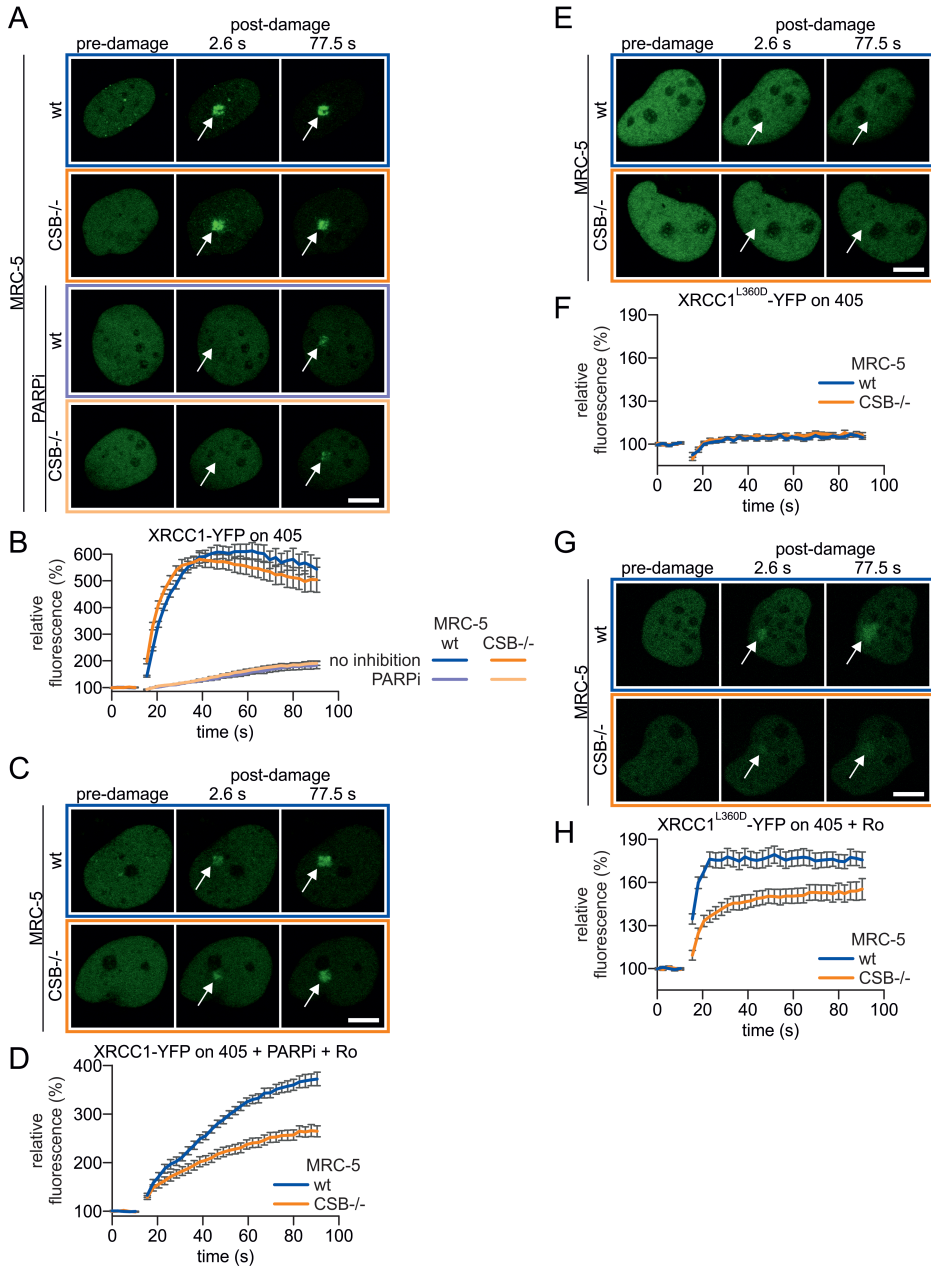


G



H

XRCC1$^{L360D}$-YFP on 405 + Ro

**Figure 2**
**CSB facilitates recruitment of XRCC1 to BER-induced single strand breaks. (A)** Representative stills of time-lapse imaging to determine accumulation kinetics of XRCC1-YFP in CSB-proficient or CSB-deficient MRC-5 cells on direct SSBs (405 nm laser micro-irradiated regions, indicated by arrows) in the absence (upper two panels) or presence of 15 µM PJ-34 to inhibit PARPs (lower two panels). **(B)** Accumulation kinetics of XRCC1-YFP at micro-irradiated areas (as shown in A). The mean relative fluorescence intensity is plotted against time in seconds. **(C)** Representative stills of time-lapse imaging to determine accumulation kinetics of XRCC1-YFP in CSB-proficient (upper panel) or CSB-deficient (lower panel) MRC-5 cells on BER induced SSBs cells at micro-irradiated (405 nm laser) subnuclear regions, indicated by arrows, in the presence of 10 µM Ro 19-8022 photosensitizer and 15 µM PJ-34. **(D)** Accumulation kinetics of XRCC1-YFP on BER induced SSBs (as shown in C). The mean relative fluorescence intensity is plotted against time in seconds. **(E)** Representative stills of time-lapse imaging to determine accumulation kinetics of the XRCC1$^{L360D}$-YFP mutant in CSB-proficient (upper panel) or CSB-deficient (lower panel) MRC-5 cells at micro-irradiated (405 nm laser) subnuclear regions, indicated by arrows. **(F)** Accumulation kinetics of the XRCC1$^{L360D}$-YFP mutant at micro-irradiated areas (as shown in E). The mean relative fluorescence intensity is plotted against time in seconds. **(G)** Representative stills of time-lapse imaging to determine accumulation kinetics of the XRCC1$^{L360D}$-YFP mutant in CSB-proficient (upper panel) or CSB-deficient (lower panel) MRC-5 cells at micro-irradiated (405 nm laser) subnuclear regions, indicated by arrows, in the presence of 10 µM Ro 19-8022 photosensitizer. **(H)** Accumulation kinetics of the XRCC1$^{L360D}$-YFP mutant at micro-irradiated areas (as shown in G). The mean relative fluorescence intensity is plotted against time in seconds. For (A, C, E and F), scale bar: 7.5 µm. For (B, D, F and H), error bars indicate the SEM of 20 cells of 2 independent, pooled experiments.

## CSB facilitates recruitment of XRCC1 to BER-intermediates

Our results show that CSB is not required for the first step of BER, i.e. loading of the glycosylase OGG1. However, CSB-deficient cells have reduced repair rates of 8-oxoG and are hyper-sensitive to oxidative DNA damage, arguing for a role of CSB in a more downstream step of the BER process ([26,27,40,41] and Fig. S1D). To further elucidate the role of CSB in BER, we addressed the question whether CSB may be required to facilitate recruitment of XRCC1 to BER. To understand whether CSB influences XRCC1 recruitment to either BER or SSBR, sub-nuclear local DNA damage was induced under two different conditions in cells stably expressing XRCC1-YFP. Firstly, for the induction of mainly direct SSBs (i.e. independent of glycosylases) we employed the 405 nm laser as was reported before [42,43]. For simplicity, DNA damage induced with those settings is named "direct SSBs" (labelled as 405 in figures). Secondly, for the induction of mainly oxidative base damage, cells were pre-incubated with a specific exogenous photosensitizer (Ro 19-8022) prior to 405 nm laser irradiation [22]. Results obtained under this condition are labelled 405 + Ro in the figures. Under the latter condition mainly BER-induced SSBs will be formed.

XRCC1-YFP, stably expressed in both CSB-proficient and deficient MRC-5 cells showed an equally robust and rapid accumulation in locally 405 nm laser irradiated areas (direct SSBs) (Fig. 2A, B). These data show that CSB is not involved in XRCC1 loading at direct SSBs. Previous studies have shown a strong PARP-dependent recruitment of XRCC1 to direct SSBs [18,43,44]. Consistently, the addition of the PARP-inhibitor PJ-34 [37] nearly completely abolished the recruitment of XRCC1 to direct SSBs, which again appeared independent of CSB (Fig. 2A, B).

Next, we measured XRCC1 accumulation on BER-induced SSBs generated by 405 nm laser irradiation in the presence of the photosensitizer Ro 19-8022. Pre-treating cells with the PARP-inhibitor PJ-34, allowed us to measure the recruitment of XRCC1 specifically to BER-induced SSBs (Fig. 2C, D). Strikingly, under those conditions we now observed a marked CSB-dependency for the recruitment of XRCC1, while active parylation by PARP was not required. When XRCC1-YFP and mCherry-CSB were co-expressed in CSB-deficient cells we find a clear co-localization at the local oxidative damage site (Fig. S2A), supporting the CSB-dependent XRCC1 recruitment.

The use of PARP inhibitors may result in the accumulation of trapped PARP-1 at the site of damage which may further interfere with BER progression [21]. To overcome this potential PARP-inhibitor side effect, we used a mutated XRCC1 (XRCC1$^{L36oD}$-YFP), carrying a point mutation in the BRCT1 domain that abolishes the interaction with PARP-1 and was shown to impede XRCC1 accumulation on direct SSBs [18]. As anticipated, no accumulation of the XRCC1$^{L36oD}$-YFP mutant on direct SSBs, in either wt or CSB-deficient cells, was detected (Fig. 2E, F). Interestingly however, recruitment of this XRCC1$^{L36oD}$-YFP mutant to BER-intermediates (e.g. BER-induced SSBs) exhibited a strong dependency on CSB (Fig. 2G, H). These results were verified in HeLa (CSB-proficient) and CS1AN (CSB-deficient) cells, ruling out a cell type specific effect (Fig. S1H). These data further corroborate that part of the XRCC1 accumulation on BER-induced SSBs is independent of PARP, but is facilitated by CSB. Previously, it was found that OGG1 expression is reduced in CSB-deficient cells, which may contribute to the reduced XRCC1 recruitment in CSB-deficient cells. However, in our CSB-deficient cells we did not observe any significant OGG1 reduction (Fig. 1SG), indicating that XRCC1 recruitment is facilitated by the presence of CSB.

**Figure 3**

**XRCC1 binding to BER induced breaks is sensitive to inhibition of transcription. (A)** Representative stills of time-lapse imaging to determine accumulation kinetics of XRCC1$^{L360D}$-YFP in untreated (upper panel) or transcription inhibited (DRB, 100 μM) MRC-5 cells at micro-irradiated (405 nm laser) subnuclear regions, indicated by arrows, in the presence of 10 μM Ro 19-8022 photosensitizer. Scale bar: 7.5 μm. **(B)** Accumulation kinetics of XRCC1$^{L360D}$-YFP at micro-irradiated areas (as shown in A). The mean relative fluorescence intensity is plotted against time in seconds. Error bars indicate the SEM of 20 cells of 2 independent, pooled experiments. **(C)** Accumulation kinetics of XRCC1$^{L360D}$-YFP expressed in HeLa cells at micro-irradiated areas in the presence of 5 μM Ro 19-8022 photosensitizer in either untreated cells or in the presence of transcription inhibitor (DRB, 100 μM). **(D)** Accumulation kinetics of OGG1-dsRed expressed in HeLa cells at micro-irradiated areas in the presence of 5 μM Ro 19-8022 photosensitizer in either untreated cells or in the presence of transcription inhibition (DRB, 100 μM). All graphs are representative for two independent experiments (at least 11 cells) and show the mean relative fluorescence intensity ± SEM.

## Recruitment of XRCC1 during BER is sensitive to inhibition of transcription

Since CSB recruitment to local oxidative base damage occurs in a transcription-dependent manner [22], we tested whether the recruitment of XRCC1 to BER-induced SSBs is also dependent on transcription. To test this, we used cells expressing the XRCC1$^{L360D}$-YFP mutant that only accumulates on BER-induced SSBs (Fig. 2G, H). Pretreatment of MRC-5 wt cells for 2 h with the transcription inhibitor DRB strongly reduced the accumulation of XRCC1$^{L360D}$-YFP to locally generated BER-induced SSBs (Fig. 3A, B). Similar reduction in accumulation of XRCC1$^{L360D}$-YFP to local oxidative damage was observed after treatment with

the transcription inhibitor Actinomycin-D (Fig. S2B, C). This transcription-dependent accumulation of XRCC1 was reproduced in HeLa cells expressing XRCC1$^{L360D}$-YFP (Fig. 3C and Fig. S2C, D). In contrast, the CSB-independent accumulation of dsRed tagged OGG1 appeared independent of transcription (Fig. 3D).
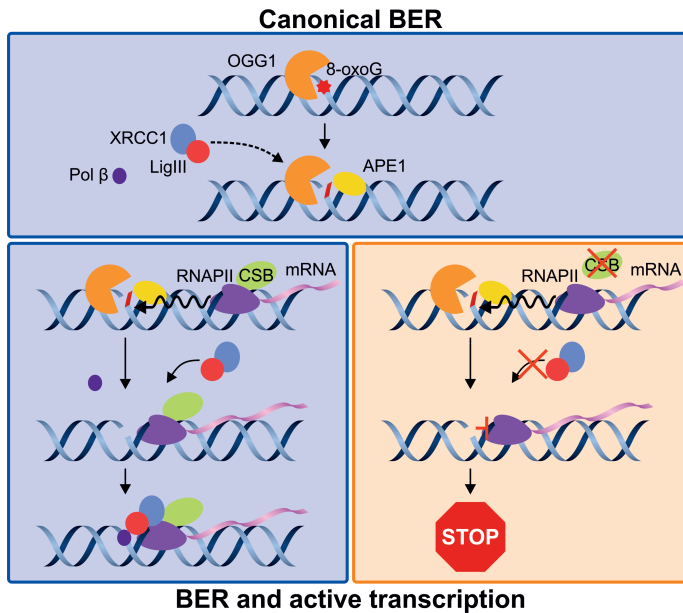


**Figure 4**
**Proposed model for the CSB function in the repair of oxidative DNA damage.** The upper panel represents the classical BER initiation on 8-oxoG lesions (red star) by the concerted action of the OOG1 glycosylase (orange sphere) and APE1 (yellow ball), subsequent recruitment of the XRCC1/LigaseIII complex (blue and red balls, respectively) and DNA Polymerase β (Pol β, dark purple ball) through interaction with the glycosylase further completes repair. The lower panels represent a situation in which an elongating RNA polymerase II complex (RNAPII, purple sphere, direction indicated by curved arrow) runs into a BER-intermediate (e.g. BER-generated SSB) that likely caused inhibition of RNAPII elongation. When CSB (green ball) is present (lower left panel, blue shaded) it will assist in loading the XRCC1/Ligase III (LigIII) complex (blue and red balls, respectively) to stalled RNAPII on BER-intermediates to facilitate the assembly of downstream BER factors, such as DNA Polymerase β (Pol β, dark-purple ball) and stimulate BER progression. In the absence of CSB (lower right panel, orange shaded), BER progression will be limited.

## DISCUSSION

Based on our results we propose a model in which CSB facilitates the recruitment of XRCC1 to transcription complexes that are stalled at BER intermediates generated during oxidative DNA damage repair (Fig. 4 lower panels). We speculate that the combined presence of CSB and XRCC1 assist downstream BER steps. Our previous work [22] already showed a transcription-dependent recruitment of CSB to 8-oxoG. Surprisingly however, targeting of the initiating glycosylase OGG1 to those lesions appeared independent of CSB and transcription (Fig. 1A,B), arguing for a transcription-dependent role of CSB beyond initial damage recognition. This observation is in line with earlier observations that the minor helix distorting 8-oxoG lesions do not interfere with RNAPII elongation [29,31,45] and would thus not require CSB. In contrast bulky DNA lesions (e.g. UV-induced photoproducts) that block RNAPII elongation trigger the recruitment of CSB to initiate classical TC-NER [46]. However, BER-intermediates (e.g. AP-sites, SSBs) generated either by bifunctional glycosylases (such as OGG1) or as a consequence of APE1 action and not yet fully processed by downstream BER steps may create a local structural DNA disturbance at which RNAPII complexes can stall and trigger CSB recruitment to facilitate XRCC1 binding [47]. Surprisingly however, upon OGG1 depletion by siRNA we did not observe a significant reduction of the XRCC1 recruitment (Fig. S2E, F). The absence of an effect of OGG1 depletion is likely explained by (partly) redundant glycosylases that compensate for the loss of OGG1 [48], or that the remaining OGG1 after incomplete knock down is sufficient to initiate BER. In addition, 405 nm laser-irradiation in the presence of Ro 19-08022 will induce, next to the predominant 8-oxoG lesions, also other types of oxidative base damage which will be targeted by other glycosylases and thus also create BER-intermediates. Nevertheless, the notion from our previous study [18] that overexpression of OGG1 (assumed to create more BER-intermediates) caused a stronger accumulation of XRCC1L360D at local oxidative DNA damage, strongly supports our model. Indeed, earlier studies have shown that these BER-intermediates do stall RNAPII [29-31,49]. Our findings support the concept that elongating RNAPII, by virtue of its DNA-translocating activity, scans DNA for perturbations, either bulky lesions or BER-intermediates [50]. It is thus likely that CSB comes into play at these BER-intermediate stalled RNAPII complexes, similarly as to its role in TC-NER. Stalled RNAPII complexes at BER-intermediates will likely disturb efficient progression of the BER reaction as the presence of these bulky molecular complexes may hamper efficient loading of downstream factors (DNA polymerase β or the ligase complex).

**5**

Different functions for CSB in TC-NER have been proposed, ranging from: being a chromatin-remodeling factor, or a recruitment platform for downstream NER factors, to pushing back or facilitating ubiquitylation and subsequent degradation of stalled RNAPII complexes to provide more efficient access of NER factors [23]. The exact role of CSB in facilitating BER needs to be determined, similarly to its still enigmatic role in TC-NER. It is possible that the proposed chromatin-remodeling function of CSB, in addition to its role in coordinating TC-NER, may create a permissive chromatin environment to enable better access to repair factors. Recently, evidence has accumulated that indeed chromatin reorganization is strongly associated to TC-NER [33,51-53]. Strikingly, in addition to a role of FACT in stimulating transcription restart in conjunction to TC-NER [33], also a role of FACT in facilitating BER was established [32]. In our model we propose that transcription (when stalled at repair-intermediates) interferes with optimal recruitment or loading of downstream BER factors. It is thus conceivable that a BER-coordinating process is operational to prevent a clash between transcription and BER. The observed relocation of the BER machinery, including XRCC1 and Ligase3 to euchromatic (transcriptional active) regions in response to oxidative stress, might reflect such a mechanism to stimulate BER-efficiency in these regions to avoid interference with transcription [18,20,39]. The compromised progression of the BER reaction due to interference with stalled transcription complexes on reaction intermediates, suggests a joint role for CSB and XRCC1 in coordinating this specific BER reaction. In addition to a pivotal organizing role for XRCC1 in SSB repair [44,54], it seems also important in coordinating BER reactions that are confronted with stalled RNAPII, likely through its scaffolding function and multiple established interactions with BER factors. BER-intermediates that are (partly) shielded by stalled transcription complexes may need CSB to help a rapid loading of XRCC1. BER coordination, mediated by XRCC1, may become more important under specific circumstances, such as in transcribed genes, on lesions that are difficult to process, or at specific genomic loci or chromatin compaction-status that hamper efficient BER progression [50]. CSB may be required for efficient loading of XRCC1, possibly by restructuring the stalled transcription machinery to allow exposure of glycosylase-generated intermediates. Strikingly, active parylation is not required for the recruitment of XRCC1 to BER-intermediate-stalled transcription complexes, whereas parylation is essential for loading to BER-unrelated SSBs. These observations do however not preclude a role of parylation in further downstream BER events, which was suggested previously [55].

# Supplementary data

Supplementary Data are available at NAR online.

## Acknowledgements
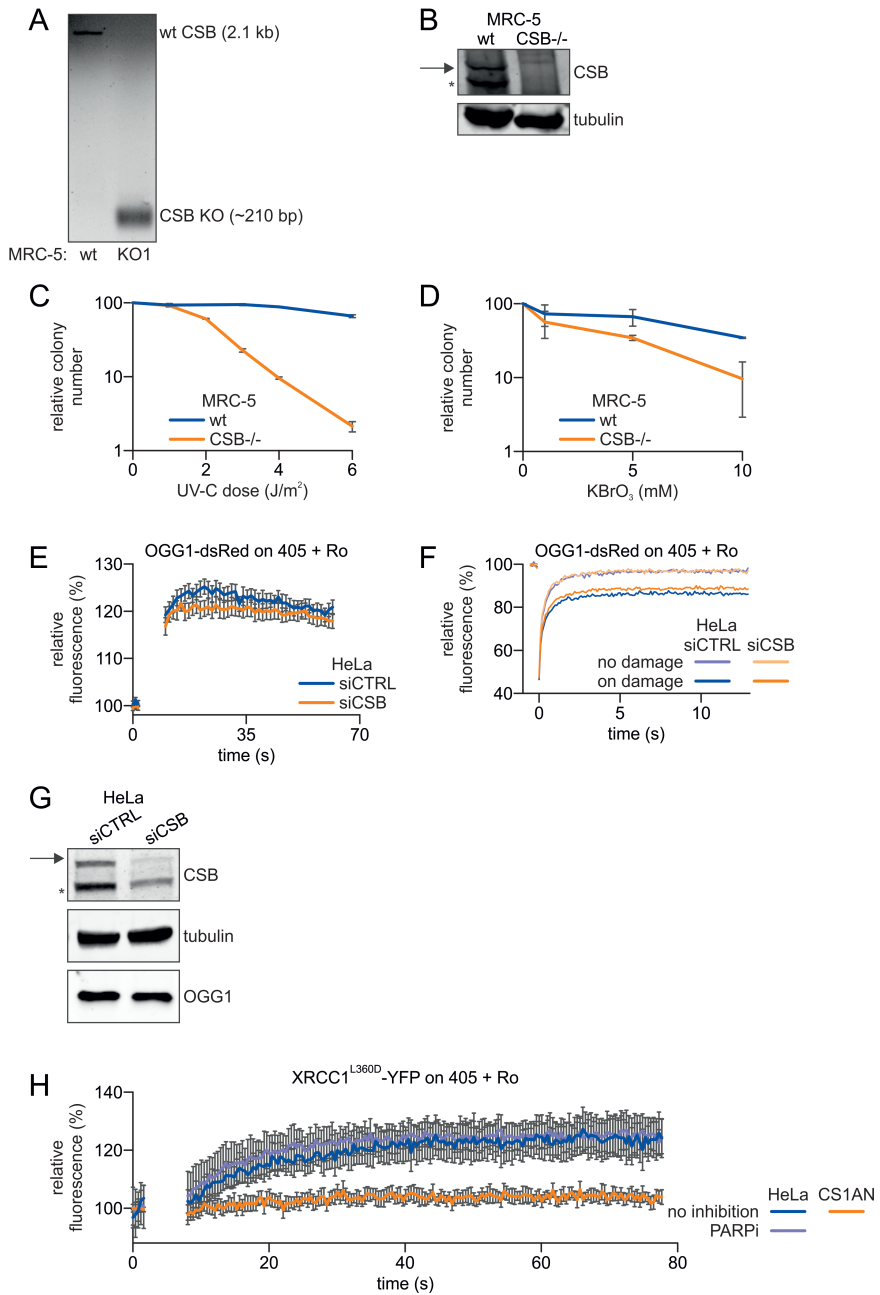
## Funding

## Conflict of interest

The authors declare to have no conflict of interest.

**5**

# References

1. Hoeijmakers,J.H. (2009) DNA damage, aging, and cancer. *The New England journal of medicine*, **361**, 1475-1485.
2. Wallace,S.S. (2014) Base excision repair: a critical player in many games. *DNA Repair*, **19**, 14-26.
3. Cadet,J., Douki,T. and Ravanat,J.L. (2011) Measurement of oxidatively generated base damage in cellular DNA. *Mutat. Res.*, **711**, 3-12.
4. Shibutani,S., Takeshita,M. and Grollman,A.P. (1991) Insertion of specific bases during DNA synthesis past the oxidation-damaged base 8-oxodG. *Nature*, **349**, 431-434.
5. Radicella,J.P., Dherin,C., Desmaze,C., Fox,M.S. and Boiteux,S. (1997) Cloning and characterization of hOGG1, a human homolog of the OGG1 gene of Saccharomyces cerevisiae. *Proc. Natl. Acad. Sci. U. S. A.*, **94**, 8010-8015.
6. Izumi,T., Hazra,T.K., Boldogh,I., Tomkinson,A.E., Park,M.S., Ikeda,S. and Mitra,S. (2000) Requirement for human AP endonuclease 1 for repair of 3'-blocking damage at DNA single-strand breaks induced by reactive oxygen species. *Carcinogenesis*, **21**, 1329-1334.
7. Vidal,A.E., Boiteux,S., Hickson,I.D. and Radicella,J.P. (2001) XRCC1 coordinates the initial and late stages of DNA abasic site repair through protein-protein interactions. *EMBO J.*, **20**, 6530-6539.
8. Wilson,D.M. and Thompson,L.H. (1997) Life without DNA repair. *Proc. Natl. Acad. Sci. U.S.A.*, **94**, 12754-12757.
9. Marsin,S., Vidal,A.E., Sossou,M., Menissier-de Murcia,J., Le Page,F., Boiteux,S., de Murcia,G. and Radicella,J.P. (2003) Role of XRCC1 in the coordination and stimulation of oxidative DNA damage repair initiated by the DNA glycosylase hOGG1. *J. Biol. Chem.*, **278**, 44068-44074.
10. Caldecott,K.W. (2003) XRCC1 and DNA strand break repair. *DNA Repair*, **2**, 955-969.
11. Caldecott,K.W. (2007) Mammalian single-strand break repair: mechanisms and links with chromatin. *DNA Repair*, **6**, 443-453.
12. Hanzlikova,H., Gittens,W., Krejcikova,K., Zeng,Z. and Caldecott,K.W. (2017) Overlapping roles for PARP1 and PARP2 in the recruitment of endogenous XRCC1 and PNKP into oxidized chromatin. *Nucleic Acids Res.*, **45**, 2546–2557.
13. Pascucci,B., Maga,G., Hubscher,U., Bjoras,M., Seeberg,E., Hickson,I.D., Villani,G., Giordano,C., Cellai,L. and Dogliotti,E. (2002) Reconstitution of the base excision repair pathway for 7,8-dihydro-8-oxoguanine with purified human proteins. *Nucleic Acids Res.*, **30**, 2124-2130.
14. Kubota,Y., Nash,R.A., Klungland,A., Schar,P., Barnes,D.E. and Lindahl,T. (1996) Reconstitution of DNA base excision-repair with purified human proteins: interaction between DNA polymerase beta and the XRCC1 protein. *EMBO J.*, **15**, 6662-6670.
15. Menoni,H., Gasparutto,D., Hamiche,A., Cadet,J., Dimitrov,S., Bouvet,P. and Angelov,D. (2007) ATP-dependent chromatin remodeling is required for base excision repair in conventional but not in variant H2A.Bbd nucleosomesv. *Mol. Cell. Biol.*, **27**, 5949-5956.
16. Menoni,H., Shukla,M.S., Gerson,V., Dimitrov,S. and Angelov,D. (2012) Base excision repair of 8-oxoG in dinucleosomes. *Nucleic Acids Res.*, **40**, 692-700.
17. Odell,I.D., Barbour,J.E., Murphy,D.L., Della-Maria,J.A., Sweasy,J.B., Tomkinson,A.E., Wallace,S.S. and Pederson,D.S. (2011) Nucleosome disruption by DNA ligase III-XRCC1 promotes efficient base excision repair. *Mol. Cell. Biol.*, **31**, 4623-4632.
18. Campalans,A., Kortulewski,T., Amouroux,R., Menoni,H., Vermeulen,W. and Radicella,J.P. (2013) Distinct spatiotemporal patterns and PARP dependence of XRCC1 recruitment to single-strand break and base excision repair. *Nucleic Acids Res.*, **41**, 3115-3129.
19. Campalans,A., Marsin,S., Nakabeppu,Y., O'Connor,T.R., Boiteux,S. and Radicella,J.P. (2005) XRCC1 interactions with multiple DNA glycosylases: a model for its recruitment to base excision repair. *DNA Repair*, **4**, 826-835.
20. Campalans,A., Moritz,E., Kortulewski,T., Biard,D., Epe,B. and Radicella,J.P. (2015) Interaction with OGG1 is required for efficient recruitment of XRCC1 to base excision repair and maintenance of genetic stability after exposure to oxidative stress. *Mol. Cell. Biol.*, **35**, 1648-1658.
21. Strom,C.E., Johansson,F., Uhlen,M., Szigyarto,C.A., Erixon,K. and Helleday,T. (2011) Poly (ADP-ribose) polymerase (PARP) is not involved in base excision repair but PARP inhibition traps a single-strand intermediate. *Nucleic Acids Res.*, **39**, 3166-3175.
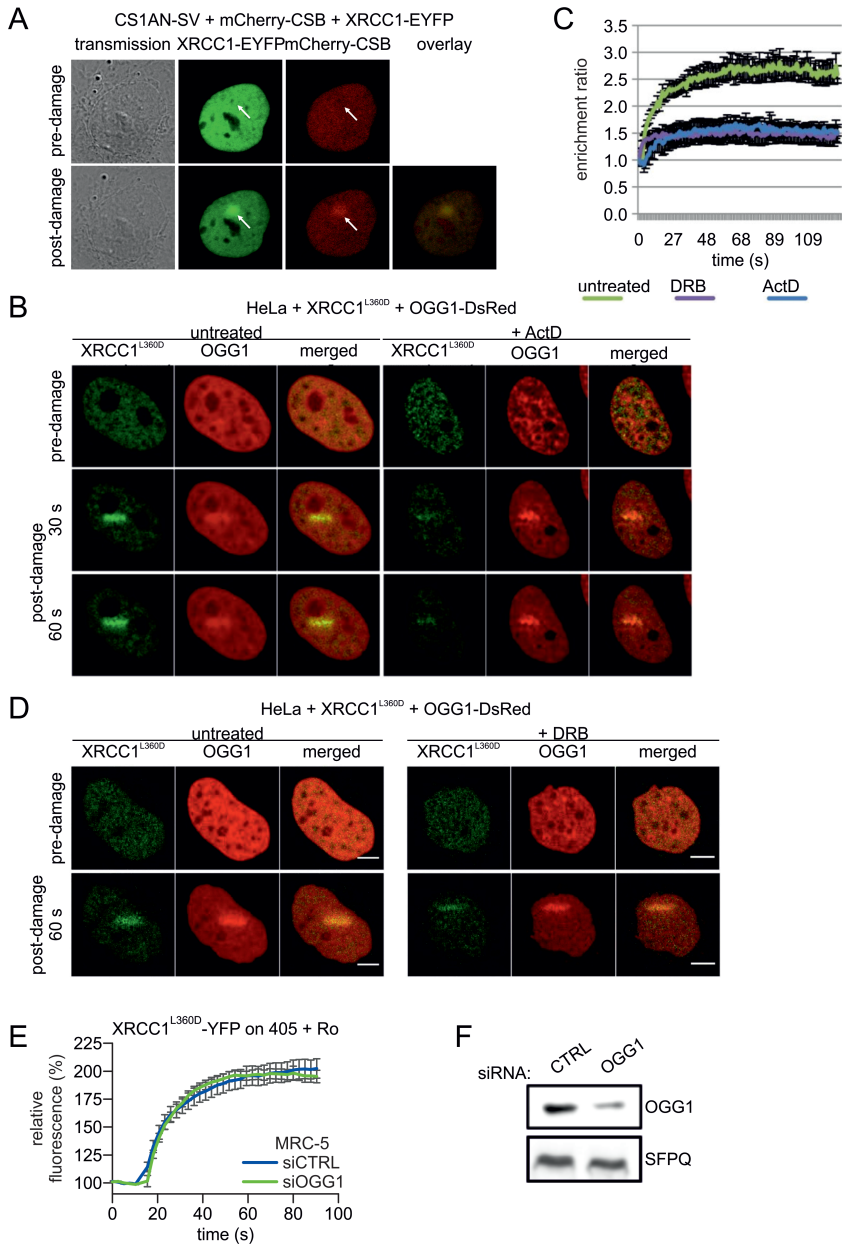
22. Menoni,H., Hoeijmakers,J.H. and Vermeulen,W. (2012) Nucleotide excision repair-initiating proteins bind to oxidative DNA lesions in vivo. *J. Cell Biol.*, **199**, 1037-1046.

23. Marteijn,J.A., Lans,H., Vermeulen,W. and Hoeijmakers,J.H. (2014) Understanding nucleotide excision repair and its roles in cancer and ageing. *Nat. Rev. Mol. Cell. Biol.*, **15**, 465-481.

24. Dianov,G., Bischoff,C., Sunesen,M. and Bohr,V.A. (1999) Repair of 8-oxoguanine in DNA is deficient in Cockayne syndrome group B cells. *Nucleic Acids Res.*, **27**, 1365-1368.

25. Osterod,M., Larsen,E., Le Page,F., Hengstler,J.G., Van Der Horst,G.T., Boiteux,S., Klungland,A. and Epe,B. (2002) A global DNA repair mechanism involving the Cockayne syndrome B (CSB) gene product can prevent the in vivo accumulation of endogenous oxidative DNA base damage. *Oncogene*, **21**, 8232-8239.

26. Stevnsner,T., Muftuoglu,M., Aamann,M.D. and Bohr,V.A. (2008) The role of Cockayne Syndrome group B (CSB) protein in base excision repair and aging. *Mech. Ageing Dev.*, **129**, 441-448.

27. Tuo,J., Chen,C., Zeng,X., Christiansen,M. and Bohr,V.A. (2002) Functional crosstalk between hOgg1 and the helicase domain of Cockayne syndrome group B protein. *DNA Repair*, **1**, 913-927.

28. Singh,S.K., Szulik,M.W., Ganguly,M., Khutsishvili,I., Stone,M.P., Marky,L.A. and Gold,B. (2011) Characterization of DNA with an 8-oxoguanine modification. *Nucleic Acids Res.*, **39**, 6789-6801.

29. Kathe,S.D., Shen,G.P. and Wallace,S.S. (2004) Single-stranded breaks in DNA but not oxidative DNA base damages block transcriptional elongation by RNA polymerase II in HeLa cell nuclear extracts. *J. Biol. Chem.*, **279**, 18511-18520.

30. Khobta,A., Kitsera,N., Speckmann,B. and Epe,B. (2009) 8-Oxoguanine DNA glycosylase (Ogg1) causes a transcriptional inactivation of damaged DNA in the absence of functional Cockayne syndrome B (Csb) protein. *DNA Repair*, **8**, 309-317.

31. Kitsera,N., Stathis,D., Luhnsdorf,B., Muller,H., Carell,T., Epe,B. and Khobta,A. (2011) 8-Oxo-7,8-dihydroguanine in DNA does not constitute a barrier to transcription, but is converted into transcription-blocking damage by OGG1. *Nucleic Acids Res.*, **39**, 5926-5934.

32. Charles Richard,J.L., Shukla,M.S., Menoni,H., Ouararhni,K., Lone,I.N., Roulland,Y., Papin,C., Ben Simon,E., Kundu,T., Hamiche,A. *et al.* (2016) FACT Assists Base Excision Repair by Boosting the Remodeling Activity of RSC. *PLoS Genet.*, **12**, e1006221.

33. Dinant,C., Ampatziadis-Michailidis,G., Lans,H., Tresini,M., Lagarou,A., Grosbart,M., Theil,A.F., van Cappellen,W.A., Kimura,H., Bartek,J. *et al.* (2013) Enhanced chromatin dynamics by FACT promotes transcriptional restart after UV-induced DNA damage. *Mol. Cell*, **51**, 469-479.

34. Sanjana,N.E., Shalem,O. and Zhang,F. (2014) Improved vectors and genome-wide libraries for CRISPR screening. *Nat. Methods*, **11**, 783-784.

35. Campeau,E., Ruhl,V.E., Rodier,F., Smith,C.L., Rahmberg,B.L., Fuss,J.O., Campisi,J., Yaswen,P., Cooper,P.K. and Kaufman,P.D. (2009) A versatile viral system for expression and depletion of proteins in mammalian cells. *PLoS One*, **4**, e6529.

36. van Cuijk,L., van Belle,G.J., Turkyilmaz,Y., Poulsen,S.L., Janssens,R.C., Theil,A.F., Sabatella,M., Lans,H., Mailand,N., Houtsmuller,A.B. *et al.* (2015) SUMO and ubiquitin-dependent XPC exchange drives nucleotide excision repair. *Nat. Commun.*, **6**, 7499.

37. Garcia Soriano,F., Virag,L., Jagtap,P., Szabo,E., Mabley,J.G., Liaudet,L., Marton,A., Hoyt,D.G., Murthy,K.G., Salzman,A.L. *et al.* (2001) Diabetic endothelial dysfunction: the role of poly(ADP-ribose) polymerase activation. *Nat. Med.*, **7**, 108-113.

38. Bensaude,O. (2011) Inhibiting eukaryotic transcription: Which compound to choose? How to evaluate its activity? *Transcription*, **2**, 103-108.

39. Amouroux,R., Campalans,A., Epe,B. and Radicella,J.P. (2010) Oxidative stress triggers the preferential assembly of base excision repair complexes on open chromatin regions. *Nucleic Acids Res.*, **38**, 2878-2890.

40. Ropolo,M., Degan,P., Foresta,M., D'Errico,M., Lasiglie,D., Dogliotti,E., Casartelli,G., Zupo,S., Poggi,A. and Frosina,G. (2007) Complementation of the oxidatively damaged DNA repair defect in Cockayne syndrome A and B cells by Escherichia coli formamidopyrimidine DNA glycosylase. *Free Radic. Biol. Med.*, **42**, 1807-1817.

41. Guo,J., Hanawalt,P.C. and Spivak,G. (2013) Comet-FISH with strand-specific probes reveals transcription-coupled repair of 8-oxoGuanine in human cells. *Nucleic Acids Res.*, **41**, 7700-7712.

**5**

42. Kong,X., Mohanty,S.K., Stephens,J., Heale,J.T., Gomez-Godinez,V., Shi,L.Z., Kim,J.S.,Yokomori,K. and Berns,M.W. (2009) Comparative analysis of different laser systems to study cellular responses to DNA damage in mammalian cells. *Nucleic Acids Res.*, **37**, e68.

43. Lan,L., Nakajima,S., Oohata,Y., Takao,M., Okano,S., Masutani,M., Wilson,S.H. and Yasui,A. (2004) In situ analysis of repair processes for oxidative DNA damage in mammalian cells. *Proc. Natl. Acad. Sci. U.S.A.*, **101**, 13738-13743.

44. El-Khamisy,S.F., Masutani,M., Suzuki,H. and Caldecott,K.W. (2003) A requirement for PARP-1 for the assembly or stability of XRCC1 nuclear foci at sites of oxidative DNA damage. *Nucleic Acids Res.*, **31**, 5526-5533.

45. Charlet-Berguerand,N., Feuerhahn,S., Kong,S.E., Ziserman,H., Conaway,J.W., Conaway,R. and Egly,J.M. (2006) RNA polymerase II bypass of oxidative DNA damage is regulated by transcription elongation factors. *EMBO J.*, **25**, 5481-5491.

46. Steurer,B. and Marteijn,J.A. (2016) Traveling Rocky Roads: The Consequences of Transcription-Blocking DNA Lesions on RNA Polymerase II. *J. Mol. Biol.*, **429**, 3146-3155

47. Nazarkina,Z.K., Khodyreva,S.N., Marsin,S., Lavrik,O.I. and Radicella,J.P. (2007) XRCC1 interactions with base excision repair DNA intermediates. *DNA Repair*, **6**, 254-264.

48. Klungland, A., Rosewell, I., Hollenbach, S., Larsen, E., Daly, G., Epe, B., Seeberg, E., Lindahl, T. and Barnes, D.E. (1999) Accumulation of premutagenic DNA lesions in mice defective in removal of oxidative base damage. Proc Natl Acad Sci U S A, **96**, 13300-13305.

49. Tornaletti,S., Maeda,L.S., Kolodner,R.D. and Hanawalt,P.C. (2004) Effect of 8-oxoguanine on transcription elongation by T7 RNA polymerase and mammalian RNA polymerase II. *DNA Repair*, **3**, 483-494.

50. Menoni,H., Di Mascio,P., Cadet,J., Dimitrov,S. and Angelov,D. (2017) Chromatin associated mechanisms in base excision repair - nucleosome remodeling and DNA transcription, two key players. *Free Radic. Biol. Med.*, **107**, 159-169.

51. Adam,S., Polo,S.E. and Almouzni,G. (2013) Transcription recovery after DNA damage requires chromatin priming by the H3.3 histone chaperone HIRA. *Cell*, **155**, 94-106.

52. Aydin,O.Z., Vermeulen,W. and Lans,H. (2014) ISWI chromatin remodeling complexes in the DNA damage response. *Cell Cycle*, **13**, 3016-3025.

53. Oksenych,V., Zhovmer,A., Ziani,S., Mari,P.O., Eberova,J., Nardo,T., Stefanini,M., Giglia-Mari,G., Egly,J.M. and Coin,F. (2013) Histone methyltransferase DOT1L drives recovery of gene expression after a genotoxic attack. *PLoS Genet.*, **9**, e1003611.

54. Okano,S., Lan,L., Caldecott,K.W., Mori,T. and Yasui,A. (2003) Spatial and temporal cellular responses to single-strand breaks in human cells. *Mol. Cell. Biol.*, **23**, 3974-3981.

55. Flohr,C., Bürkle,A., Radicella,J.P. and Epe,B. (2003) Poly(ADP-ribosyl)ation accelerates DNA repair in a pathway dependent on Cockayne syndrome B protein. *Nucleic Acids Res.*, **31**, 5332-5337.

**5**

A — wt CSB (2.1 kb), CSB KO (~210 bp), MRC-5: wt KO1

B — MRC-5 wt CSB-/-, CSB, tubulin

C — relative colony number vs UV-C dose (J/m²), MRC-5 wt, CSB-/-

D — relative colony number vs KBrO₃ (mM), MRC-5 wt, CSB-/-

E — OGG1-dsRed on 405 + Ro, relative fluorescence (%) vs time (s), HeLa siCTRL, siCSB

F — OGG1-dsRed on 405 + Ro, relative fluorescence (%) vs time (s), HeLa siCTRL siCSB, no damage, on damage

G — HeLa siCTRL siCSB, CSB, tubulin, OGG1

H — XRCC1^L360D-YFP on 405 + Ro, relative fluorescence (%) vs time (s), HeLa CS1AN, no inhibition, PARPi

**Supplemental Figure 1**

**(A)** To verify the CSB knock out in MRC-5 cells, PCR amplification over the deleted exon 3 of the endogenous CSB gene was performed. Lane 1 (wt) shows the PCR product of wt CSB with the expected 2.1 kb band, lane 2 shows the PCR product of the knock out (KO) clone in which exon 3 of CSB is deleted, producing a PCR product with the expected 210 bp. **(B)** Protein expression was analyzed by Western blotting, probed with anti- CSB and anti-tubulin (loading control) antibodies. The arrow indicates the full length CSB protein and * indicates a splice-variant creating the CSB-PiggyBac fusion protein. Colony survival of MRC-5 wt (blue) and MRC-5 CSB-deficient (orange) cells following **(C)** UV irradiation **(D)** or treatment with potassium bromate (KBrO) to induce oxidative damage. The percentage of 3 surviving cells is plotted against the applied UV-C (J/m2) or KBrO3 (mM) dose. Data represent at least two independent experiments. **(E)** Accumulation kinetics of OGG1-DsRed stably expressed in HeLa cells after silencing CSB (siCSB) or a negative silencing control (siCTRL) (knock-down, shown in panel (H)) at micro-irradiated (405 nm laser) subnuclear regions in the presence of 5 µM Ro 19-8022 photosensitizer (n = 15 cells ± SEM). **(F)** FRAP analysis of OGG1-DsRed stably expressed in HeLa cells after silencing CSB (siCSB) or a negative silencing control (siCTRL) at locally damaged areas (on damage) or at a similar sized area without DNA damage (no damage) (n = 15 cells ± SEM). **(G)** The efficiency of siRNA mediated knock down of CSB and the effect of its depletion on OGG1 expression was evaluated using Western blotting probed with CSB, Tubulin and OGG1 antibodies. The arrow indicates the position of the full length CSB protein and asterisk (*) points to the position of the CSB-PiggyBac fusion protein. Anti-Tubulin was used a loading control. **(H)** Accumulation kinetics of the XRCC1L360D-YFP mutant at micro-irradiated areas in the presence of 5 µM Ro 19-8022 photosensitizer. The mean relative fluorescence intensity is plotted against time in seconds. Graphs represent the mean relative fluorescence intensity of at least 6 cells ± SEM.

5

A  CS1AN-SV + mCherry-CSB + XRCC1-EYFP
transmission  XRCC1-EYFP  mCherry-CSB  overlay
pre-damage
post-damage

B  HeLa + XRCC1$^{L360D}$ + OGG1-DsRed
untreated / + ActD
XRCC1$^{L360D}$  OGG1  merged  XRCC1$^{L360D}$  OGG1  merged
pre-damage
post-damage 30 s
post-damage 60 s

C
enrichment ratio
time (s)
untreated  DRB  ActD

D  HeLa + XRCC1$^{L360D}$ + OGG1-DsRed
untreated / + DRB
XRCC1$^{L360D}$  OGG1  merged  XRCC1$^{L360D}$  OGG1  merged
pre-damage
post-damage 60 s

E  XRCC1$^{L360D}$-YFP on 405 + Ro
relative fluorescence (%)
time (s)
MRC-5
siCTRL
siOGG1

F  siRNA: CTRL  OGG1
OGG1
SFPQ

**Supplemental Figure 2**

**(A)** Representative stills of time-lapse imaging of stably expressing XRCC1-EYFP (green) and mCherry-CSB (red) in CS1AN-SV cells, show co-localization (overlay) of CSB and XRCC1 at damage (405 nm in the presence of 10 μM Ro 19-8022 photosensitizer). Arrows point to position of the local oxidative DNA damage. **(B, C)** XRCC1 binding to BER induced breaks is reduced after transcription inhibition. **(B)** Representative stills of time-lapse imaging to determine accumulation kinetics of XRCC1$^{L360D}$-YFP and OGG1-DsRed in untreated (left panel) or transcription inhibited (1μg/ml Actinomycin D, ActD, right panel) in HeLa cells at damaged (405 nm laser + 10 μM Ro 19-8022) subnuclear regions, indicated by arrows. **(C)** Accumulation kinetics of XRCC1$^{L360D}$-YFP at micro-irradiated areas (as shown in A). The mean relative fluorescence intensity is plotted against time in seconds. Error bars indicate the standard deviation of 20 cells of 2 independent, pooled experiments. **(D)** Representative stills of time-lapse imaging to determine accumulation kinetics of XRCC1$^{L360D}$-YFP and OGG1-DsRed in untreated (left panel) or transcription inhibited (DRB, 100 μM, right panel) in HeLa cells at damaged (405 nm laser + 10 μM Ro 19-8022) subnuclear regions. **(E)** Accumulation kinetics of XRCC1$^{L360D}$-YFP at damaged areas were determined in control, or in siRNA-mediated OGG1 knock down MRC-5 cells. Damage was induced by 10 μM Ro 19-8022 photosensitizer. Error bars indicate the standard deviation of 10 cells. **(F)** Western blot of siRNA (control; CTRL and OGG1 targeting) treated MRC5 cells that stably express XRCC1$^{L360D}$-YFP), probed with OGG1 and SFPQ antibodies.

5

# Appendix

Summary

Samenvatting

Zusammenfassung

Curriculum Vitae

List of Publications

PhD-portofolio

Acknowledgements/Danksagung/
Dankwoord

# Summary

DNA, the carrier of the genetic information of all organisms, is vulnerable to chemical changes induced by processes in the cell as well as by environmental DNA damaging agents, including chemicals in food and air pollution and by radiation. Even the apparent harmless radiation from sunlight is dangerous for DNA. Sunlight includes the invisible UV-light, which can damage DNA by inducing specific lesions, such as cyclobutane pyrimidine dimers (CPD) and 6-4 pyrimidine-pyrimidone photoproducts (6-4PPs). Damaged DNA severely affects its normal function, *i.e.*: duplication (replication) of DNA required for cell propagation and transcription, the process that reads the information stored in genes. Both replication and transcription are vital for cells and organisms. Moreover, persistent DNA damage can result in alterations of the original DNA code (mutations) and can lead to the development of cancer and accelerated ageing. It is thus crucial to protect DNA against damage and, if present, to quickly remove DNA damage.

To circumvent the serious consequences of DNA damage, cells are equipped with the so-called DNA damage response (DDR), which is a collection of several DNA repair systems and signalling pathways. This thesis is mainly focused on one such DNA repair system, Transcription-Coupled Nucleotide Excision Repair (TC-NER). TC-NER removes helix-distorting DNA lesions, such as those induced by UV-light, in actively transcribed genes. The progression of transcription is blocked when RNA polymerase II (RNAP II) encounters such a helix distorting lesion. This results in perturbed transcription, the disturbance of internal cellular processes and jeopardizes normal cell function. Stalled RNAP II initiates the recruitment of TC-NER factors to the lesion site, such as the Cockayne Syndrome proteins A (CSA) and B (CSB) and the UV-stimulated scaffolding protein A (UVSSA). The assembly of these factors translates into active TC-NER, channelling into the unwinding of the DNA and subsequent dual incisions in the DNA around the lesion. The excised DNA fragment of about 22 to 30 nucleotides is then removed, and the resulting single-strand gap is filled by DNA synthesis and sealed by ligation, which completes the repair.

Two syndromes are linked to defective TC-NER: Cockayne Syndrome (CS) and UV-sensitivity syndrome (UV$^S$S). Mutations in the *CSA* and *CSB* genes are causative of CS, while most UV$^S$S patients have a mutation in the *UVSSA* gene. Both syndromes are characterized by a TC-NER deficiency upon UV-light induced DNA damage and patients show photosensitivity. Strikingly however,

CS patients show additional severe clinical abnormalities which are absent in UV$^S$S patients, such as growth failure, progressive neurodevelopmental defects and premature ageing.

The remarkable differences between CS and UV$^S$S are hypothesized to be caused by functions of CSA and CSB in other processes and pathways, for example in oxidative DNA damage repair. Byproducts of normal cell metabolism can cause a variety of different types of oxidative DNA damage, such as 8-oxo-7,8-dihydroguanine (8-oxoG), one of the most abundant oxidative DNA lesions. Since it was found that CSA- and CSB-deficient cells are also hypersensitive to oxidative DNA lesions, it was suggested that endogenously produced DNA damage cannot be removed from the transcribed strand in these cells. The gradual accumulation of stalled RNAP II at persistent DNA lesions induces transcription stress, causing a disturbed cellular homeostasis, senescence or even apoptosis, eventually leading to the salient progressive CS-specific features.

Background to the experimental work in this thesis on the DDR, its biological significance and a general introduction to DNA repair, focussing on TC-NER, and the controversy regarding the various explanations of the phenotypical differences between CS and UV$^S$S were introduced and discussed in **Chapter 1**. In **Chapter 2** the development and application of a novel method, called amplified Unscheduled DNA Synthesis (AUDS), for detecting excision-based DNA repair activity is described. Previously, no user-friendly, single cell assay was available for assessing the activity of specific excision-based DNA repair, such as TC-NER and Base Excision Repair (BER). Our newly developed, immunofluorescence-based, method allows to directly measure TC-NER activity, already at low, physiological relevant UV-C doses, such as 2 J/m$^2$. This novel procedure was applied and appeared to be instrumental to further dissect TC-NER, focussing on the role of UVSSA, described in Chapters 3 and 4.

In **Chapter 3** we investigated the mechanisms by which UVSSA is recruited to UV-induced DNA damage. In line with previous data from our lab, but in contrast to other reports, we could confirm a CSA- and CSB-independent accumulation of UVSSA. With live cell imaging we found that especially the DUF2043 domain, and not the VHS domain of UVSSA is involved in the accumulation of UVSSA at UV-damaged areas in the nucleus. By analysing proteins that specifically interact with the DUF2043 domain, we aimed to identify novel factors involved in the binding of UVSSA to TC-NER complexes. We compared the potential difference

of interactors between full length UVSSA and the two domain deletion mutants and identified the two subunits of the FACT complex, Spt16 and SSRP1, as specific binders of the DUF2043 domain. We showed that depletion of Spt16 specifically affects the accumulation of UVSSA but not of the other TC-NER factors. The presented data further helps to elucidate the molecular function of UVSSA and contributed to understand the many aspects of TC-NER regulation.

The involvement of UVSSA in UV-damage repair has been widely accepted, whereas its role in the repair of oxidative DNA damage has been questioned. Surprisingly however, we showed that UVSSA is involved in the repair of oxidative DNA damage by using the sensitive AUDS assay. These unanticipated findings prompted us to further explore whether UVSSA has potential functions in the repair of oxidative DNA damage which were described in **Chapter 4**. Interestingly, we found that the accumulation of UVSSA on oxidative DNA damage is neither dependent on the DUF2043 domain, nor on the Spt16 subunit of FACT, as both were previously identified to be required for its accumulation on UV-damage. To identify proteins involved in the damage-specific function of UVSSA, *i.e.* proteins that bind to UVSSA either after UV-irradiation or after oxidative DNA damage induction, we used a quantitative mass spectrometry approach. We identified the NuRD complex and the Mediator complex, both involved in transcription and RNA metabolism, as UV-specific UVSSA-interactors, *i.e.* not enriched in their association to UVSSA upon oxidative damage. Nucleotide binding and mitochondrial function proteins and complexes were identified as specific UVSSA interactors upon oxidative damage. Interestingly, oxidative damage causes a decreased interaction of UVSSA with especially proteins involved in RNA processing. This indicates that, in situations of differing DNA damage, UVSSA interacts with different complexes, and thus likely exhibits different functions. These data challenge the hypothesis that the different phenotypes of CS and UV$^S$S are a result of CSA and CSB being involved in the repair of oxidative DNA damage, and UVSSA is not.

To further elucidate the involvement of TC-NER factors in the repair of oxidative DNA damage, we analysed the significance and mechanism of the accumulation of CSB on oxidative DNA damage in **Chapter 5.** Previously, our lab reported this accumulation to be transcription-dependent. We identified a role for CSB in facilitating the transcription-dependent recruitment of X-ray repair cross-complementing protein 1 (XRCC1) to single strand breaks (SSBs), which are formed as intermediate products of the BER reaction. This finding contrasts to the known accumulation of XRCC1 on BER-unrelated SSBs, which is CSB and

transcription independent. We propose a model in which BER progression on active genes is facilitated by CSB through enabling the recruitment of XRCC1 to RNAP II shielded lesions. These observations further strengthen the hypothesis of the involvement of TC-NER factors in the response to oxidative DNA damage, the possible existence of a dedicated transcription-associated BER pathway and that TC-NER factors are involved in different repair pathways.

In **Chapter 6** the main data and results of the experimental work compiled in this thesis are summarized and discussed, complemented with a discussion on future directions of research for gaining more insight in the function and regulation of TC-NER, BER and the factors involved.

## Samenvatting

DNA, de drager van genetische informatie van alle organismen, is kwetsbaar voor chemische veranderingen veroorzaakt door processen in de cel alsmede DNA beschadigende factoren in het milieu, waaronder chemicaliën in voedsel en de lucht en straling. Zelfs de onschuldig lijkende straling van zonlicht is gevaarlijk voor DNA. De onzichtbare UV-straling, aanwezig in zonlicht, kan DNA beschadigen door het toebrengen van specifieke laesies, zoals cyclobutaan-pyrimidine-dimeren (CPD) en 6-4 pyrimidine-pyrimidone-phosphoproducten (6-4PPs). DNA beschadigingen verstoren de normale functies van DNA; zoals de verdubbeling (replicatie) van DNA, wat nodig is voor iedere celdelingen en de transcriptie van DNA, het proces waarbij de informatie die ligt opgeslagen in genen wordt gelezen. Zowel replicatie en transcriptie zijn van levensbelang voor cellen en organismen. Bovendien kunnen persisterende DNA-beschadigingen blijvende veranderingen in de originele DNA-code (mutaties) veroorzaken en daarmee leiden tot de ontwikkeling van kanker en versneld ouder worden. Het is dus uitermate belangrijk om DNA te beschermen en om de reeds opgelopen schade snel te repareren.

Om ernstige consequenties van DNA-schade te vermijden, zijn cellen uitgerust met de zogeheten DNA damage response (DDR), een verzameling van verschillende DNA-reparatie systemen en signaleringsroutes. Dit proefschrift is voornamelijk gefocust op één van deze reparatie systemen, Transcription-Coupled Nucelotide Excision Repair (TC-NER). TC-NER verwijdert helix-deformerende DNA-laesies, zoals die gevormd door UV-straling, uit genen die transcriptie ondergaan. De voortgang van transcriptie wordt geblokkeerd zodra RNA-polymerase II (RNAP II) een helix-deformerende laesie tegen komt. Dit leidt tot onderbroken transcriptie, het verstoren van interne cellulaire processen en brengt de normale cel-functies in gevaar. Gehinderd RNAP II initieert het rekruteren van TC-NER factoren, zoals de Cockayne Syndrome eiwitten A (CSA) en B (CSB) en UV-stimulated scaffolding protein A (UVSSA), naar de beschadigde locatie op het DNA. Het samenkomen van deze factoren leidt tot TC-NER-activatie, waarbij aan weerszijde van de schade een incisie in het DNA gemaakt wordt. Een fragment van ongeveer 30 nucleotiden rond de laesie wordt vervolgens verwijderd en het complementaire, enkelstrengs DNA wordt ingevuld doormiddel van DNA-synthese. Het nieuwe DNA wordt vervolgens geligeerd aan het oorspronkelijke DNA waarmee de reparatie is voltooid.

Aangeboren afwijkingen in TC-NER veroorzaken twee verschillende syndromen: Cockayne Syndrome (CS) en UV-sensitivity syndrome (UV$^S$S). CS wordt veroorzaakt door mutaties in de *CSA* en *CSB* genen, terwijl de meeste UV$^S$S-patiënten een mutatie in het *UVSSA* gen hebben. Patiënten van beide aandoeningen vertonen overgevoeligheid voor zonlicht omdat ze, door een gebrekkige TC-NER reactie, DNA-schades veroorzaakt door UV-licht niet kunnen verwijderen. Naast zonlicht gevoeligheid lijden CS-patiënten, in tegenstelling tot UV$^S$S-patiënten, ook aan ernstige groeibeperkingen, progressieve neurologische degeneratie en versnelde veroudering. Deze opmerkelijke verschillen tussen CS en UV$^S$S worden verondersteld het resultaat te zijn van verstoringen in andere DNA reparatie processen en signaleringsroutes waarin CSA en CSB een rol spelen, bijvoorbeeld de reparatie van oxidatieve DNA-schade. Bijproducten van normaal metabolisme kunnen in cellen verschillende typen oxidatieve DNA schade aanrichten, zoals 8-oxo-7,8-dihydroguanine (8-oxoG), één van de meest voorkomende oxidatieve DNA-laesies. De ontdekking van hypergevoeligheid van CSA- en CSB-deficiënte cellen voor oxidatieve DNA-laesies, leidde tot de suggestie dat DNA-schade van endogene oorsprong in deze cellen niet kan worden verwijderd van DNA strengen die transcriptie ondergaan. De geleidelijke accumulatie van gehinderd RNAP II bij niet-gerepareerde DNA-laesies induceert transcriptiestress wat een verstoorde cellulaire homeostase of zelfs apoptose veroorzaakt en uiteindelijk leidt tot de opvallende progressieve, CS-specifieke afwijkingen.

In **Hoofdstuk 1** wordt begeleidende achtergrondinformatie geven voor het in dit proefschrift beschreven experimentele werk. Naast een algemene inleiding over de oorzaak en gevolgen van DNA schade wordt ook de cellulaire respons op DNA schade (DDR) kort besproken. Aangezien de focus van het experimentele werk gericht is op TC-NER, zal dit uitgebreider worden belicht en zal nader worden ingegaan op de controverse over de verschillende verklaringen van de fenotypische verschillen tussen CS en UV$^S$S. **Hoofdstuk 2** beschrijft de ontwikkeling en toepassing van een nieuwe methode, amplified Unscheduled DNA Synthesis (AUDS) genaamd, voor de detectie van op excisie-gebaseerde DNA reparatie activiteit. Voorheen was er geen gebruiksvriendelijke enkele-cel-analyse beschikbaar om de activiteit te meten van specifieke excisie DNA repair processen, zoals TC-NER en Base Excision Repair (BER). Onze nieuw ontwikkelde, op immunofluorescentie gebaseerde, methode maakt het mogelijk om direct TC-NER te meten, zelfs bij lage, fysiologisch relevante UV-C doses, zoals na UV-bestraling met slechts 2 J/m$^2$. Deze nieuwe procedure hebben we toegepast voor de verdere analyse van TC-NER in hoofdstukken 3 en 4 waarin de rol van UVSSA centraal staat.

In **Hoofdstuk 3** onderzochten we het mechanisme waardoor UVSSA wordt gerekruteerd naar UV-geïnduceerde DNA-schade. In overeenstemming met eerdere experimenten van ons laboratorium vonden we dat UVSSA accumuleert op DNA schade in een CSA- en CSB-onafhankelijke manier, dit in tegenstellingen tot bevindingen van andere laboratoria. Met behulp van microscopie van levende cellen, met een zogenaamde confocale microscoop, konden we aantonen dat het DUF2043- en niet het VHS-domein van het UVSSA eiwit betrokken is bij de ophoping van UVSSA in UV-beschadigde gebieden in de celkern. Door eiwitten die specifiek met het DUF2043-domein interacteren te analyseren, probeerden we nieuwe factoren te identificeren die betrokken zijn bij de binding van UVSSA aan TC-NER-complexen. Hiertoe vergeleken we, met behulp van kwantitatieve massa-spectrometrie, de verschillende eiwitten die aan het volledige UVSSA-eiwit of aan de twee verschillende domein-deletiemutanten binden. Op deze manier identificeerden we de eiwitten Spt16 en SSRP1, die samen het FACT-complex vormen, als specifieke bindingspartners van het DUF2043-domein. We lieten zien dat specifiek het wegnemen van Spt16, de accumulatie van UVSSA op DNA schade verminderde, maar niet dat van andere TC-NER factoren. De gepresenteerde data dragen bij aan een beter begrip van de moleculaire functie van UVSSA en de vele aspecten van TC-NER-regulatie.

Het idee dat UVSSA een rol speelt in de reparatie van UV-schade wordt breed gedragen, echter de betrokkenheid van UVSSA bij de reparatie van oxidatieve DNA-schade wordt betwijfeld. Opvallenderwijs lieten wij met behulp van de AUDS-assay zien dat UVSSA weldegelijk een rol speelt in de reparatie van oxidatieve DNA-schade. Dit onvoorziene resultaat dreef ons ertoe om in **Hoofdstuk 4** de betrokkenheid van UVSSA in de oxidatieve DNA-schade respons verder te bestuderen. We vonden dat de accumulatie van UVSSA op oxidatieve DNA-schade onafhankelijk is van zowel het DUF2043-domein als het Spt16 onderdeel van FACT, twee factoren waarvan we eerder in hoofdstuk 3 lieten zien dat ze nodig waren voor UVSSA-accumulatie op UV-schade. Om de eiwitten die betrokken zijn bij de schade-specifieke functie van UVSSA te identificeren, dat zijn eiwitten die specifiek aan UVSSA binden na of blootstelling aan UV-licht of na oxidatieve schade inductie, maakten we gebruik van kwantitatieve massaspectrometrie. We identificeerden het NuRD complex en het Mediator complex, beide betrokken in transcriptie en RNA-metabolisme, als UV-specifieke UVSSA-interactiepartners. Dat wil zeggen dat deze complexen bij UV-schade, in tegenstelling tot bij oxidatieve schade, verhoogde associatie met UVSSA vertoonde. Nucleotide binding- en mitochondriële functie-eiwitten werden geïdentificeerd als oxidatief-specifieke UVSSA-interactiepartners. Opmerkelijk

is dat oxidatieve DNA schade een verminderde interactie veroorzaakt van UVSSA met eiwitten betrokken bij het verwerken van RNA. Dit suggereert dat afhankelijk van de DNA-schade, UVSSA met andere complexen interacties aangaat en dus waarschijnlijk een andere functie vervult. Deze bevindingen staan haaks op de hypothese dat de fenotypische verschillen tussen CS en UV$^S$S het resultaat zijn van het feit dat UVSSA niet betrokken is bij de reparatie van oxidatieve schade, waar CSA en CSB dat wel zijn.

Om de betrokkenheid van TC-NER factoren in de reparatie van oxidatieve DNA-schade nader te bestuderen, analyseerden we in **Hoofdstuk 5** hoe en waarom CSB bindt aan oxidatieve DNA-schade. Voorheen hebben we in ons laboratorium gevonden dat deze binding afhankelijk is van transcriptie. We konden aantonen dat CSB nodig is voor de transcriptie afhankelijke rekrutering van X-ray repair cross-complementing protein 1 (XRCC1) naar single strand breaks (SSBs). SSBs zijn een tussenproduct van de BER-reactie. Dit resultaat staat in contrast met de bekende accumulatie van XRCC1 op BER-ongerelateerde SSBs, wat onafhankelijk is van zowel CSB als transcriptie. Op grond van deze resultaten stellen we een model voor waarin CSB XRCC1 kan rekruteren naar de door RNAP II afgeschermde laesies, waardoor de voortgang van BER op actieve genen mogelijk gemaakt wordt. Deze bevindingen ondersteunen de hypothese dat TC-NER factoren een rol spelen in de respons op oxidatieve DNA-schade, het mogelijke bestaan van een exclusief transcriptie-geassocieerd BER proces en dat TC-NER factoren betrokken zijn in verschillende reparatie processen.

In **Hoofdstuk 6** worden de voornaamste data en resultaten van het experimentele werk verzameld in dit proefschrift samengevat en bediscussieerd. Daarbij worden ook toekomstige onderzoeksrichtingen besproken, die meer inzicht zouden kunnen geven in functie en regulatie van TC-NER, BER en de factoren die daarin een rol spelen.

# Zusammenfassung

Die DNA, der Träger der genetischen Information aller Organismen, ist anfällig für chemische Veränderungen die durch Vorgänge in der Zelle oder durch DNA-schädigende Agenzien aus der Umgebung induziert werden. Das schließt Chemikalien in der Nahrung und aus der Luft sowie Strahlungseinflüsse ein. Selbst die scheinbar harmlose Strahlung des Sonnenlichts ist potentiell schädlich für die DNA. Das Sonnenlicht umfasst auch die unsichtbare UV-Strahlung, welche die DNA durch die Induktion spezifischer Veränderungen wie cyclobutane pyrimidine dimers (CPD) und 6-4 pyrimidine-pyrimidone photoproducts (6-4PPs) schädigt. Die DNA-Schäden beeinflussen die normalen Funktionen der Erbsubstanz: die Verdopplung (Replikation) der DNA bei der Zellteilung und die Transkription, also den Prozess des Auslesens der in den Genen enthaltenen Information.

Sowohl Replikation als auch Transkription sind lebenswichtig für Zellen und Organismen. Darüber hinaus kann anhaltende DNA-Schädigung den ursprünglichen genetischen Code durch Mutationen verändern und zur Entstehung von Krebs und beschleunigter Alterung führen. Deshalb ist es für Organismen lebenswichtig die DNA gegen Schäden zu schützen und vorhandene Schäden schnell zu beseitigen.

Zur Vermeidung der ernsthaften Folgen von DNA-Schäden sind alle Zellen mit sogenannten DNA damage response (DDR) Systemen ausgestattet, einer Sammlung von verschiedenen DNA-Reparatursystemen und Signalwegen. Diese Doktorarbeit befasst sich hauptsächlich mit einem dieser DNA-Reparatursysteme, der Transkriptions-gekoppelten Nukleotid-Exzisions-Reparatur (Transcription-coupled Nucleotide Excision Repair, TC-NER). TC-NER entfernt helix-deformierende DNA-Schäden in aktiv transkribierten Genen, wie sie beispielsweise durch UV-Strahlung ausgelöst werden. Das Fortschreiten der Transkription wird verhindert, wenn die RNA-Polymerase II (RNAP II) auf eine helix-deformierende Verletzung trifft. Die führt zu einer Störung der Transkription, zur Beeinträchtigung interner zellulärer Prozesse und zur Gefährdung der normalen Zellfunktion. Die steckengebliebene RNAP II initiiert die Anlagerung von TC-NER Faktoren an der Stelle des Schadens, wie z.B. Cockayne Syndrom Protein A (CSA) und B (CSB) und UV-stimulated scaffolding protein A (UVSSA). Die Aggregation dieser Faktoren resultiert in aktivierter TC-NER, was zur Entspannung der DNA und anschließenden doppelte Einschnitten um die Verletzung führt. Das ausgeschnittene DNA-Fragment mit einer Länge

von ca. 30 Nukleotiden wird dann entfernt, und die entstandene Einzelstrang-DNA durch DNA-Synthese aufgefüllt. Die Reparatur wird durch das Schließen der Lücke durch Ligation abgeschlossen.

Zwei Syndrome stehen in Verbindung mit einem defekten TC-NER: das Cockayne-Syndrome (CS) und das UV-sensitivity syndrome (UV$^S$S). Mutationen in den Genen für *CSA* und *CSB* sind ursächlich für CS, während die meisten UV$^S$S Patienten eine Mutation im *UVSSA* Gen aufweisen. Beide Syndrome sind charakterisiert durch ein Defizit in TC-NER nach UV-induzierter DNA-Schädigung, und die betroffenen Patienten sind lichtempfindlich. Auffallend ist, dass CS-Patienten zusätzliche ein schweres klinisches Erscheinungsbild zeigen, das bei UV$^S$S-Patienten fehlt, wie z.B. Wachstumsstörungen, progressive neurologische Entwicklungsdefekte und vorzeitiges Altern.

Die bemerkenswerten Unterschiede zwischen CS und UV$^S$S werden einer Hypothese folgend durch Funktionen von CSA und CSB in anderen Prozessen und Reparaturmechanismen verursacht, wie z.B. in der oxidativen DNA-Schädigungs-Reparatur. Nebenprodukte des normalen zellulären Metabolismus können eine Reihe verschiedener Typen von oxidativen DNA-Schäden verursachen, wie 8-oxo-7,8-dihydroguanine (8-oxoG), einer der häufigsten oxidativen DNA-Verletzungen. Nachdem man herausgefunden hat, dass CSA- und CSB-defekte Zellen auch überempfindlich gegenüber diesen oxidativen DNA-Verletzungen sind, wurde angenommen, dass endogen erzeugte DNA-Schäden in diesen Zellen nicht aus dem transkribierten DNA-Strang entfernt werden können. Die allmähliche Anreicherung von blockierter RNAP II an persistierenden DNA-Verletzungen induziert Transkriptions-Stress, und führt zu einer gestörten zellulären Homöostase, Alterung oder sogar Zelltod (Apoptose), was schließlich zu den markant progressiven CS-spezifischen Merkmalen führt.

Der Hintergrund der experimentellen Arbeiten in dieser Promotionsschrift über DDR, ihrer biologischen Signifikanz und eine generelle Einleitung zur DNA-Reparatur mit einem Schwerpunkt auf TC-NER und die Kontroverse bezüglich der verschiedenen Erklärungen der phänotypischen Unterschiede zwischen CS und UV$^S$S werden im **Kapitel 1** vorgestellt und diskutiert. Im **Kapitel 2** wird die Entwicklung und Anwendung einer neuen Methodik, amplified Unscheduled DNA Synthesis (AUDS) genannt, zur Ermittlung exzisions-basierter DNA-Reparatur-Aktivitäten beschrieben. Zuvor war kein benutzerfreundlicher Einzelzell-Test zur Abschätzung der Aktivität von spezifischer exzisions-basierter DNA-Reparatur, wie TC-NER und Base Excision Repair (BER), verfügbar. Unsere neu entwickelte,

immunfluoreszenz-basierte Methode ermöglicht nicht nur die direkt Messung der TC-NER Aktivität, sondern erlaubt mit ihrer hohen Empfindlichkeit auch die Analyse der TC-NER-Aktivität bei geringen, physiologisch relevanten UV-C Dosen von etwa 2 J/m$^2$. Dieses neue Verfahren war hilfreich für die weitere Analyse von TC-NER mit Blick auf die Rolle von UVSSA, wie in den Kapiteln 3 und 4 beschrieben.

Im **Kapitel 3** werden die Mechanismen untersucht, durch die UVSSA an UV-induzierten DNA-Schäden rekrutiert wird. Im Einklang mit früheren Daten konnte eine CSA- und CSB-unabhängige Anreicherung von UVSSA nachgewiesen werden. Durch Live Cell Imaging fanden wir heraus, dass insbesondere die DUF2043 Domäne, und nicht die VHS-Domäne, an der der Akkumulation von UVSSA an UV-geschädigten Bereichen im Zellkern beteiligt ist. Durch die Analyse von Proteinen, die spezifisch mit der DUF2043-Domäne interagieren, versuchten wir neue Faktoren zu identifizieren, die an der Bindung von UVSSA an TC-NER-Komplexen beteiligt sind. Wir verglichen den möglichen Unterschied der Bindungspartner von komplettem UVSSA und den beiden Domänen-Deletions-Mutanten und konnten die beiden Untereinheiten des FACT-Komplexes, Spt16 und SSPR1, als spezifische Bindungspartner der DUF2043-Domäne identifizieren. Wir zeigten weiterhin, dass die Verminderung von Spt16 spezifisch die Anreicherung von UVSSA, aber nicht die der anderen TC-NER-Faktoren betrifft. Die vorgelegten Daten helfen ferner, die molekulare Funktion von UVSSA zu erhellen und tragen zum Verständnis der vielen Aspekte der TC-NER-Regulierung bei.

Während die Mitwirkung von UVSSA in der UV-Schaden-Reparatur weitgehend akzeptiert ist, wurde dessen Rolle bei der Reparatur oxidativer DNA-Schäden angezweifelt. Überraschenderweise konnten wir durch die Verwendung des AUDS-Verfahrens nachweisen, dass UVSSA an der Reparatur von oxidativen DNA-Schäden beteiligt ist. Dieser unerwartete Befund regte uns dazu an, weiter nachzuforschen, ob UVSSA mögliche Funktionen in der Reparatur oxidativer DNA-Schäden hat, was im **Kapitel 4** beschrieben wird. Wir fanden heraus, dass die Akkumulation von UVSSA bei oxidativen Schäden weder von der DUF2043-Domäne noch von der Spt16-Untereinheit von FACT abhängt, wie es für die ihre Akkumulation aufgrund von UV-Schäden erforderlich war. Um mögliche Faktoren oder Komplexe zu identifizieren, die in an der schadens-spezifischen Funktion von UVSSA beteiligt sind, verwendeten wir einen quantitative Massen-Spektroskopie-Ansatz. Wir zielten darauf ab, mögliche Unterschiede von UVSSA Bindunspartnern als Antwort auf UV- oder oxidative Schädigung zu

identifizieren. Wir fanden heraus, dass der NuRD-Komplex und der Mediator-Komplex, die beide an der Transkription und dem RNA-Metabolismus beteiligt sind, UV-spezifische Bindungspartner von UVSSA sind, d.h. in ihrer Assoziation mit UVSSA nach oxidativen Schäden nicht angereichert werden. Nukleotide-bindende und Mitochondrial-funktionelle Proteine und Komplexe wurden als spezifische UVSSA Bindungspartner nach oxidativen Schäden identifiziert. Interessanterweise verursacht oxidativer Schaden eine verringerte Interaktion von UVSSA insbesondere mit solchen Proteinen, die an der RNA-Prozessierung beteiligt sind. Dies zeigt, dass bei unterschiedlichen DNA-Schäden UVSSA mit verschiedenen Komplexen interagiert und somit unterschiedliche Funktion besitzt.

Diese Daten stellen die Hypothese in Frage, dass die unterschiedlichen Phänotypen von CS und UV$^S$S auf CSA und CSB zurückzuführen sind, die an der Reparatur oxidativer DNA-Schäden beteiligt sind, während UVSSA daran nicht beteiligt ist.

Um die Beteiligung der TC-NER-Faktoren bei der Reparatur oxidativer DNA-Schäden weiter zu erhellen, haben wir die Bedeutung und den Mechanismus der Akkumulation von CSB bei oxidativer DNA-Schädigung im **Kapitel 5** untersucht. In der Vergangenheit hat unser Labor bereits berichtet, dass diese Akkumulation von der Transkription abhängt. Wir konnten eine Rolle von CSB bei der Anreicherung von X-Ray Repair Cross-complementing Protein 1 (XRCC1) an Einzelstrangbrüchen, welche intermediäre Produkte der BER Reaktion sind, nachweisen. Dieser Befund steht im Widerspruch zur bekannten Anreicherung von XRCC1 an BER-unabhängigen Einzelstrangbrüchen, welche CSB- und transkriptions-unabhängig ist. Wir schlagen ein Model vor, in dem das Fortschreiten von BER an aktiven Genen durch CSB unterstützt wird, indem es die Rekrutierung von XRCC1 an von RNAP II abgedeckten Verletzungen erlaubt. Diese Beobachtungen unterstützen die Hypothese der Beteiligung von TC-NER-Faktoren als Reaktion auf oxidative DNA-Schäden und die Existenz eines zugehörigen transkriptions-assoziierten BER-Pfads sowie einer Beteiligung der TC-NER-Faktoren an verschiedene Reparatur-Mechanismen.

Im **Kapitel 6** werden die wichtigsten Daten und Ergebnisse der vorliegenden experimentellen Arbeit zusammengetragen und diskutiert, ergänzt um eine Diskussion der künftigen Richtung der Forschung, um ein tieferes Verständnis der Funktion und Regulation von TC-NER, BER und der beteiligten Faktoren zu erlangen.

## Curriculum Vitae

Franziska Wienholz was born on 31 march 1987 in Herdecke, Germany. In 2006 she graduated from Städtisches Gymnasium Gevelsberg (secondary school) in Germany. She started her study Medical Biology at the Radboud University Nijmegen in the Netherlands. During her master study she conducted two research internships, the first at the Radboud Institute for Molecular Life Sciences at the Department of Biochemistry of Integrated Systems under the supervision of Dr. Roland Brock and Dr. Merel Adjobo-Hermans. For her second internship she moved to the UK for conducting research at GlaxoSmithKline in Stevenage under the supervision of Dr. Laurens Kruidenier and Dr. Palwinder Mander. In 2012 she started her PhD research at the department of Molecular Genetics at the Erasmus MC. The research was conducted in the group of Prof. Dr. Wim Vermeulen under the supervision of Dr. Jurgen Marteijn and is presented in this thesis.

Since October 2017 she is working for Corning Life Sciences as Scientific Support Specialist.

## List of Publications

**The transcription-coupled DNA repair-initiating protein CSB promotes XRCC1 recruitment to oxidative DNA damage.**
H. Menoni, F. Wienholz, A.F. Theil, R.C. Janssens, H. Lans, A. Campalans, J.P. Radicella, J.A. Marteijn and W. Vermeulen. *Nucleic Acids Research* (2018).

**Live-cell analysis of endogenous GFP-RPB1 uncovers rapid turnover of initiating and promoter-paused RNA Polymerase II.**
B. Steurer, R.C. Janssens, B. Geverts, M.E. Geijer, F. Wienholz, A.F. Theil, J. Chang, S. Dealy, J. Pothof, W.A. van Cappellen, A.B. Houtsmuller and J.A. Marteijn. *Nucleic Acids Research* (2018).

**Amplification of unscheduled DNA synthesis signal enables fluorescence-based single cell quantification of transcription-coupled nucleotide excision repair.**
F. Wienholz, W. Vermeulen and J. A. Marteijn. *Nucleic Acids Research* (2017).

**A ubiquitylation site in Cockayne syndrome B required for repair of oxidative DNA damage, but not for transcription-coupled nucleotide excision repair.**
Ranes, M., S. Boeing, Y. Wang, F. Wienholz, H. Menoni, J. Walker, V. Encheva, P. Chakravarty, P. O. Mari, A. Stewart, G. Giglia-Mari, A. P. Snijders, W. Vermeulen and J. Q. Svejstrup. *Nucleic Acids Research* (2016).

# PhD Portofolio

**Name:** Franziska Wienholz
**PhD period:** Sep. 2012 – Aug. 2017

**ErasmusMC Department:** Molecular Genetics
**Research School:** MGC

**Promoter:** Prof. Dr. Wim Vermeulen
**Supervisor:** Dr. Jurgen Marteijn

|  | Year | Workload (ECTS/hours) | |
|---|---|---|---|
| **General Courses** | | | |
| Biomedical English Writing and Communication | 2015 | 3 | ECTS |
| Research Integrity | 2014 | 0.3 | ECTS |
| Literature Discussion | 2014 | 2 | ECTS |
| Statistics | 2013 | 2 | ECTS |
| Cell and Developmental Biology | 2013 | 3 | ECTS |
| Genetics | 2013 | 3 | ECTS |
| Biochemistry and Biophysics | 2012 | 3 | ECTS |
| Safely Working in the laboratory | 2012 | 8 | hours |
| | | | |
| **Specific Courses (e.g. Research school, Medical Training)** | | | |
| Media contacts for researchers | 2015 | 2.5 | hours |
| Genome Maintenance and Cancer | 2014 | 0.8 | ECTS |
| MGC Technology Facilities | 2014 | 0.4 | ECTS |
| Research Management for PhD-students | 2014 | 1 | ECTS |
| Leica Confocal Introduction Course | 2012 | 3 | hours |
| Cellular Imaging | 2012 | 1.8 | ECTS |
| | | | |
| **Seminars and Workshops** | | | |
| Amy & Friends Patientendag | 2014 | 0.15 | ECTS |
| Indesign CS6 Workshop | 2014 | 0.15 | ECTS |
| MGC PhD Workshop | 2013-2015 | 38 | hours |
| MGC Symposium | 2012, 2013 | 0.6 | ECTS |

|  | Year | Workload (ECTS/hours) | |
|---|---|---|---|
| **(Inter)national Conferences** | | | |
| Responses to DNA Damage: from molecule to disease | | | |
|   Egmond aan Zee, Poster presentation | 2016 | 8 | hours |
| Benzon Symposium: Nuclear Regulation by Ubiquitin | | | |
|   Copenhagen, Denmark, Poster presentation | 2014 | 30 | hours |
| Dutch Chromatin Meeting & NVBMB Fall Symposium | | | |
|   Rotterdam | 2013 | 8 | hours |
| | | | |
| **Supervising/Teaching** | | | |
| Journal Club BSc Nanobiology | 2014 | 0.15 | ECTS |
| Practical Genetics BSc Nanobiology | 2013-2016 | 12 | hours |
| Master student | 2013-2014 | 10 | months |

# Acknowledgements/Danksagung/Dankwoord

Was ein spannendes Ende einer noch spannenderen Zeit!
I want to thank everyone who supported, helped and guided me during the exciting time that I spent in the NER lab at Erasmus MC.

Om te beginnen, Jurgen, mijn directe begeleider. Heel erg bedankt voor wat je me hebt geleerd afgelopen jaren. Onder anderen het opzetten en uitvoeren van efficiënte experimenten (ook al voegde ik stiekem toch nog extra condities toe) en hoe ik mezelf moet motiveren en moest door zetten. Bedankt voor je geduld tijdens mijn schrijfproces. Ik kon altijd rekenen op je steun; niet in de laatste plaats toen Joris en ik een gezin begonnen. Ik wil je natuurlijk ook bedanken voor het delen van je 'vieze plaatjes collectie'.

Wim, ik noem je hier als tweede, maar als lab-leider en hart-onder-de-riem-steker, verdien je zonder einige twijfel een gedeeld eertse plek. Dank je wel voor de aangename tijd, de lange discussies, je open deur (in tegenstelling tot de deuren van vele duitse autoriteit personen) en het corrigeren van mijn Nederlands!

Dear Cristina, when you joined the lab, we immediately hit it off. You have been my true confidant throughout this journey. We shared highs and lows, both in the lab and in our private lives. I am truly grateful for your friendship which I am confident will last for years to come. I wish you and Ovidiu the best of luck for your shared future and lots of adventures. Maybe, one day, we can return the chandelier.

Dear Yasemin, when you joined us our threesome of musketeers was complete! I was really happy to have you as a friend directly next to me in the office to share jokes, frustrations and a supervisor with. I feel fortunate that I was able witness Maarten and you getting married. The two of you have always shown us incredible hospitality, which, on your wedding I experienced, was amplified by your extended family. Thank you for being not only a colleague, but also my friend!

Jana, during our time in the lab, we both were involved in significant genetic cloning experiments. I do believe that New Year's Eve 2016 gave us good directions for our futures: We read our fortunes with molten lead in water (futures which involved tadpoles for everyone it appeared). I wish you, Jurai and the kids a fantastic future, be it with or without even more tadpoles.

Hannes, dank je wel dat je Jurgen wilde afleiden wanneer ik er tussenuit wilde knijpen. Bedankt Hannes voor je geruststellende woorden en je positieve energie.

Dear Alice, you have spent a significant time with me during my second year. Thank you very much for your great help with setting up the CRISPR-Cas method and for your great enthusiasm and your independence. Every now and then I keep thinking about our cow-adventure in Germany. Thank you for teaching me that Cognac is the solution to all of life's problems.

Maria, thank you for your advice and support. Our talks were always encouraging as you convinced me of and showed appreciation for my own capabilities and talents. You are a very motivating and inspiring person.

Karen, heel erg bedankt voor de strakke organisatie van alle mogelijk labspullen en alles eromheen (je weet zelfs, hoe veel waarde ik op Ordnung leg).

Dear Masaki, thank you for accepting my invasion into your working space, for teaching me Japanese words and for helping me out!

I want to thank you, Hervé, for our collaboration on XRCC1-CSB and your proposals for improvement.

Dear Alex, thank you so much for many advices and for sharing your enthusiasm for experiments with me.

I want to thank Imke, Serena, Arjan, Loes, Maikel, Kasper, Petra, Niels, Özge, Mariangela, Barbara, Roel, Marit, Angela, Mervin, Di and all other, old, new and infinite members of the NER lab I might be forgetting for making my time in Rotterdam enjoyable.

Heel veel dank aan de keuken-ladies voor een altijd lieve lach en heel veel hulp. Doppio-Man, heel erg bedankt voor de vele hartjes in mijn koffies. A special thanks to Justus Jonas, Peter Shaw and Bob Andrews for keeping me company at the long hours behind the microscope.

I want to thank all the following people who crossed my path and inspired me: Frau Rüth, Sir Alfred Russel Wallace, Mary Berry, Merri Garton, Andre Mayr, Jörg Kriegsmann, Anneke van der Noord, Dr. Pal Mander, Dr. Laurens Kruidenier,

Prof. Dr. E. van Zoelen, Dr. Merel Adjobo-Hermans and Dr. Peter Weiser.

I am grateful for all my new colleagues at Corning who have given me a warm welcome and support as I am discovering my new world.

Andrea, Fritzi, Judith, Julia, Lea und Yvonne – vielen lieben Dank, dass ihr es trotz meines chronischen Zeitmangels schafft, meine Freunde zu bleiben!

Lieve Fardo und Beat, thank euch zo much für de many Abendteuer.

Bedankt Wouter en Martine voor jullie steun en hulp met alles!

Für ganz viele gute Ratschläge, Rezepte mit viel zu viel Butter, Unterstützung und Bewunderung bedanke ich mich bei meinen wundervollen Omas!

Meinen lieben Schwestern möchte ich recht herzlich für die frühe (freiwillige) Unterstützung meiner biologischen Neugierig bedanken!

Liebe Mama und lieber Papa, vielen Dank, dass Ihr mich zu dem gemacht habt, was ich heute sein kann.

Liebe Ellenor, lieber Jonathan und liebes *, vielen Dank für die vielen inspirierenden Diskussionen.

♥ Beste Joris, bedankt voor alles wat wij met elkaar delen!

-----------------------------------------------------------------
I am thankful to have received the highest education possible without having to ever question the right to education or having to struggle with substantial financial support. For many girls access to education is not within the realm of possibility. Please consider donating for Girls Education at CAMFED at my fundraising campaign:

https://camfed.org/donate/personal-fundraising/612-phd-defense/